Atmos. Chem. Phys. Discuss., 13, 25649–25739, 2013
www.atmos-chem-phys-discuss.net/13/25649/2013/
doi:10.5194/acpd-13-25649-2013

Atmospheric Chemistry and Physics Discussions
Open Access

Aerosol indirect effect on the grid-scale clouds in the two-way coupled WRF-CMAQ: model description, development, evaluation and regional analysis

S. Yu[1], R. Mathur[1], J. Pleim[1], D. Wong[1], R. Gilliam[1], K. Alapaty[1], C. Zhao[2], and X. Liu[2,*]

[1]Atmospheric Modeling and Analysis Division, National Exposure Research Laboratory, US Environmental Protection Agency, Research Triangle Park, NC 27711, USA
[2]Atmospheric Sciences and Global Change Division, Pacific Northwest National Laboratory, Richland, WA, USA
[*]now at: Department of Atmospheric Science, University of Wyoming, Laramie, WY 82071, USA

Received: 9 August 2013 – Accepted: 11 September 2013 – Published: 7 October 2013

Correspondence to: S. Yu (yu.shaocai@epa.gov)

Published by Copernicus Publications on behalf of the European Geosciences Union.

Abstract

This study implemented first, second and glaciation aerosol indirect effects (AIE) on resolved clouds in the two-way coupled WRF-CMAQ modeling system by including parameterizations for both cloud drop and ice number concentrations on the basis of CMAQ-predicted aerosol distributions and WRF meteorological conditions. The performance of the newly-developed WRF-CMAQ model, with alternate CAM and RRTMG radiation schemes, was evaluated with the observations from the CERES satellite and surface monitoring networks (AQS, IMPROVE, CASTNet, STN, and PRISM) over the continental US (CONUS) (12 km resolution) and eastern Texas (4 km resolution) during August and September of 2006. The results at the AQS surface sites show that in August, the normalized mean bias (NMB) values for $PM_{2.5}$ over the eastern (EUS) and western US (WUS) are 5.3 % (–0.1 %) and 0.4 % (–5.2 %) for WRF-CMAQ/CAM (WRF-CMAQ/RRTMG), respectively. The evaluation of $PM_{2.5}$ chemical composition reveals that in August, WRF-CMAQ/CAM (WRF-CMAQ/RRTMG) consistently underestimated the observed SO_4^{2-} by −23.0 % (−27.7 %), −12.5 % (−18.9 %) and −7.9 % (−14.8 %) over the EUS at the CASTNet, IMPROVE and STN sites, respectively. Both models (WRF-CMAQ/CAM, WRF-CMAQ/RRTMG) overestimated the observed mean OC, EC and TC concentrations over the EUS in August at the IMPROVE sites. Both models generally underestimated the cloud field (shortwave cloud forcing (SWCF)) over the CONUS in August due to the fact that the AIE on the subgrid convective clouds was not considered when the model simulations were run at the 12 km resolution. This is in agreement with the fact that both models captured SWCF and longwave cloud forcing (LWCF) very well for the 4 km simulation over the eastern Texas when all clouds were resolved by the finer domain. Both models generally overestimated the observed precipitation by more than 40 % mainly because of significant overestimation in the southern part of the CONUS in August. The simulations of WRF-CMAQ/CAM and WRF-CMAQ/RRTMG show dramatic improvements for SWCF, LWCF, cloud optical depth (COD), cloud fractions and precipitation over the ocean relative to those of

ACPD
13, 25649–25739, 2013

WRF default cases in August. The model performance in September is similar to that in August except for greater overestimation of $PM_{2.5}$ due to the overestimations of SO_4^{2-}, NH_4^+, NO_3^-, and TC over the EUS, less underestimation of clouds (SWCF) over the land areas due to about 10 % due to the lower SWCF values and less convective clouds in September.

1 Introduction

Atmospheric emissions resulting from consumption of fossil fuels by human activities contribute to climate change and degrade air quality. Aerosol particles can influence the Earth's climate both directly by scattering and absorption of incoming solar radiation and terrestrial outgoing radiation, and indirectly by affecting cloud radiative properties through their role as cloud condensation nuclei (CCN) and ice nuclei (IN) (Twomey, 1974, 1991; Charlson et al., 1992; Yu, 2000; Yu et al., 2000, 2001a, b, 2003, 2006; Yu and Zhang, 2011; Lohmann and Feichter, 2005; Menon et al., 2002, 2008; IPCC, 2007; DeFelice et al., 1997; Chapman et al., 2009; Gustafson et al., 2007; Zhang et al., 2010a, b, 2012; Tao et al., 2012; Hansen et al., 1997; Haywood and Boucher, 2000; Ramanathan et al., 2001; Rosenfeld et al., 2008; Saxena and Yu, 1998; Saxena et al., 1997; Yu et al., 2006, 2012a, b). The so-called aerosol indirect effect (AIE) can be split into the first, second, and glaciation indirect aerosol effects. For a given cloud liquid water content, an increase in the cloud droplet number concentration implies a decrease in the effective radius, thus increasing the cloud albedo; this is known as the first AIE (or cloud albedo effect) and was first estimated by Twomey (1974). The second AIE is based on the idea that decreasing the mean droplet size in the presence of enhanced aerosols decreases the cloud precipitation efficiency, producing clouds with a larger liquid water content and longer lifetime (cloud lifetime effect) and its recognition is commonly attributed to Albrecht (1989). The "glaciation AIE" is based on the idea that increases in IN because of enhanced aerosols (dust, organic carbon, black carbon and sulfate) result in more frequent glaciation of a super-cooled liquid water cloud

ACPD
13, 25649–25739, 2013

due to the difference in vapor pressure over ice and water and increase in the amount of precipitation via the ice phase, leading to decrease of cloud cover and the shorter cloud lifetime (IPCC, 2007; Lohmann, 2002). The first and second AIEs have negative radiative effect at the top of atmosphere (TOA), while the glaciation AIE has positive effect. As summarized by Lohmann and Feichter (2005) and IPCC (2007), other aerosol indirect effects may include the semi-direct effect, which refers to an evaporation of cloud droplets caused by the absorption of solar radiation by soot, and the thermodynamic effect which refers to a delay of the onset of freezing by the smaller cloud droplets causing super-cooled clouds to extend to colder temperature (precipitation suppression). The IPCC (2007) concludes that increasing concentrations of the long-lived greenhouse gases have led to a combined radiative forcing +2.63 [±0.26] $\mathrm{W\,m^{-2}}$, and the total direct aerosol radiative forcing is estimated to be −0.5 [±0.4] $\mathrm{W\,m^{-2}}$, with a *medium-low* level of scientific understanding, while the radiative forcing due to the cloud albedo effect (also referred to as first indirect), is estimated to be −0.7 [−1.1, +0.4] $\mathrm{W\,m^{-2}}$, with a *low* level of scientific understanding. Clearly, the great uncertainty in the indirect aerosol forcing for the assessment of climate forcing by anthropogenic aerosols must be reduced.

Numerous investigations provide observational evidence of the AIE. For example, the presence of non-precipitating supercooled liquid water near cloud tops because of the over-seeding from both smokes over Indonesia and urban pollution over Australia (Rosenfeld, 1999, 2000) has been identified. Rosenfeld et al. (2007) found that on the basis of the analysis of more than 50 yr of observations at Mt. Hua near Xi'an in China, the observed orographic precipitation decreased by 30–50 % during the hazy conditions in the presence of high levels of aerosols and small CCN. On the basis of the extensive ground-based and global A-Train (CALIPSO and MODIS) observations during the past 10 yr, Li et al. (2011) found the strong climate effects of aerosols on clouds and precipitation. Lin et al. (2006) found the evidence that high biomass burning-derived aerosols were correlated with elevated cloud top heights, large anvils and more rainfall on the basis of satellite observations over the Amazon basin. En-

ACPD
13, 25649–25739, 2013

hanced rainfall in the coastal NW Atlantic region (Cerveny et al., 1998) and downwind of Mexico city urban area (Jauregui et al., 1996) and paper mills (Eagen et al., 1974) is attributed to the effects of giant CCN. However, it is impossible to evaluate the AIE with observations directly because the AIE is traditionally estimated on the basis of the difference of model results between the present day and pre-industrial times, and the observational records (satellite and other long-term records) are not long enough to characterize conditions during the pre-industrial times (IPCC, 2007). However, the satellite retrievals of various cloud parameters provide indirect means for evaluating the model simulations. For example, the cloud droplet effective radii retrieved from the satellite of the Advanced Very High Resolution Radiometer (AVHRR) (Han et al., 1994) have been used to evaluate the global model simulations (Rotstayn, 1999; Ghan et al., 2001a, b, c; Ghan and Easter, 2006).

The chemistry-aerosol-cloud-radiation-climate interactions are complex and can be nonlinear. To realistically simulate these interactions, a fully online-coupled meteorology-air quality model is needed. Although there are a large number of online coupled global meteorology-air quality models with various degrees of coupling (very limited prognostic gaseous and aerosol species and/or aerosol-cloud-radiation process representation) to air quality (Granier and Brasseur, 1991; Rasch et al., 2000; Taylor and Penner, 1994; Jacobson, 1994, 2006), even fewer coupled meteorology-air quality models at urban and regional scale exist due to the fact that mesoscale meteorology models and air quality models were developed separately. The history and current status of the development and application of online-coupled meteorology and air quality models have been reviewed by Zhang (2008). As summarized by Pleim et al. (2008), there are three approaches to couple meteorology and air quality models. The first approach is to simply add atmospheric chemistry to the existing meteorology models such as MM5/Chem (Grell et al., 2000) and WRF/Chem (Grell et al., 2005). The second approach is to integrate meteorology and atmospheric chemistry from the beginning such as GATOR-GCMOM model (Jacobson, 2001a, b). The third approach is to combine existing meteorology and air quality models into a single executable program

ACPD
13, 25649–25739, 2013

with 2-way meteorological and chemical data exchange such as the two-way coupled WRF-CMAQ model (Wong et al., 2012). Each approach has its own advantages and disadvantages. For example, the advantage of the third approach is to allow using the existing computational and numerical techniques in each model (meteorology and air quality) and leverage future development in each model by maintaining equivalent one-way capability. The two-way coupled WRF-CMAQ model is developed with the third approach by integrating WRF and CMAQ models into a single executable program in which CMAQ can be executed as a stand-alone model or part of the coupled system without any code changes (Wong et al., 2012). The WRF-CMAQ model is a community online-coupled model which is publicly available and allows contributions from the community.

In this work, we implement the indirect effects of aerosols on the microphysical and radiative properties of clouds (including first, second and glaciation indirect aerosol forcing) in the two-way coupled WRF-CMAQ. The cloud droplet number concentrations were calculated from the CMAQ-predicted aerosol particles using a parameterization based on a maximum supersaturation determined from a Gaussian spectrum of updraft velocities and the internally mixed aerosol properties within each mode (Abdul-Razzak and Ghan, 2002). The cloud condensation nuclei (CCN) concentrations at six supersaturations (0.02 %, 0.05 %, 0.1 %, 0.2 %, 0.5 %, 1.0 %) are estimated. The cloud ice number concentrations for the CMAQ-predicted sulfate, black carbon and dust were estimated with an ice nucleation scheme in the NCAR Community Atmospheric Model (CAM) (Liu et al., 2007). The resulting cloud drop and ice number concentrations are added to the Morrison cloud microphysics scheme (Morrison et al., 2009, 2005) and this allows us to estimate aerosol effects on cloud and ice optical depth and microphysical process rates for indirect aerosol radiative forcing (including first, second and glaciations indirect aerosol forcing) by tying a two-moment treatment of cloud water (mass and number) and cloud ice (mass and number) to precipitation (the Morrison et al., 2-moment cloud microphysics scheme, Morrison et al., 2009, 2005) and two radiation schemes (the Rapid Radiative Transfer Model for GCMs (RRTMG) (Iacono

ACPD
13, 25649–25739, 2013

et al., 2008) and CAM, Collins et al., 2004) in the WRF model. The RRTMG and CAM radiation schemes are used because these two schemes are used in many studies. The simulations with the newly-developed WRF3.3-CMAQ5.0 model are carried out at a 4 km resolution model grid over east Texas (Fig. 1a) and a 12 km resolution model grid over the continental US (Fig. 1b) for the summer of 2006. The model performance for cloud properties (e.g., cloud optical depth (COD), cloud fractions), shortwave cloud forcing (SWCF), longwave cloud forcing (LWCF) and $PM_{2.5}$, its chemical composition and precursors is examined with satellite observation data (CERES) and the surface monitoring networks (AIRNOW, IMPROVE, CASTNet, STN, PRISM) during August and September of 2006.

2 Model description and simulation design

2.1 Two-way coupled WRF-CMAQ

The two-way coupled WRF-CMAQ modeling system (Pleim et al., 2008; Mathur et al., 2010; Wong et al., 2012) was developed by linking the Weather Research and Forecasting (WRF) model (Skamarock et al., 2008) and Community Multiscale Air Quality (CMAQ) model (Eder and Yu, 2006; Mathur et al., 2008; Eder et al., 2010, 2009). A brief summary relevant to the present study is presented here. In this system, radiative effects of aerosols and the cloud droplets diagnosed from the activation of CMAQ-predicted aerosol particles interact with the WRF radiation calculations, resulting in a "2-way" coupling between atmospheric dynamic and chemical modeling components (Pleim et al., 2008; Mathur et al., 2010). Figure 2 shows a schematic coupling for the WRF and CMAQ modeling system which includes three components: WRF, CMAQ and a coupler. In the coupled system, CMAQ is added as a subroutine in WRF and can be executed as a stand-alone model or part of the coupled system without any code changes. The coupler serves as an inter-model translator by transferring meteorological data from WRF to CMAQ and CMAQ-predicted aerosol data from CMAQ to WRF in

ACPD
13, 25649–25739, 2013

memory. In the coupler, a subroutine called AQPREP prepares virtual meteorological files in forms compatible for CMAQ to use directly without writing the physical files, and another subroutine FEEDBACK, which is called within the aerosol module in CMAQ, is used to compute aerosol properties and transfer the related aerosol data from CMAQ to WRF for direct and indirect aerosol forcing calculations. The call frequency is a user defined environmental variable as a ratio of the WRF to CMAQ time steps and is used in the coupled system to determine how many times WRF is called for each CMAQ call. WRF integrates at a very fine time step while the minimum synchronization time step in CMAQ is determined by the horizontal wind speed Courant condition in model layers lower than ~700 hPa; the coupling frequency is flexible and can be specified by the user. This is a mechanism to balance computational performance while allowing the user to couple the models as tightly as needed. The preliminary results of the two-way coupled WRF-CMAQ model with direct aerosol effect only for a ten-day simulation of a wildfire event in California during 20–29 June 2008, showed that the coupled model can improve the accuracy of both meteorology and air quality simulations for these cases with high aerosol loading when the direct aerosol effect is included (Wong et al., 2012). In this work, the AIE in the two-way coupled WRF-CMAQ model is implemented by adding a subroutine called CMAQ-mixactivate which calculates both cloud droplet and ice number concentrations on the basis of the CMAQ-predicted aerosol particles and the WRF meteorological conditions (see Figs. 2 and 3) and will be described in detail below. Like CMAQ, the subroutine CMAQ_mixactivate is added as a subroutine in WRF and is called just after CMAQ is called in order to use the results of CMAQ simulations.

Table 1 summarizes the model configurations and components used in this study. The physics package of the WRF (ARW) includes the Kain–Fritsch (KF2) cumulus cloud parameterization (Kain and Fritsch, 1990, 1993; Kain, 2004), Asymmetric Convective Model (ACM2) planetary boundary layer (PBL) scheme (Pleim, 2007a, b), RRTMG (Iacono et al., 2008) and CAM (Collins et al., 2004) shortwave and longwave radiation schemes, Morrison et al., 2-moment cloud microphysics (Morrison et al., 2009, 2005; Morrison and Pinto, 2006), and Pleim-Xiu (PX) land-surface scheme (Pleim and Xiu, 1995, 2003; Xiu and Pleim, 2001). Note that the KF2 cumulus cloud scheme was turned off for the model simulations at the 4 km resolution model grid. The meteorological initial and lateral boundary conditions were derived from a combination of North American Mesoscale (NAM) model analyses and forecasts at 3 h intervals developed by the National Center for Environmental Prediction (NCEP). The Carbon Bond chemical mechanism (CB05) (Yarwood et al., 2005) has been used to represent photochemical reaction pathways. Emissions are based on the 2005 National Emission Inventory (NEI) (available at www.epa.gov/ttnchief1/net/2005inventory.html) and BEIS v3.14 for year 2006. The mobile source emissions were generated by EPA'S MOBILE6 model.

The aerosol module in CMAQ is described by Binkowski and Roselle (2003) and updates are described by Bhave et al. (2004), Yu et al. (2007a), Carlton et al. (2010), Foley et al. (2010), and Appel et al. (2013). The size distribution of aerosols in tropospheric air quality models can be represented by the sectional approach (Zhang et al., 2002, 2012), the moment approach (Yu et al., 2003), and the modal approach (Binkowski and Roselle, 2003). In the aerosol module of CMAQ, the aerosol distribution is modeled as a superposition of three lognormal modes that correspond nominally to the ultrafine (diameter (Dp) $< 0.1\,\mu m$), fine ($0.1\,\mu m < Dp < 2.5\,\mu m$), and coarse ($Dp > 2.5\,\mu m$) particle size ranges. Each lognormal mode is characterized by total number concentration, geometric mean diameter and geometric standard deviation. Table 2 lists the aerosol species for each mode in the latest aerosol module AERO6 of CMAQ version 5.0 which is used in this study. As summarized by Foley et al. (2010), there are three main increments for the new aerosol module including improved treatment of secondary organic aerosol (SOA), a new heterogeneous N_2O_5 hydrolysis parameterization and a new treatment of gas-to-particle mass transfer for coarse particles with the update of the in-line treatment of sea-salt emissions. In the previous aerosol module, SOA was formed by absorptive partitioning of condensable oxidation products of monoterpenes (ATRP1, ATRP2), long alkanes (~ 8 carbon atoms) (AALK), low-yield aromatic

ACPD
13, 25649–25739, 2013

products (based on *m*-xylene data) (AXYL1, AXYL2), and high-yield aromatics (based on toluene data) (ATOL1, ATOL2). The updates to the representation of SOA include several recently identified SOA formation pathways from isoprene (AISO1, AISO2), benzene (ABNZ1, ABNZ2), sesquiterpenes (ASQT), in-cloud oxidation of glyoxal and methylglyoxal (AORGC), particle-phase oligomerization (aged SOA, AOLGA, AOLGB), acid enhancement of isoprene SOA (AISO3), and NOx-dependent SOA yields from aromatic compounds (ATOL3, AXYL3, ABNZ3) (see Table 2, Carlton et al., 2010). Note that ATOL3, AXYL3, ABNZ3, AISO3, AOLGA, AOLGB and AORGC are non-volatile SOA. Primary organic aerosols (POA) is separated into primary organic carbon (APOC) and primary noncarbon organic mass (APNOM) (POA = APOC + APNOM) and soil is calculated as SOIL = 2.20Al + 2.49Si + 1.63Ca + 2.42Fe + 1.94Ti (Simon et al., 2011). Note that "OTHR" specie in Table 2 refers to unspecified anthropogenic mass which comes from the emission inventory in $PM_{2.5}$, i.e., $[PM_{2.5}] = [SO_4^{2-}] + [NH_4^+] + [NO_3^-] + [OM] + [EC] + [SOIL] + [OTHR]$. The model results for $PM_{2.5}$ concentrations are obtained by summing aerosol species concentrations over the first two modes. Generally speaking, the modal approach offers the advantage of being computationally efficient, whereas the sectional representation provides more accuracy at the expense of computational cost (Yu et al., 2007a, b, 2004, 2005, 2008; McKeen et al., 2007; Liu et al., 2011). The chemical boundary conditions (BCs) for the CMAQ model simulation over the CONUS were provided by an annual 2006 GEOS-Chem (Bey et al., 2001) simulation.

2.2 Aerosol-cloud-radiation interaction: indirect effects

A flow diagram for calculation of AIE in the two-way coupled WRF-CMAQ model is shown in Fig. 3.

2.2.1 First and second indirect aerosol forcing

To estimate the first and second indirect aerosol forcing, the cloud droplet number concentrations are diagnosed from the activation of CMAQ-predicted aerosol particles using a aerosol activation scheme for multiple externally mixed lognormal modes, with each mode composed of uniform internal mixtures of soluble and insoluble material developed by Abdul-Razzak and Ghan (2002, 2000). The detailed description of the aerosol activation scheme is given by Abdul-Razzak and Ghan (2002, 2000). Here a brief summary relevant to the present study is presented. The aerosol number concentration of a multimode lognormal distribution can be expressed as

$$\frac{dn}{dr} = \sum_{i=1}^{I} \frac{N_i}{\sqrt{2\pi}\ln\sigma_i} \exp\left(-\frac{1}{2} \frac{\ln^2\left(\frac{r}{r_{g,i}}\right)}{\ln^2(\sigma_i)} \right) \tag{1}$$

where N_i is the total number concentration, $r_{g,i}$ is the geometric mean dry radius, and σ_i is the geometric standard deviation for each aerosol mode i, $i = 1, 2, \ldots I$. The smallest activation dry radius ($r_{cut,i}$) for each mode is (Abdul-Razzak and Ghan, 2002, 2000):

$$r_{cut,i} = r_{g,i} \left(\frac{S_{m,i}}{S_{max}} \right)^{\frac{2}{3}} \tag{2}$$

where the critical supersaturation ($S_{m,i}$) for activating particles and ambient maximum supersaturation (S_{max}) are given by (Abdul-Razzak and Ghan, 2002, 2000; Abdul-Razzak et al., 1998):

$$S_{m,i} = \frac{2}{\sqrt{B_i}} \left(\frac{A}{3r_{g,i}} \right)^{\frac{3}{2}} \tag{3}$$

Discussion Paper | Discussion Paper | Discussion Paper | Discussion Paper |

ACPD

13, 25649–25739, 2013

Aerosol indirect effect in the two-way coupled WRF-CMAQ

S. Yu et al.

$$S_{\max} = \frac{1}{\left\{\sum \frac{1}{S_{m,i}^2}\left[0.5\exp(2.5\ln^2\sigma_i)\left(\frac{\xi}{\eta_i}\right)^{\frac{3}{2}} + (1+0.25\ln\sigma_i)\left(\frac{S_{m,i}^2}{\eta_i+3\xi}\right)^{\frac{3}{4}}\right]\right\}^{\frac{1}{2}}} \tag{4}$$

Where

$$\xi = \frac{2A}{3}\left(\frac{\alpha V}{G}\right)^{\frac{1}{2}} \tag{5}$$

$$\eta_i = \frac{(\alpha V/G)^{\frac{3}{2}}}{2\pi\rho_w\gamma N_i} \tag{6}$$

$$A = \frac{2\sigma_w M_w}{\rho_w RT} \tag{7}$$

Here A is coefficient of the curvature effect (Kelvin term) in the Köhler equation, V is the updraft velocity, the growth coefficient (G) represents diffusion of heat and moisture to the particles (gas kinetic effects), ρ_w is the water density, M_w is the molecular weight of water, R is the molar gas constant, T is the temperature, σ_w is the surface tension of water, α and γ are size-invariant coefficients in the supersaturation balance equation (Leaitch et al., 1986; Abdul-Razzak et al., 1998). The hygroscopicity parameter (B_j) (solute effect, Raoult term) in the Köhler equation for component j can be expressed as (Pruppacher and Klett, 1997; Abdul-Razzak et al., 1998)

$$B_j = \frac{M_w v_j \phi_j \varepsilon_j / M_{a,j}}{\rho_w/\rho_{a,j}} \tag{8}$$

where v_j, ϕ_j, ε_j, $M_{a,j}$ and $\rho_{a,j}$ are the number of ions the salt dissociates into (von't Hoff factor for solute in solution), osmotic coefficient, the mass fraction of soluble material (1 for water soluble material and 0 for insoluble material), molecular weight and density for

ACPD
13, 25649–25739, 2013

component j, respectively. The volume mean hygroscopicity parameter ($\overline{B_i}$) for aerosol mode i can be calculated as follows (Hanel, 1976; Pruppacher and Klett, 1997; Abdul-Razzak et al., 1998):

$$\overline{B_i} = \frac{\sum_{j=1}^{J} (B_{i,j} q_{i,j} / \rho_{a,i,j})}{\sum_{j=1}^{J} (q_{i,j} / \rho_{a,i,j})} \quad (9)$$

where $q_{i,j}$, and $\rho_{a,i,j}$ are mass mixing ratio, and density for component j in aerosol mode i, respectively. Petters and Kreidenweis (2007) summarized the hygroscopicity B value ranges for different compounds on the basis of different measurements and estimations from the different investigators. Note that the single parameter κ value in Petters and Kreidenweis (2007) is practically equivalent to the hygroscopicity B value here (Liu and Wang, 2010). Koehler et al. (2009) estimated that the hygroscopicity B values for $(NH_4)_2SO_4$, and NaCl ranged from 0.33 to 0.72 and 0.91 to 1.33, respectively. The hygroscopicity values for anthropogenic SOA range from 0.06 to 0.14 (Prenni et al., 2007) and for biogenic SOA range from 0.06 to 0.23 (Prenni et al., 2007; King et al., 2010). Elemental carbon is generally considered as non-hygroscopic ($B = 0$). Jimenez et al. (2009) showed that the hygroscopicity of SOA changes from 0 to 0.2 because of its aging in the atmosphere. On the basis of the measurements for three mineral dust samples (dust from Canary Island, outside Cairo and Arizona Test Dust), Koehler et al. (2009) reported that the hygroscopicity values for the minimally-processed dust particles vary from 0.01 to 0.08 with a suggested median value of 0.03. In this study, the hygroscopicity B value for ASO4, ANO3, ANH4 and AORGC are assumed to be 0.5. The hygroscopicity B value of 0.14 is used for the SOA species (AALK, AXYL, ATOL, ABNZ, ATRP, AISO and ASQT). The hygroscopicity B value for aged SOA (AOLGA and AOLGB) is assumed to be 0.20. Table 3 lists the molecular weight, density and hygroscopicity B values for each component used in this study.

ACPD
13, 25649–25739, 2013

After the smallest activation dry radius ($r_{\mathrm{cut},i}$) for each mode is determined, the total number (N_{act}, i.e., cloud droplet number) and mass (M_{act}) activated for each mode can be calculated as follows (Abdul-Razzak and Ghan, 2002, 2000):

$$N_{\mathrm{act}} = \sum_{i=1}^{I} N_i \frac{1}{2}[1 - \mathrm{erf}(u_i)] \tag{10}$$

$$M_{\mathrm{act}} = \sum_{i=1}^{I} M_i \frac{1}{2}\left[1 - \mathrm{erf}\left(u_i - \frac{3\sqrt{2}}{2}\ln(\sigma_i)\right)\right] \tag{11}$$

where

$$u_i = \frac{2\ln(S_{\mathrm{m},i}/S_{\mathrm{max}})}{3\sqrt{2}\ln(\sigma_i)}. \tag{12}$$

The total aerosol number and mass concentrations are separated into interstitial (refers to aerosol particles that do not activate to form cloud droplets) and cloud-borne (activated) portions based on the values of activated fractions with the above equations. It is also assumed that all cloud droplets are formed either when a cloud forms within a layer or as air flows into the cloud. For stratiform (resolved) clouds, the scheme of activation (Ghan et al., 1997; Abdul-Razzak and Ghan, 2002, 2000) only accounts for both resolved and turbulent transport of air into the base of the cloud but neglects droplet formation on the sides and top of the cloud. An implicit numerical integration scheme for treatment of cloud droplet nucleation and vertical diffusion of cloud droplets simultaneously is performed by expressing cloud droplet nucleation in terms of a below-cloud droplet number concentration diagnosed from the nucleation flux and the eddy diffusivity (Abdul-Razzak and Ghan, 2002, 2000). When a cloud dissipates in a grid cell, cloud droplets evaporate and aerosols are resuspended, i.e., they transfer from the cloud-borne to the interstitial state. The newly-simulated cloud droplet number concentrations are updated due to the transport processes like other species in the model

ACPD
13, 25649–25739, 2013

before being added to the Morrison et al., 2-moment cloud microphysics scheme (Morrison et al., 2009, 2005). The Morrison cloud microphysics scheme predicts both number concentrations and mass mixing ratios of five hydrometer types (cloud droplets, ice crystals, rain droplets, snow particles and graupel particles) and water vapor, and describes several microphysical processes which include auto-conversion, self-collection, collection between hydrometeor species, freezing, cloud ice nucleation and droplet activation by aerosols and sedimentation. The resulting cloud drop number concentrations were supplied to the Morrison cloud microphysics scheme to allow estimation of aerosol effects on cloud optical depth and microphysical process rates for indirect aerosol radiative forcing (including first and second indirect aerosol forcing) by tying a two-moment treatment of cloud water (mass and number) to precipitation (the Morrison cloud microphysics scheme) and two alternate radiation schemes (RRTMG and CAM) in the WRF model. It should be noted that the original default aerosol activation processes which are based on Khvorostyanov and Curry (1999) were turned off in the study to avoid to double accounting of the aerosol activation. Radiation schemes used in the numerical models are very sensitive to the effective radius; Slingo (1990) showed that decreasing the effective radius of cloud droplets from 10 to 8 µm would result in atmospheric cooling that could offset global warming from doubling the CO_2 content of the atmosphere. In the Morrison cloud microphysics scheme, the cloud drop effective radius (r_e) is defined as the ratio of the third to the second moment of the gamma droplet size distribution as follows (Morrison and Grabowski, 2007):

$$r_e = \frac{\Gamma(\mu+4)}{2\lambda\Gamma(\mu+3)} \quad (13)$$

where Γ is the Euler gamma function and cloud droplet number concentrations ($N_c(D)$) are assumed to follow gamma size distribution:

$$N_c(D) = N_{c,0} D^{\mu} e^{-\lambda D} \quad (14)$$

where D, $N_{c,0}$ and λ are diameter, the "intercept" parameter, and slope parameter, respectively. $\mu = 1/\eta^2 - 1$ is the spectral parameter (η is the ratio between the standard

ACPD
13, 25649–25739, 2013

deviation of the spectrum and the mean radius for the relative radius dispersion) and η is calculated as follows (Martin et al., 1994; Morrison and Grabowski, 2007):

$$\eta = 0.0005714 N_c + 0.2714 \quad (15)$$

where N_c is the cloud droplet number concentration (cm^{-3}). These cloud droplet effective radii from the Morrison cloud microphysics scheme are used in the RRTMG (or CAM) radiation schemes directly and this will affect the radiation fields accordingly.

2.2.2 Glaciation indirect aerosol forcing

To estimate the glaciation indirect aerosol forcing, the cloud ice number concentrations were estimated from the activation of the CMAQ-predicted sulfate, black carbon, dust and organic aerosols with an ice nucleation scheme used in the NCAR CAM (Liu et al., 2007). The detailed description of the ice nucleation scheme is given by Liu et al. (2007) and Liu and Penner (2005). Briefly, in this scheme, the ice crystal number concentration ($N_{i,a}$) from homogeneous nucleation ($-60\,^{\circ}C < T < -35\,^{\circ}C$) is a function of temperature (T), updraft velocity (w) and sulfate aerosol number concentration (N_a) and is calculated as follows:

For higher T and lower w (the fast-growth regime):

$$N_{i,a} = \min\left\{\exp(a_2 + b_2 T + c_2 \ln w) N_a^{a_1 + b_1 T + c_1 \ln w}, N_a\right\}, \quad (16)$$

while for lower T and higher w (the slow-growth regime):

$$N_{i,a} = \min\left\{\exp(a_2 + (b_2 + b_3 \ln w) T + c_2 \ln w) N_a^{a_1 + b_1 T + c_1 \ln w}, N_a\right\}. \quad (17)$$

In Eqs. (16) and (17), a_1, a_2, b_1, b_2, b_3, c_1 and c_2 are coefficients for the homogeneous nucleation parameterization. The ice crystal number concentrations ($N_{i,s}$) formed from

ACPD
13, 25649–25739, 2013

immersion nucleation of soot or mineral dust (N_s) through the heterogeneous nucleation on the basis of classic nucleation theory (Pruppacher and Klett, 1997) are calculated as follows:

$$N_{i,s} = \min\left\{\exp((a_{21}\ln w + a_{22}) + (a_{11}\ln w + a_{12})T)N_s^{(b_{21}\ln w + b_{22})+(b_{11}\ln w + b_{12})T}, N_s\right\} \quad (18)$$

where a_{11}, a_{12}, a_{21}, a_{22}, b_{11}, b_{12}, b_{21}, and b_{22} are coefficients.

In the original version of the ice nucleation scheme in the NCAR CAM (Liu et al., 2007), the deposition/condensation nucleation of ice crystals in mixed-phase clouds is represented by the Meyers et al. (1992) formulation which does not allow ice number concentration to depend on the aerosol number concentration. In the new version used in this work, the ice number concentration from the deposition/condensation nucleation on dust/metallic, black carbon and organic aerosols with the size interval $\mathrm{d}\log D_x$ is estimated by the approach of Phillips et al. (2008) as follows

$$N_{i,X} = \int_{\log(0.1\,\mu\mathrm{m})}^{\infty} \{1 - \exp[-\mu_X(D_X, S_i, T)]\} \times \frac{\mathrm{d}n_X}{\mathrm{d}\log(D_X)}\mathrm{d}\log(D_X) \quad (19)$$

$$\mu_X = H_X(S_i, T)\xi(T)\left(\frac{a_X n_{IN,1,*}}{\Omega_{X,1,*}}\right) \times \frac{\mathrm{d}\Omega_X}{\mathrm{d}n_X} \text{ for } T < 0\,^\circ\mathrm{C} \text{ and } 1 < S_i \leq S_i^w \quad (20)$$

$$n_{IN,1,*}(T, S_i) = \psi c \exp[12.96(S_i - 1) - 0.639] \text{ for } T \geq -25,^\circ\mathrm{C} \text{ and } 1 < S_i \leq S_i^w \quad (21)$$

Where X represents dust/metallic, black carbon and organic aerosols, μ_X is the average of the number of activated ice embryos per insoluble aerosol particle of size D_X, $\frac{\mathrm{d}\Omega_X}{\mathrm{d}n_X} \approx \pi D_X$, n_X is the number mixing ratio of aerosols in group X, S_i is the saturation ratio of water vapor with respect to ice, T is temperature, ψ is assumed to be $0.058707\gamma/\rho_c\,\mathrm{m^3\,kg^{-1}}$ ($\gamma = 2$ and $\rho_c = 0.76\,\mathrm{kg\,m^{-3}}$), $c = 1000\,\mathrm{m^{-3}}$, and $H_x(S_i, T)$ is an empirically determined fraction (Phillips et al., 2008). The ice number concentrations from the contact freezing of cloud droplets by dust particles are estimated with the

Discussion Paper | Discussion Paper | Discussion Paper | Discussion Paper |

ACPD

13, 25649–25739, 2013

Aerosol indirect effect in the two-way coupled WRF-CMAQ

S. Yu et al.

approach of Young (1974) as follows (Liu et al., 2007):

$$n_{\text{frz, cnt}} = 4\pi r_v N_d N_{\text{cnt}} D_{\text{cnt}} / \rho_0 \quad (22)$$

where

$$N_{\text{cnt}} = N_{a0}(270.16 - T)^{1.3} \quad (23)$$

$$D_{\text{cnt}} = \frac{k_B T C_c}{6\pi\mu r_{\text{cnt}}} \quad (24)$$

where r_v, N_d, ρ_0, N_{a0}, k_B, r_{cnt}, C_c, μ and T are the volume mean droplet radius, cloud droplet number concentration, air density, number concentration of dust particles for each mode (dust accumulation and coarse modes), the Boltzmann constant, the aerosol (dust) number mean radius, the Cunningham correction factor, viscosity of air and temperature, respectively. The original contact freezing scheme in the Morrison cloud microphysics scheme which is based on the approach of Meyers et al. (1992) is turned off in this study. The resulting cloud ice number concentrations were added to the Morrison cloud microphysics scheme to allow estimation of aerosol effects on ice optical depth and microphysical process rates for indirect glaciation aerosol radiative forcing by tying a two-moment treatment of cloud ice (mass and number) to precipitation (the Morrison cloud microphysics scheme) and two radiation schemes (RRTMG and CAM) in the WRF model. Calculation of ice effective radius is complicated by the nonspherical geometry of ice crystals. In the Morrison cloud microphysical scheme, the parameterization of Fu (1996) for derivation of ice effective diameter ($D_{e,i}$) is employed as follows (Morrison and Grabowski, 2007):

$$D_{e,i} = 2\sqrt{3}\text{IWC}/(3\rho_i A_c) \quad (25)$$

Where IWC is the ice water content and A_c is the projected area of the crystals from the given A (projected area)–D (dimension) relationship integrated over the size distribution (Morrison and Grabowski, 2007). The A–D relationship varies as a function of crystal habit, degree of riming and particle size. These ice effective radii from the Morrison cloud microphysics scheme are used in the RRTMG and CAM radiation schemes directly and this will affect the radiation fields accordingly.

3 Observational data sets

3.1 $PM_{2.5}$ and its chemical components observations at the surface sites

Over the continental United States, four surface monitoring networks for $PM_{2.5}$ measurements were employed in this evaluation: Interagency Monitoring of Protected Visual Environments (IMPROVE), Speciated Trends Network (STN), Clean Air Status Trends Network (CASTNet) and Air Quality System (AQS), each with its own and often disparate sampling protocol and standard operating procedures. In the IMPROVE network, two 24 h samples are collected on quartz filters each week, on Wednesday and Saturday, beginning at midnight local time (Sisler and Malm, 2000). The observed $PM_{2.5}$, SO_4^{2-}, NO_3^-, EC and OC data are available at 155 rural sites across the continental United States. The STN network (http://www.epa.gov/air/data/aqsdb.html) follows the protocol of the IMPROVE network (i.e., every third day collection) with the exception that most of the sites are in urban areas. The observed $PM_{2.5}$, SO_4^{2-}, NO_3^-, and NH_4^+ data are available at 182 STN sites within the model domain. The CASTNet (http://www.epa.gov/castnet/) collected the concentration data at predominately rural sites using filter packs that are exposed for 1 week intervals (i.e., Tuesday to Tuesday). The aerosol species at the 82 CASTNet sites used in this evaluation include: SO_4^{2-}, NO_3^-, and NH_4^+. The hourly near real-time $PM_{2.5}$ data at 840 sites in the continental United States are measured by tapered element oscillating microbalance (TEOM) instruments at the US EPA's AQS network sites. The hourly, near real-time O_3 data for 2006 at 1138 measurement sites in the continental United States are available from the US EPA's AQS network, resulting in nearly 1.2 million hourly O_3 observations for the studied period.

ACPD
13, 25649–25739, 2013

3.2 Satellite cloud observations from CERES

The NASA Clouds and Earth's Radiant Energy System (CERES) is a suite of satellite-based instruments designed to measure the top-of-atmosphere (TOA) radiation fields simultaneously with cloud properties. The CERES scanners operated on three satellites (the Tropical Rainfall Measuring Mission (TRMM), Moderate Resolution Imaging Spectroradiometer (MODIS) *Terra* and *Aqua* satellites) in which data from the TRMM Visible Infrared Scanner (VIRS) (Kummerow et al., 1998) and the MODIS *Terra* and *Aqua* (Barnes et al., 1998) are used for discriminating between clear and cloudy scenes, and for retrieving the properties of clouds and the aerosols. In this study, the monthly data of cloud properties are obtained from the CERES SSF (Single Scanner Footprint) 1deg Product Edition2.6 (CERES Terra SSF1deg-lite_Ed2.6) which was released on 11 July 2011 (Wielicki et al., 2006; http://ceres-tool.larc.nasa.gov/ord-tool/jsp/SSF1degSelection.jsp). Monthly means are calculated using the combination of observed and interpolated parameters from all days containing at least one CERES observation. CERES SSF1deg provides CERES-observed temporally interpolated top-of-atmosphere (TOA) radiative fluxes and coincident MODIS-derived cloud and aerosol properties at daily and monthly 1°-regional, zonal and global time-space scales. The cloud parameters used in this study include cloud area fraction (day-night), liquid water path, water particle radius, ice particle effective radius, cloud visible optical depth (day-night). The TOA radiation fluxes include shortwave flux (clear-sky and all-sky) and longwave flux (clear-sky and all-sky). Following Harrison et al. (1990), the shortwave (longwave) cloud forcing SWCF (LWCF) at the TOA was calculated as the difference between the clear-sky reflected shortwave (outgoing longwave) radiation and the all-sky reflected shortwave (outgoing longwave) radiation at the TOA for both models and observations.

4 Results and discussion

4.1 Model performance evaluation for $PM_{2.5}$, O_3 and $PM_{2.5}$ chemical composition

To evaluate model performance, regression statistics along with three measures of bias (the mean bias (MB), normalized MB (NMB) and normalized MB factor (NMBF)), and three measures of error (the root mean square error (RMSE), normalized mean error (NME) and normalized mean error factor (NMEF)), and correlation coefficient (*r*) (Yu et al., 2006; Gustafson and Yu, 2012) were calculated. Following the protocol of the IMPROVE network, the daily (24 h) $PM_{2.5}$ concentrations at the AQS sites were calculated from midnight to midnight local time of the next day on the basis of hourly $PM_{2.5}$ observations. The results are summarized in Tables 4–6 for August 2006 and in Tables 7 and 8 for September 2006.

4.1.1 $PM_{2.5}$ and O_3 at the AQS sites

Table 4 and Fig. 4a clearly indicate that over the CONUS, both models (WRF-CMAQ/CAM and WRF-CMAQ/RRTMG) reproduced the majority of the observed daily maximum 8 h O_3 with values > 40 ppbv within a factor of 1.5 for August of 2006. The NMB and NME are −0.1 % (15.0 %) and −0.4 % (14.8 %) for WRF–CMAQ/CAM (WRF–CMAQ/RRTMG), respectively, when only data of maximum 8 h O_3 with concentrations > 40 ppbv are considered. These values are much lower than the corresponding results when all data are considered, indicating the overestimation in the low O_3 concentration range contributes significantly to the overall overestimation for both models, especially when only data over the eastern Texas domain are used, as shown in Table 4. The overestimation in the low O_3 concentration range could be indicative of titration by NO in urban plumes that the model does not resolve because many AQS sites are located in urban areas as pointed out by Yu et al. (2007). One of the reasons for more O_3 over-estimation for the 4 km resolution simulations relative to the 12 km resolution simulation

Discussion Paper | Discussion Paper | Discussion Paper | Discussion Paper |
ACPD
13, 25649–25739, 2013
Aerosol indirect effect in the two-way coupled WRF-CMAQ
S. Yu et al.

over the eastern Texas is because of boundary conditions used in the 4 km simulations although the model performance for O_3 is still reasonably well because the NMB values are less than 37 % as listed in Table 4. The model performance for both models for O_3 concentrations is similar.

The model performance for $PM_{2.5}$ at the AQS sites for August of 2006 is summarized in Tables 5 and 6, and Fig. 5. Following Eder and Yu (2006), the results over the COUNS were separated into the eastern (EUS, longitude > −100° W) and western US (WUS, longitude < −100° W). Figure 5 indicates that both models captured the majority of observed daily $PM_{2.5}$ values within a factor of 2, but generally underestimated the observations at the high $PM_{2.5}$ concentration range. The domain wide mean values of MB and RMSE for all daily $PM_{2.5}$ at the AQS sites for August of 2006 over the EUS are 0.81 (−0.02) and 10.70 (10.20) $\mu g\,m^{-3}$ for WRF-CMAQ/CAM (WRF-CMAQ/RRTMG), respectively, and those for NMB and NME are 5.3 (−0.1) % and 49.9 (48.6) % for WRF-CMAQ/CAM (WRF-CMAQ/RRTMG), respectively. The results over the WUS are similar to those over the EUS. Generally, WRF-CMAQ/CAM simulated higher $PM_{2.5}$ levels than WRF-CMAQ/RRTMG.

The model performance for $PM_{2.5}$ at the AQS sites during September of 2006 is summarized in Tables 7 and 8. There are greater overestimations of $PM_{2.5}$ in September relative to those in August. Over the EUS, WRF-CMAQ/CAM and WRF-CMAQ/RRTMG overestimated the observed $PM_{2.5}$ at the AQS sites by a factor of 1.30 and 1.27), respectively, as indicated by normalized mean bias factor (NMBF) (Yu et al., 2006). According to the results at these STN urban sites which also have consistent overestimation of $PM_{2.5}$, the overestimations of $PM_{2.5}$ at these urban locations by both models primarily result from the overestimations of SO_4^{2-}, NH_4^+, NO_3^-, and TC over the EUS. Over the WUS, WRF-CMAQ/CAM and WRF-CMAQ/RRTMG overestimated the observed $PM_{2.5}$ at the AQS sites by a factor of 1.65 and 1.55, respectively, mainly due to the overestimations of TC according to the results at the STN urban sites in Table 7b.

The results over the eastern Texas domain for both 4 km and 12 km resolution simulations are summarized in Tables 6 and 8. For August of 2006, both WRF-CMAQ/CAM

ACPD
13, 25649–25739, 2013

and WRF-CMAQ/RRTMG overestimated the observed $PM_{2.5}$ at the AQS sites mainly because of the overestimation of TC according to the results at the STN urban sites as shown in Table 6. Table 6 also shows that the less overestimations of $PM_{2.5}$ for the 12 km resolution simulations relative to the 4 km resolution simulations are due to the fact that the results of the 12 km resolution simulations have more underestimations of SO_4^{2-}, NH_4^+, and NO_3^- for both models. This is because of the underestimation of cloud fields in the 12 km resolution simulations as indicated in Sect. 4.2 below. Similar performance trends in the two models are also noted for September of 2006, as shown in Table 8. However, the model performance for SO_4^{2-} is very good with the NMB < ±6 %.

4.1.2 $PM_{2.5}$ and its chemical composition at the CASTNet, IMPROVE, STN sites

Over the EUS for the 12 km resolution simulations of August 2006, the examination of the domain-wide bias and errors (Table 5a and Figs. 6 and 7) for different networks reveals that the WRF-CMAQ/CAM (WRF-CMAQ/RRTMG) consistently underestimated the observed SO_4^{2-} by −23.0 % (−27.7 %), −12.5 % (−18.9 %) and −7.9 % (−14.8 %) at the CASTNet, IMPROVE and STN sites, respectively. Both models underestimated the observed NH_4^+ at the CASTNet sites (by −23.0 % for WRF-CMAQ/CAM and −27.7 % for WRF-CMAQ/RRTMG) and had a good performance at the STN sites with the NMB < ±7 %. Both models overestimated the observed SO_2 by more than 98 % at the CASTNet sites. The comparison of the modeled and observed total sulfur (SO_4^{2-} + SO_2) at the CASTNet sites in Fig. 8 and Table 5a reveals that both models overestimated the observed total sulfur systematically and the modeled mean total sulfur values are higher than the observations by 25.3 % and 21.8 % for WRF-CMAQ/CAM and WRF-CMAQ/RRTMG, respectively. This indicates too much SO_2 emission in the emission inventory and that not enough gaseous SO_2 concentrations were oxidized to produce aerosol SO_4^{2-} in the models. Although the NMB values for aerosol NO_3^- are less than 60 % as shown in Table 5a, the poor model performance for NO_3^- (see scatter plot in Fig. 6a and correlation < 0.40 in Table 5a) is related in part to volatility issues of measurements associated with NO_3^-, and their exacerbation because of uncertainties associated with SO_4^{2-} and total NH_4^+ simulations in the model (Yu et al., 2005). Table 5a indicates that both models overestimated the observed mean OC, EC and TC concentrations at the IMPROVE sites by 25.9 %, 54.9 % and 31.9 % for WRF-CMAQ/CAM, respectively, and by 23.8 %, 52.2 % and 29.7 % for WRF-CMAQ/RRTMG, respectively. As pointed by Yu et al. (2012a), since the IMPROVE and the model emission inventory use the thermo-optical reflectance (TOR) method to define the split between OC and EC while the STN network used the thermo-optical transmittance (TOT) method, only the determination of total carbon (TC = OC + EC) is comparable between these two analysis protocols. Therefore, Table 5a only lists the performance results for TC comparisons from the STN sites. The very small NMB values (< ±3 %) but large NME values (> 48 %) for both models indicated that there is a large compensation error between the overestimation and underestimation of the observed TC concentrations at the STN sites in the model simulations. The model performances for $PM_{2.5}$ at the IMPROVE and STN sites are reasonably good with the NMB values of −13.2 % and −0.7 % for WRF-CMAQ/CAM, respectively, and −16.8 % and −6.2 % for WRF-CMAQ/RRTMG, respectively. One of the reasons for the consistent underestimations of $PM_{2.5}$ is because of the consistent underestimation of SO_4^{2-} due to the fact that the model generally underestimated the cloud field as analyzed below, which caused underestimation of aqueous SO_4^{2-} production.

Over the WUS for the 12 km resolution simulations of August 2006, Table 5b shows that WRF-CMAQ/CAM (WRF-CMAQ/RRTMG) still consistently underestimated the observed SO_4^{2-} by −23.9 % (−24.5 %), and −4.2 % (−9.5 %) at the CASTNet, and STN sites, respectively, while both models had slight overestimations of the observed SO_4^{2-} at the IMPROVE sites with the NMB < 15 %. Both models underestimated the observed NH_4^+ at both CASTNet and STN sites by more than 34 %. Both models also overestimated the observed SO_2 by more than 47 % at the CASTNet sites. The comparison of the modeled and observed total sulfur (SO_4^{2-} + SO_2) at the CASTNet sites in Fig. 8 and Table 5b reveals that both models had good performance for the observed total

ACPD
13, 25649–25739, 2013

sulfur with NMB < 6 %. This indicates reasonable total SO_2 emission in the emission inventory and that gaseous SO_2 concentrations were not oxidized enough to produce aerosol SO_4^{2-} in the models over the WUS. Like the EUS, both models have poor performance for aerosol NO_3^- but had serious underestimations at all networks by more than a factor of 2, especially at both CASTNet and STN sites, as shown in Fig. 6b and Table 5b. This indicates too low NOx emissions in the emission inventory over the WUS. Table 5b indicates that both models overestimated the observed mean OC, EC and TC concentrations at the IMPROVE sites by more than 38.6 % while both models had slight underestimations of TC at the STN sites by less than 13 %. The model performances for $PM_{2.5}$ at the IMPROVE and STN sites are reasonably good with the NMB values < 15 %.

The results for September are different from those of August in the following aspects over the EUS and WUS. Over the EUS, both models had slight overestimations of SO_4^{2-} at both IMPROVE and STN sites with the NMB < 20 % but slight underestimations at CASTNet sites with NMB < −11 % as shown in Table 7a. This is consistent with the fact that both models generally overestimated the cloud field for September as analyzed below. Both models consistently overestimated NH_4^+ in September by more than 20 %, especially at CASTNet sites. Both models also had consistent overestimations of the observed SO_2 and total sulfur at the CASTNet sites like August, and consistent overestimations of mean OC, EC and TC concentrations at the IMPROVE sites by more than 32 %. The model performance for $PM_{2.5}$ at the IMPROVE and STN sites is reasonably good with general consistent overestimations instead of underestimations. Table 7a shows that both models generally overestimated all $PM_{2.5}$ species (SO_4^{2-}, NO_3^-, NH_4^+, OC, EC, TC) at IMROVE and STN sites.

Over the WUS for September, both models had similar performance for SO_4^{2-}, NH_4^+, SO_2, and total sulfur to those of August for different networks. Like August, both models had consistent overestimations of OC, EC and TC concentrations at the IMPROVE sites but also had overestimation of TC at the STN sites as shown in Table 7b in September. Both models had more overestimations of $PM_{2.5}$ at the IMPROVE and

STN sites in September than August over the WUS due to the fact that both models overestimated TC more in September than August.

4.2 Model performance evaluation for cloud properties (SWCF, LWCF, COD, and cloud fraction) with CERES satellite observations

To gain insights into the model performance for the parameterizations of cloud-mediated radiative-forcing due to aerosols (i.e., indirect aerosol forcing) in the two-way coupled WRF-CMAQ modeling system, the CERES satellite observations of cloud properties (SWCF, LWCF, COD, and cloud fraction) were used. To compare the model results with the CERES observations, the $1.0^{\circ} \times 1.0^{\circ}$ CERES data are interpolated to the model domains for the 12 km resolution over the CONUS and the 4 km resolution over eastern Texas. The results for SWCF, LWCF, |SWCF|/LWCF, COD and cloud fractions over land and ocean areas of the EUS and WUS are shown in Figs. 9–12, 13–16, 17–18, 19–21 and 22–23, respectively. Tables 9 to 12 statistically summarize the model performance for each case in August and September. For reference, the results for the WRF only with the RRTMG and CAM radiation schemes are also shown in Figures and Tables. As shown in Figs. 9, 11–13 and 15–21, the model performances are very different over land and ocean areas for the 12 km resolution simulations over the CONUS domain. Therefore, the results over land and ocean areas are presented separately for these simulations in the following analysis.

4.2.1 SWCF and LWCF comparisons

Cloud radiative forcing depends on both cloud radiative properties and cloud microphysical properties. The SWCF is mostly dominated by low and middle clouds except in regions of deep convection, where very bright stratiform anvils may contribute significantly; whereas the LWCF is mostly dominated by high clouds (Lauer et al., 2009). The ratio of |SWCF| and LWCF ($N = |SWCF|/LWCF$) can be used to indicate averaged cloud height, e.g., smaller N with higher clouds (Su et al., 2010). As summarized by Taylor (2012), |SWCF| ≫ LWCF for low clouds, stratocumulus and cumulus and LWCF ≫ |SWCF| for high clouds, cirrus and cirrostratus (Hartmann and Doelling, 1991; Stephens, 2005), whereas there is a cancelation between SWCF and LWCF (|SWCF| ≈ LWCF) for deep convective clouds (Kiehl and Ramanathan, 1990; Kiehl, 1994b).

Over the land areas of the EUS in August of 2006 as shown in Tables 9 and 10, the domain means of the CERES observations, WRF-CMAQ/CAM, WRF-CMAQ/RRTMG, WRF/CAM, and WRF/RRTMG for SWCF (LWCF) are −60.90 (30.26), −53.75 (21.83), −47.23 (20.95), −51.13 (37.28), and −39.36 (26.98) watts m^{-2}, respectively. Over the land areas of the WUS in August of 2006, the domain means of the CERES observations, WRF-CMAQ/CAM, WRF-CMAQ/RRTMG, WRF/CAM, and WRF/RRTMG for SWCF (LWCF) are −37.18 (30.33), −27.58 (19.97), −24.76 (19.58), −39.54 (46.10), and −27.71 (29.23) watts m^{-2}, respectively. According to the CERES observations, the SWCF values over the land of the EUS are much more negative than those of the WUS, whereas their LWCF values are very close. The NMB values for SWCF (LWCF) over the land of the EUS in August of 2006 are −11.74 % (−27.86 %) and −22.45 % (−30.76 %) for WRF-CMAQ/CAM, WRF-CMAQ/RRTMG, respectively, whereas over the land of WUS, they are −25.82 % (−34.15 %) and −33.40 % (−35.45 %), respectively. The consistent underestimations of SWCF and LWCF by both WRF-CMAQ/CAM, WRF-CMAQ/RRTMG indicate that the WRF-CMAQ model generally underestimated the cloud field, although the WRF-CMAQ/CAM produced more cloud than the WRF-CMAQ/RRTMG over the CONUS (both EUS and WUS) in August of 2006. The model performance for the land of the EUS is slightly better than the WUS. The results over eastern Texas from the 12 km resolution simulations are similar to those over the CONUS as shown in Table 9. One of the reasons for the underestimation of cloud in both WRF-CMAQ/CAM, WRF-CMAQ/RRTMG is that the subgrid convective clouds do not include these aerosol indirect effects which may pose an issue for these 12 km simulations. This is in agreement with the fact that both WRF-CMAQ/CAM, WRF-CMAQ/RRTMG captured SWCF and LWCF very well for the 4 km simulation over east-

ACPD
13, 25649–25739, 2013

ern Texas with the NMB values < ±10 % as shown in Figs. 11 and 15 and Tables 9 and 10. This is because the 4 km simulations were able to resolve subgrid convective clouds and include the aerosol effects.

Over the ocean areas of the EUS in August 2006, the NMB values for SWCF (LWCF) are −7.75 % (−19.99 %) and −23.69 % (−27.70 %) for WRF-CMAQ/CAM, WRF-CMAQ/RRTMG, respectively, whereas over the ocean areas of WUS, they are 9.20 % (−27.90 %) and −14.64 % (−34.79 %), respectively. WRF-CMAQ/CAM performed better for both SWCF and LWCF than WRF-CMAQ/RRTMG. CAM and RRTMG radiation schemes used different parameterizations to calculate the optical properties of cloud, in part, leading to the different results for WRF-CMAQ/CAM and WRF-CMAQ/RRTMG. Figures 11 and 15, and Tables 9 and 10 indicate that the WRF only cases (both WRF/CAM and WRF/RRTMG) did not perform as well as WRF-CMAQ, especially over the ocean areas, due to the fact that in the default WRF, cloud effective radii over the land and ocean are assumed to be 8.0 and 14.0 µm, respectively, and ice effective radius is assumed to be 14.0 µm in the formulation for calculation of effective radius originally developed by J. T. Kiehl (1994a). The results in Figs. 11 and 15 strongly indicate that the assumption of 14.0 µm of cloud effective radius over the ocean is not reasonable because the WRF-only cases completely misplaced cloud locations with negative correlations as shown in Tables 9 and 10. The results of WRF-CMAQ/CAM, WRF-CMAQ/RRTMG have significant improvements for both SWCF and LWCF predictions over both ocean and land relative to those of the WRF only cases. Grabowski (2006) also found that the formulations for the calculations of cloud effective radius have significant impact on the estimation of indirect aerosol effects.

Over the land areas of both EUS and WUS for September 2006, both WRF-CMAQ/CAM and WRF-CMAQ/RRTMG captured SWCF slightly better than those of August of 2006 with the NMB values < −5 % as shown in Table 9, and Figs. 11 and 12. Both WRF-CMAQ/CAM and WRF-CMAQ/RRTMG also underestimated both SWCF and LWCF values over the land areas as in August 2006, possibly because the AIE on subgrid convective clouds is not included for the model simulations at the 12 km resolu-

ACPD
13, 25649–25739, 2013

tion. The SWCF values for September are about 10 % lower than August over the land areas as shown in Table 9. Over the ocean areas for September of 2006, both WRF-CMAQ/CAM and WRF-CMAQ/RRTMG captured both SWCF and LWCF very well with the slightly overestimations (NMB values < 16 %). For the 4 km simulation over eastern Texas in September, both WRF-CMAQ/CAM, WRF-CMAQ/RRTMG captured SWCF and LWCF very well with the NMB values < ±12 % for SWCF and NMB values < ±21 % for LWCF as shown in Figs. 12 and 16 and Tables 9 and 10. Similar to August 2006, the results of WRF-CMAQ/CAM, WRF-CMAQ/RRTMG have significant improvements for both SWCF and LWCF with much better correlations relative to those of WRF default cases at 12 km resolutions, especially over the ocean. For the 4 km simulations over eastern Texas, both WRF-CMAQ/CAM and WRF-CMAQ/RRTMG have significantly better performance for SWCF than the corresponding WRF/CAM and WRF/RRTMG in both August and September in terms of the NMB values as listed in Table 9, whereas for LWCF in Table 10, both WRF-CMAQ/CAM and WRF-CMAQ/RRTMG have better performance in August and close performance in September relative to the corresponding WRF/CAM and WRF/RRTMG. This indicates that it is necessary to include the aerosol fields from the air quality model (CMAQ here) in the meteorological models (WRF here) to simulate cloud fields.

The ratios of |SWCF| and LWCF (N values) in Fig. 17 shows that over both land and ocean areas of the EUS in August 2006, both WRF-CMAQ/CAM and WRF-CMAQ/RRTMG performed very well when the N values $\lesssim$2.5 but significantly overestimated observed N values when N $\gtrsim$2.5, indicating that both models overestimated low clouds, stratocumulus and cumulus. On the other hand, over both land and ocean areas of the WUS in August 2006, both WRF-CMAQ/CAM and WRF-CMAQ/RRTMG performed very well when $\sim 0.2 < N \lesssim 2.5$ and significantly overestimated the observed N values when $N \gtrsim 2.5$ or $N \lesssim 0.2$ as shown in Fig. 17, suggesting that both models underestimated high clouds, cirrus and cirrostratus but overestimated low clouds, stratocumulus and cumulus over the land and ocean areas of the WUS. Figure 17 also shows that there are not many high clouds, cirrus and cirrostratus over both land and

ACPD
13, 25649–25739, 2013

ocean areas of the EUS in August 2006 according to both observations and model results in September. The results also indicate that the WRF default cases underestimate the observed N values when $N \gtrsim 2.0$ for the whole domain, indicating that both WRF/CAM and WRF/RRTMG underestimated low clouds, stratocumulus and cumulus everywhere. Both WRF-CMAQ/CAM and WRF-CMAQ/RRTMG performed very well when $\sim 0.2 < N \lesssim 2.5$ over the model domain, much better than the corresponding WRF/CAM and WRF/RRTMG, indicating the importance for including the aerosol effect in the meteorological models.

The results of the N values for September 2006 in Fig. 18 are similar to those for August except that WRF default cases (WRF/CAM and WRF/RRTMG) also overestimated low clouds, stratocumulus and cumulus over the model domain and the land areas of the WUS and that there were not many high clouds, cirrus and cirrostratus according to both observations and model results.

4.2.2 COD comparisons

The COD values are determined by the cloud liquid water path (LWP) and cloud effective radius, and LWP is strongly dependent on external dynamical forcing parameters, such as large-scale divergence rate (Ghan et al., 2001a; Lu and Seinfeld, 2005; Seinfeld and Pandis, 1998). Comparisons of mean COD from models with observations for August are shown in Fig. 19 and their scatter plots are shown in Figs. 20 and 21. Table 11 statistically summarizes the results of model performances. Over the land areas of both EUS and WUS in August and September, both WRF-CMAQ/CAM and WRF-CMAQ/RRTMG consistently underestimated observed COD with more underestimation over the WUS as shown in Table 11 and Figs. 20 and 21, being consistent with generally underestimations of SWCF as indicated in Sect. 4.2.1. Over the ocean areas of both EUS and WUS in August and September, WRF-CMAQ/CAM captured the observed COD very well with the NMB values $< \pm 10\,\%$, whereas WRF-CMAQ/RRTMG underestimates the observed COD by more than 28 %. The results of COD for the 4 km simulation over the eastern Texas are better than those of the 12 km simulations over

ACPD
13, 25649–25739, 2013

Aerosol indirect effect in the two-way coupled WRF-CMAQ

S. Yu et al.

the land of the EUS in August for both WRF-CMAQ/CAM and WRF-CMAQ/RRTMG as shown in Table 11. However, in September, the results of COD for the 4 km simulations over the eastern Texas are not better relative to those of the 12 km simulations. One of the reasons for this is that in September, all model results (WRF-CMAQ/CAM, WRF-CMAQ/RRTMG, WRF/CAM and WRF/RRTMG) underestimated COD significantly in the 4 km simulations but not for the 12 km simulations as shown in Table 11 and Fig. 21. Relative to the WRF default cases (WRF/CAM and WRF/RRTMG), the results of WRF-CMAQ/CAM and WRF-CMAQ/RRTMG have significant improvements for COD performance as shown in Table 1 and Figs. 20 and 21.

4.2.3 Cloud fraction comparisons

In the satellite observation, cloud fraction or cloud cover is defined as the number of cloudy pixels divided by the total number of pixels. In the WRF model, cloud fraction is calculated on the basis of the relative humidity and liquid water substance with the parameterization of Randall (1995) following Hong et al. (1998). The model performances for the cloud fractions are shown in the scatter plots of Figs. 22 and 23 and summarized in Table 12. WRF-CMAQ/CAM captured cloud fractions very well over the whole model domain (land and ocean) in both August and September with the NMB values $< \pm 10$ % and correlations > 0.9 and WRF-CMAQ/RRTMG also did very well with the slightly higher NMB values and lower correlations as shown in Table 12 and Figs. 22 and 23. All models (WRF-CMAQ/CAM, WRF-CMAQ/RRTMG, WRF/CAM and WRF/RRTMG) captured the observed cloud fractions well for the 4 km simulation over the eastern Texas in both August and September with the NMB values $< \pm 12$ % and correlations > 0.74 as shown in Table 12. On the other hand, the WRF default cases (WRF/CAM and WRF/RRTMG) significantly misplaced the locations of clouds over the land and ocean in both August and September even with negative correlations, especially for August and over the ocean areas as shown in Figs. 22 and 23. This is consistent with the results of SWCF in Sect. 4.2.1.

ACPD
13, 25649–25739, 2013

Title Page
Abstract | Introduction
Conclusions | References
Tables | Figures
◀ | ▶
◀ | ▶
Back | Close
Full Screen / Esc
Printer-friendly Version
Interactive Discussion

4.3 Precipitation evaluation

The monthly gridded cumulative precipitation data at the 4 km resolution over the CONUS from the Parameter–Elevation Regressions on Independent Slopes Model (PRISM; Daly et al., 1994; Daly, 2002) were regridded to the 12 km CONUS domain to evaluate the model performance for precipitation. The spatial difference of monthly mean precipitations between observations and models are shown in Figs. 24 (August) and 25 (September). The scatter plots are shown in Figs. 26 and statistical results are summarized in Table 13. Figure 24 and Table 12 indicates that both WRF-CMAQ/CAM and WRF-CMAQ/RRTMG generally overestimated the observed precipitation by more than 40 % mainly because of significant overestimation in the southern part of the CONUS in August. Both WRF-CMAQ/CAM and WRF-CMAQ/RRTMG significantly improved the underestimation of precipitation over the central part of the CONUS and overestimation over the New Mexico regions in August relative to their corresponding WRF default cases (WRF/CAM and WRF/RRTMG) as shown in Fig. 24. In September, all models (WRF-CMAQ/CAM, WRF-CMAQ/RRTMG, WRF/CAM, and WRF/RRTMG) reproduce the observed precipitation reasonably well with the NMB values < 40 %, although all models consistently underestimated the observations as shown in Table 13 and Fig. 25. Both WRF-CMAQ/CAM and WRF-CMAQ/RRTMG improved the underestimation of precipitation over the EUS in September with smaller NMB values relative to their corresponding WRF default cases (WRF/CAM and WRF/RRTMG) as shown in Fig. 25. It is generally accepted in the meteorological community that small scale summertime convection is more difficult to replicate with convective parameterizations because of the stochastic nature of these cells, which are often triggered by mesoscale surface forcing or outflow boundaries from other convective cells (Grell and Devenyi, 2002). September has less convection effects relative to August. For the 4 km simulations over the eastern Texas, both WRF-CMAQ/CAM and WRF-CMAQ/RRTMG improved the underestimation of precipitation in August with smaller NMB values relative to their corresponding WRF default cases (WRF/CAM and WRF/RRTMG) as shown in

ACPD
13, 25649–25739, 2013

Table 13, whereas in September, all models captured the observed precipitation well with the NMB value < ±20 %.

5 Conclusions

In this study, the AIE on the microphysical and radiative properties of clouds (including first, second and glaciation indirect aerosol forcing) have been implemented in the two-way coupled WRF-CMAQ modeling system by including parameterizations for both cloud drop and ice number concentrations on the basis of the CMAQ-predicted aerosol distributions, chemical and microphysical properties, and the WRF meteorological conditions, with a new subroutine, "CMAQ_mixactivate". The cloud drop number concentrations were estimated from the activation of CMAQ-predicted aerosol particles using an aerosol activation scheme for multiple externally mixed lognormal modes, each mode composed of a uniform internal mixtures of soluble and insoluble material developed by Abdul-Razzak and Ghan (2002, 2000), while the cloud ice number concentrations were estimated from the activation of the CMAQ-predicted sulfate, black carbon, dust and organic aerosols with an ice nucleation scheme adopted from the NCAR CAM. The resulting cloud drop and ice number concentrations are supplied to the Morrison et al., 2-moment cloud microphysics scheme by tying a two-moment treatment of cloud water (mass and number) and cloud ice (mass and number) to precipitation in the Morrison et al., 2-moment cloud microphysics scheme and two separate radiation schemes (RRTMG and CAM) in the WRF model. This allows us to estimate aerosol effects on cloud and ice optical depth and microphysical process rates for first, second and glaciation AIE. The cloud drop effective radius and cloud ice effective radius from the output of the Morrison cloud microphysics scheme are used in the RRTMG and CAM radiation schemes directly and these affect the computed radiation fields accordingly. The model performance was carried out by comparison of the model simulations with the observations from satellite and surface networks over the CONUS (12 km resolution) and eastern Texas (4 km resolution) domains in August and September of 2006.

ACPD
13, 25649–25739, 2013

The results at the AQS surface sites show that in August over the EUS the NMB and NME values for $PM_{2.5}$ are 5.3 (−0.1) % and 49.9 (48.6) % for WRF-CMAQ/CAM (WRF-CMAQ/RRTMG), respectively. The results over the WUS are similar to those over the EUS. Over the EUS in August, WRF-CMAQ/CAM (WRF-CMAQ/RRTMG) consistently underestimated the observed SO_4^{2-} by −23.0 % (−27.7 %), −12.5 % (−18.9 %) and −7.9 % (−14.8 %) at the CASTNet, IMPROVE and STN sites, respectively, and both models overestimated the observed SO_2 by more than 98 % at the CASTNet sites. Both models overestimated the observed total sulfur ($SO_4^{2-} + SO_2$) at the CASTNet sites systematically, and the modeled mean total sulfur values were higher than the observations by 25.3 % and 21.8 % for WRF-CMAQ/CAM and WRF-CMAQ/RRTMG, respectively. The observed mean OC, EC and TC concentrations over the EUS in August at the IMPROVE sites were overestimated by 25.9 %, 54.9 % and 31.9 % for the WRF-CMAQ/CAM, respectively, and by 23.8 %, 52.2 % and 29.7 % for the WRF-CMAQ/RRTMG, respectively. The model performances for $PM_{2.5}$ at the IMPROVE and STN sites over the EUS in August are reasonably good with the NMB values of −13.2 % and −0.7 % for WRF-CMAQ/CAM, respectively, and −16.8 % and −6.2 % for WRF-CMAQ/RRTMG, respectively. The results over the WUS in August are similar to those over the EUS except that both models had slight overestimations of the observed SO_4^{2-} at the IMPROVE sites with the NMB < 15 % and slight underestimations of TC at the STN urban sites by less than 13 %.

According to the CERES observations in August, the SWCF values over the land of the EUS are much higher than those of the WUS, whereas their LWCF values are very close. The NMB values for SWCF (LWCF) over the land of the EUS in August are −11.74 % (−27.86 %) and −22.45 % (−30.76 %) for WRF-CMAQ/CAM, WRF-CMAQ/RRTMG, respectively, whereas over the land of WUS, they are −25.82 % (−34.15 %) and −33.40 % (−35.45 %), respectively. One of the reasons for the underestimation of cloud in both WRF-CMAQ/CAM and WRF-CMAQ/RRTMG is that the subgrid convective clouds do not include aerosol effects in the model simulations at the 12 km resolution. This is in agreement with the fact that both models captured SWCF

ACPD
13, 25649–25739, 2013

and LWCF very well for the 4 km simulation over the eastern Texas with the NMB values $< \pm 10\,\%$. The results of the ratios of |SWCF| and LWCF indicate that in August, both models overestimated low clouds, stratocumulus and cumulus over the land and ocean areas of the EUS and that both models underestimated high clouds, cirrus and cirrostratus but overestimated low clouds, stratocumulus and cumulus over the land and ocean areas of the WUS. Over the land areas of the CONUS in August, both models consistently underestimated observed COD with more underestimation over the WUS, being generally consistent with underestimations of SWCF. Over the ocean areas in August, WRF-CMAQ/CAM captured the observed COD very well with the NMB values $< \pm 10\,\%$, whereas WRF-CMAQ/RRTMG underestimated the observed COD by more than 28 %. Both models captured cloud fractions very well over the whole model domain (land and ocean) in August. Both WRF-CMAQ/CAM and WRF-CMAQ/RRTMG generally overestimated the observed precipitation by more than 40 % mainly because of significant overestimation in the southern part of the CONUS in August. The results of WRF-CMAQ/CAM and WRF-CMAQ/RRTMG have significant improvements for SWCF, LWCF, COD, cloud fractions and precipitation over the ocean relative to those of WRF default cases in August.

The results of model performance in September are similar to those in August except that there is greater overestimation of $PM_{2.5}$ due to the overestimations of SO_4^{2-}, NH_4^+, NO_3^-, and TC over the EUS and overestimations of TC over the WUS on the basis of the results at the STN urban sites, there is less underestimation of clouds (SWCF) over the land areas due to about 10 % due to the lower SWCF values and less convective clouds relative to that in August, and all model results (WRF-CMAQ/CAM, WRF-CMAQ/RRTMG, WRF/CAM and WRF/RRTMG) underestimated COD significantly in the 4 km simulations but not for the 12 km simulations.

Since convective clouds play an important role in determining our climate state, especially for the summer season, it is imperative to include convection-aerosol interactions. Realistically, it is a big challenge to quantify the response of convective clouds to aerosols because of the complexity and nonlinearity of interactions involving photo-

ACPD
13, 25649–25739, 2013
Aerosol indirect effect in the two-way coupled WRF-CMAQ
S. Yu et al.

chemistry, aerosols, liquid and ice-phase clouds and precipitation microphysics, radiation, dynamics and surface-atmosphere exchange over a wide range of spatiotemporal scales (Seifert etal., 2012; Tao et al., 2012). The developmental work for linking the CMAQ predicted aerosol fields to the two-moment microphysics scheme in the modified Kain–Fritsch convective scheme is under way and will be accomplished in the future.

Acknowledgements. The authors would like to thank Kathleen Fahey for the constructive and very helpful comments. The United States Environmental Protection Agency through its Office of Research and Development funded and managed the research described here. It has been subjected to Agency's administrative review and approved for publication. C. Zhao and X. Liu are partially supported by the Office of Science of the US Department of Energy as part of the Regional and Global Climate Modeling Program. The CERES data were obtained from the NASA Langley Research Center EOSDIS Distributed Active Archive Center. The PRISM monthly precipitation data were downloaded from http://www.prism.oregonstate.edu/.

References

Abdul-Razzak, H. and Ghan, S. J.: A parameterization of aerosol activation. Part 2: Multiple aerosol types, J. Geophys. Res., 105, 6837–6844, 2000.

Abdul-Razzak, H. and Ghan, S. J.: A parameterization of aerosol activation. 3. Sectional representation, J. Geophys. Res., 107, 4026, doi:10.1029/2001JD000483, 2002.

Abdul-Razzak, H., Ghan, S. J., and Rivera-Carpio, C.: A parameterization of aerosol activation. Part I: Single aerosol type, J. Geophys. Res., 103, 6123–6132, 1998.

Appel, K. W., Pouliot, G. A., Simon, H., Sarwar, G., Pye, H. O. T., Napelenok, S. L., Akhtar, F., and Roselle, S. J.: Evaluation of dust and trace metal estimates from the Community Multiscale Air Quality (CMAQ) model version 5.0, Geosci. Model Dev., 6, 883–899, doi:10.5194/gmd-6-883-2013, 2013.

Albrecht, B. A.: Aerosols, cloud microphysics, and fractional cloudiness, Science, 245, 1227–1230, 1989.

Barnes, W. L., Pagano, T. S., and Salomonson, V. V.: Prelaunch characteristics of the Moderate Resolution Imaging Spectroradiometer (MODIS) on EOS-AM1, IEEE Trans. Geosci. Remote Sens., 36, 1088–1100, 1998.

Bey, I., Jacob, D. J., Yantosca, R. M., Logan, J. A., Field, B. D., Fiore, A. M., Li, Q., Liu, H. Y., Mickley, L. J., and Schultz, M. G.: Global modeling of tropospheric chemistry with assimilated meteorology: model description and evaluation, J. Geophys. Res., 106, 23073–23096, 2001.

Bhave, P. V., Roselle, S. J., Binkowski, F. S., Nolte, C. G., Yu, S. C., Gipson, G. L., and Schere, K. L.: CMAQ Aerosol Module Development: Recent Enhancements and Future Plans, Paper presented at 3rd Annual CMAS Models-3 Users' Conference, Commun. Model., and Anal. Syst. Cent., Chapel Hill, N.C., 18–20 October, 2004.

Binkowski, F. S. and Roselle, S. J.: Models-3 Community Multiscale Air Quality (CMAQ) model aerosol component: 1. Model description, J. Geophys. Res., 108, 4183, doi:10.1029/2001JD001409, 2003.

Carlton, A. G., Bhave, P. V., Napelenok, S. L., Edney, E. O., Sarwar, G., Pinder, R. W., Pouliot, G. A., and Houyoux, M.: Model representation of secondary organic aerosol in CMAQv4.7., Environ. Sci. Technol., 44, 8553–8560, 2010.

Cerveny, R. S. and Bailing Jr., R. C.: Weekly cycles of air pollutants, precipitation and tropical cyclones in the coastal NW Atlantic region, Nature, 394, 561–563, 1998.

Chapman, E. G., Gustafson Jr., W. I., Easter, R. C., Barnard, J. C., Ghan, S. J., Pekour, M. S., and Fast, J. D.: Coupling aerosol-cloud-radiative processes in the WRF-Chem model: Investigating the radiative impact of elevated point sources, Atmos. Chem. Phys., 9, 945–964, doi:10.5194/acp-9-945-2009, 2009.

Charlson, R. J., Schwartz, S. E., Hales, J. M., Cess, R. D., Coakley Jr., J. A., Hansen, J. E., and Hofmann, D. J.: Climate forcing by anthropogenic aerosols, Science, 255, 5043, 423–430, doi:10.1126/science.255.5043.423, 1992.

Collins, W. D., Rasch, P. J., Boville, B. A., Hack, J. J., MaCaa, J. R., Williamson, D. L., Kiehl, J. T., Briegleb, B. P., Bitz, C., Lin, S. J., Zhang, M., and Dai, Y.: Description of the NCAR Community Atmosphere Model (CAM3.0), NCAR Technical Note, NCAR/TN-464+STR, 226 pp., 2004.

Daly, C.: Variable Influence of Terrain on Precipitation Patterns: Delineation and Use of Effective Terrain Height in PRISM, available at: http://prism.nacse.org/pub/prism/docs/effectiveterrain-daly.pdf (last access: 30 September 2013), 2002.

Daly, C., Neilson, R. P., and Phillips, D. L.: A statistical-topographic model for mapping climatological precipitation over mountainous terrain, J. Appl. Meteor., 33, 140–158. 1994.
DeFelice, T. P., Saxena, V. K., and Yu, S. C.: On the measurements of cloud condensation nuclei (CCN) at Palmer Station, Antarctica, Atmos. Environ., 31, 4039–4044, 1997.
Eagen, R. C., Hobbs, P. V., and Radke, L. F.: Particle emissions from a large Kraft paper mill and their effects on the microstructure of warm clouds, J. App. Meteor., 13, 535–552, 1974
Eder, B. and Yu, S. C.: An evaluation of model performance of EPA models-3/CMAQ, Atmos. Environ., 40, 4811–4824, 2006.
Eder, B., Kang, D., Mathur, R., Pleim, J., Yu, S. C., Otte, T., and Pouliot. G.:. A performance evaluation of the national air quality forecast capability for the summer of 2007, Atmos. Environ., 43, 2312–2320, 2009.
Eder, B., Kang, D., Rao, S. T., Mathur, R., Yu, S. C., Otte, T., Schere, K., Wayland, R., Jackson, S., Davidson, P., and McQueen, J.: A demonstration of the use of national air quality forecast guidance for developing local air quality index forecasts, B. Am. Meteorol. Soc., 91, 313–326, doi:10.1175/2009BAMS2734.1, 2010.
Fu, Q.: An accurate parameterization of the solar radiative properties of cirrus clouds for climate models, J. Climate, 9, 2058–2082, 1996.
Foley, K. M., Roselle, S. J., Appel, K. W., Bhave, P. V., Pleim, J. E., Otte, T. L., Mathur, R., Sarwar, G., Young, J. O., Gilliam, R. C., Nolte, C. G., Kelly, J. T., Gilliland, A. B., and Bash, J. O.: Incremental testing of the Community Multiscale Air Quality (CMAQ) modeling system version 4.7, Geosci. Model Dev., 3, 205–226, doi:10.5194/gmd-3-205-2010, 2010.
Ghan, S. J. and Easter, R. C.: Impact of cloud-borne aerosol representation on aerosol direct and indirect effects, Atmos. Chem. Phys., 6, 4163–4174, doi:10.5194/acp-6-4163-2006, 2006.
Ghan, S. J., Leung, L. R., Easter, R. C., and Abdul-Razzak, H.: Prediction of droplet number in a general circulation model, J. Geophys. Res., 102, 21777–21794, 1997.
Ghan, S. J., Easter, R. C., Chapman, E. G., Abdul-Razzak, H., Zhang, Y., Leung, L. R., Laulainen, N. S., Saylor, R. D., and Zaveri, R. A.: A physically based estimate of radiative forcing by anthropogenic sulfate aerosol, J. Geophys. Res.-Atmos., 106, 5279–5293, 2001a.
Ghan, S., Laulainen, N., Easter, R., Wagener, R., Nemesure, S., Chapman, E., Zhang, Y., and Leung, R.: Evaluation of aerosol direct radiative forcing in MIRAGE, J. Geophys. Res.-Atmos., 106, 5295–5316, 2001b.

ACPD
13, 25649–25739, 2013

Aerosol indirect effect in the two-way coupled WRF-CMAQ

S. Yu et al.

Ghan, S. J., Easter, R. C., Hudson, J., and Breon, F.-M.: Evaluation of aerosol indirect radiative forcing in MIRAGE, J. Geophys. Res.-Atmos., 106, 5317–5334, 2001c.
Grabowski, W. W.: Indirect impact of atmospheric aerosols in idealized simulations of convective-radiative quasi equilibrium, J. Climate, 19, 4664–4682, 2006.
Granier, C. and Brasseur, G.: Ozone and other trace gases in the Arctic and Antarctic regions: three-dimensional model simulations, J. Geophys. Res., 96, 2995–3011, doi:10.1029/90JD01779, 1991.
Grell, G. and Devenyi, D.: A generalized approach to parameterizing convection combining ensemble and data assimilation techniques, Geophys. Res. Lett., 29, 1693, doi:10.1029/2002GL015311, 2002.
Grell, G. A., Emeis, S., Stockwell, W. R., Schoenemeyer, T., Forkel, R., Michalakes, J., Knoche, R., and Seidl, W.: Application of a multiscale, coupled MM5/chemistry model to the complex terrain of the VOTALP valley campaign, Atmos. Environ., 34, 1435–1453, 2000.
Grell, G. A., Peckham, S. E., Schmitz, R., McKenn, S. A., Frost, G., Skamarock, W. C., and Eder, B.: Fully coupled "online" chemistry within the WRF model, Atmos. Environ., 39, 6957–6975, 2005.
Gustafson Jr., W. I. and Yu, S. C.: Generalized approach for using unbiased symmetric metrics with negative values: normalized mean bias factor and normalized mean absolute error factor, Atmos. Sci. Lett., 13,262–267, doi:10.1002/asl.393, 2012.
Gustafson Jr., W. I., Chapman, E. G., Ghan, S. J., Easter, R. C., and Fast, J. D.: Impact on modeled cloud characteristics due to simplified treatment of uniform cloud condensation nuclei during NEAQS 2004, Geophys. Res. Lett., 34, L19809, doi:10.1029/2007GL030021, 2007.
Han, Q., Rossow, W. B., and Lacis A. A.:, Near-global survey of effective droplet radii in liquid water clouds using ISCCP data, J. Climate, 7, 465–497, doi:10.1175/1520-0442, 1994.
Hansen, J., Sato, M., and Ruedy, R.: Radiative forcing and climate response, J. Geophys. Res., 102, 6831–6864, 1997.
Hanel, G.: The properties of atmospheric aerosol particles as functions of the Relative humidityat thermodynamic equilibrium with the surrounding moist air, Adv. Geophys., 19, 73–188, 1976.
Harrison, E. F., Minnis, P., Barkstrom, B. R., Ramanathan, V., Cess, R. D., and Gibson, G. G.: Seasonal variation of cloud radiative forcing derived from the Earth Radiation Budget Experiment, J. Geophys. Res., 95, 18687–18703, doi:10.1029/JD095iD11p18687, 1990.

ACPD
13, 25649–25739, 2013

Hartmann, D. L. and Doelling, D.: On the net radiative effectiveness of clouds, J. Geophys. Res., 96, 869–891, 1991.
Haywood, J. and Boucher, O.: Estimates of the direct and indirect radiative forcing due to tropospheric aerosols: a review, Rev. Geophys., 38, 513–543, 2000.
Hong, S.-Y., Juang, H.-M., and Zhao, Q.: Implementation of prognostic cloud scheme for a regional spectral model, Mon. Weather Rev., 126, 2621–2639, 1998.
Iacono, M. J., Delamere, J. S., Mlawer, E. J., Shephard, M. W., Clough, S. A., and Collins, W. D.: Radiative forcing by long-lived greenhouse gases: calculations with the AER radiative transfer models, J. Geophys. Res., 113, D13103, doi:10.1029/2008JD009944, 2008.
Intergovernmental Panel on Climate Change (IPCC): Climate Change 2007: The Physical Science Basis, Contribution of Working Group I to the Fourth Assessment Report of the Intergovernmental Panel on Climate Change, Cambridge Univ. Press, New York, 2007.
Jacobson, M. Z.: Developing, coupling, and applying a gas, aerosol, transport, and radiation model to study urban and regional air pollution, Ph.D. Thesis, Department of Atmospheric Sciences, University of California, Los Angeles, 436 pp., 1994.
Jacobson, M. Z.: GATOR-GCMM: a global-through urban-scale air pollution and weather forecast model 1. Model design and treatment of subgrid soil, vegetation, roads, rooftops, water, sea, ice, and snow, J. Geophys. Res., 106, 5385–5401, 2001a.
Jacobson, M. Z.: GATOR-GCMM: 2. A study of day- and nighttime ozone layers aloft, ozone in national parks, and weather during the SARMAP Field Campaign, J. Geophys. Res., 106, 5403–5420, 2001b.
Jacobson, M. Z.: Effects of absorption by soot inclusions within clouds and precipitation on global climate, J. Phys. Chem., 110, 6860–6873, 2006.
Jauregui, E. and Romales, E.: Urban effects on convective precipitation in Mexico City, Atmos. Environ., 30, 3383–3389, 1996.
Jimenez, J. L., Canagaratna, M. R., and Donahue, N. M., et al.: Evolution of Organic Aerosols in the Atmosphere, Science, 326, 1525–1529, doi:10.1126/science.1180353, 2009.
Kain, J. S.: The Kain–Fritsch convective parameterization: an update, J. Appl. Meteor., 43, 170–181, 2004.
Kain, J. S. and Fritsch, J. M.: A one-dimensional entraining/detraining plume model and its application in convective parameterization, J. Atmos. Sci., 47, 2784–2802, 1990.

ACPD
13, 25649–25739, 2013

Kain, J. S. and Fritsch, J. M.: Convective parameterization for mesoscale models: the Kain–Fritcsh scheme, in: The Representation of Cumulus Convection in Numerical Models, in: Emanuel, K. A. and Raymond, D. J., Amer. Meteor. Soc., 246 pp., 1993.
Khvorostyanov, V. I. and Curry, J. A.: A simple analytical model of aerosol properties with account for hygroscopic growth, Part 1, Equilibrium size spectra and CCN activity spectra, J. Geophys. Res., 104, 2163–2174, 1999.
Kiehl, J. T.: On the observed near cancellation between longwave and shortwave cloud forcing in tropical regions, J. Climate, 7, 559–656, 1994a.
Kiehl, J. T.: Sensitivity of a GCM climate simulation to differences in continental versus maritime cloud drop size, J. Geophys. Res., 99, 23107–23115, 1994b.
Kiehl, J. T. and Ramanathan, V.: Comparison of cloud forcing derived from the earth radiation budget experiment with that simulated by the NCAR community climate model, J. Geophys. Res., 95, 11679–11698, 1990.
King, S. M., Rosenoern, T., Shilling, J. E., Chen, Q., Wang, Z., Biskos, G., McKinney, K. A., Pöschl, U., and Martin, S. T.: Cloud droplet activation of mixed organic-sulfate particles produced by the photooxidation of isoprene, Atmos. Chem. Phys., 10, 3953–3964, doi:10.5194/acp-10-3953-2010, 2010.
Koehler, K. A., Kreidenweis, S. M., DeMott, P. J., Petters, M. D., Prenni, A. J., and Carrico, C. M.: Hygroscopicity and cloud droplet activation of mineral dust aerosol, Geophys. Res. Lett., 36, L08805, doi:10.1029/2009GL037348, 2009.
Kummerow, C., Barnes, W., Kozu, T., Shine, J., and Simpson, J.: The Tropical Rainfall Measuring Mission System (TRMM) sensor package, J. Atmos. Oceanic Technol., 15, 809–827, 1998.
Lauer, A., Wang, Y., Phillips, V. T. J., McNaughton, C. S., Bennartz, R., and Clarke, A. D.: Simulation marine boundary layer clouds over the eastern Pacific in a regional climate model with double-moment cloud microphysics, J. Geophys. Res., 114, D21205, doi:10.1029/2009JD012201, 2009.
Leaitch, W. R., Strapp, J. W., Wiebe, H. A., Anlauf, K. G., and Isaac, G. A.: Chemical and microphysical studies of nonprecipitating summer cloud in Ontario, Canada, J. Geophys. Res., 91, 11821–11831, 1986.
Li, Z., Niu, F., Fan, J., Liu, Y., Rosenfeld, D., and Ding Y.: The long-term impacts of aerosols on the vertical development of clouds and precipitation, Nat. Geosci., 4, 888–894, doi:10.1038/ngeo1313, 2011.

ACPD
13, 25649–25739, 2013

Lin, J. C., Matsui, T., Pielke Sr., R. A., and Kummerow, C.: Effects of biomass-burning-derived aerosols on precipitation and clouds in the Amazon Basin: a satellite-based empirical study, J. Geophys. Res., 111, D19204, doi:10.1029/2005JD006884, 2006
Liu, P., Zhang, Y., Yu, S. C., and Schere, K. L.: Use of a process analysis tool for diagnostic study on fine particulate matter predictions in the U.S. Part II: Process analysis and sensitivity simulations, Atmos. Pollut. Res., 2, 61–71, 2011.
Liu, X. and Penner, J. E.: Ice nucleation parameterization for global models, Meteor. Z., 14, 499–514, 2005.
Liu, X. and Wang, J.: How important is organic aerosol hygroscopicity to aerosol indirect forcing?, Environ. Res. Lett., 5, 044010, doi:10.1088/1748-9326/5/4/044010, 2010.
Liu, X., Penner, J. E., Ghan, S. J., and Wang, M.: Inclusion of ice microphysics in the NCAR community atmospheric model version 3 (CAM3), J. Climate, 20, 4526–4547, 2007.
Liu, Y., Daum, P. H., and McGraw, R. L.: Size truncation effect, threshold behavior, and a new type of autoconversion parameterization, Geophys. Res. Lett., 32, L11811, doi:10.1029/2005GL022636, 2005.
Lohmann, U.: A glaciation indirect aerosol effect caused by soot aerosols, Geophys. Res. Lett., 29, 1052, doi:10.1029/2001GL014 357, 2002.
Lohmann, U. and Feichter, J.: Global indirect aerosol effects: a review, Atmos. Chem. Phys., 5, 715–737, doi:10.5194/acp-5-715-2005, 2005.
Lu, M.-L. and Seinfeld, J. H.: Study of the aerosol indirect effect by large-eddy simulation of marine stratocumulus, J. Atmos. Sci., 62, 3909–3932, 2005.
Martin, G. M., Johnson, D. W., and Spice, A.: The measurement and parameterization of effective radius of droplets in warm stratiform clouds, J. Atmos. Sci., 51, 1823–1842, 1994.
Mathur, R., Yu, S. C., Kang, D., and Schere, K. L.: Assessment of the winter-time performance of developmental particulate matter forecasts with the Eta-CMAQ modeling system, J. Geophys. Res., 113, D02303, doi:10.1029/2007JD008580, 2008.
Mathur, R., Pleim, J., Wong, D., Otte, T., Gilliam, R., Roselle, S., Young, J., Binkowski, F., and Xiu, A.: The WRF-CMAQ integrated on-line modeling system: development, testing and initial application, in: Air Pollution Modeling and Its Application XX, edited by: Steyn, D. G. and Rao, S. T., doi:10.1007/978-90-481-3812-8, Springer, the Netherlands, 155–159, 2010.
McKeen, S., Chung, S. H., Wilczak, J., Grell, G., Djalalova, I., Peckham, S., Gong, W., Bouchet, V., Moffet, R., Tang, Y., Carmichael, G. R., Mathur, R., and Yu, S. C.: The eval-

uation of several $PM_{2.5}$ forecast models using data collected during the ICARTT/NEAQS 2004 field study, J. Geophys. Res., 112, D10S20, doi:10.1029/2006JD007608, 2007.
Menon, S., Hansen, J. E., Nazarenko, L., and Luo, Y.: Climate effects of black carbon aerosols in China and India, Science, 297, 2250–2253, 2002.
Menon, S., Del Genio, A. D., Kaufman, Y. J., Koch, D., Bennartz, R., Loeb, N., and Orlikowski, D.: Analyzing signatures of aerosol-cloud interactions with satellite retrievals and the GISS GCM to constrain the aerosol indirect effect, J. Geophys. Res., 113, D14S22, doi:10.1029/2007JD009442, 2008.
Meyers, M. P., DeMott, P. J., and Cotton, W. R.: New primary ice nucleation parameterization in an explicit model, J. Appl. Meteor., 31, 708–721, 1992.
Morrison, H. and Grabwski, W. W.: Comparison of bulk and bin warm-rain microphysics models using a kinematic framework, J. Atmos. Sci., 64, 2839–2861, 2007.
Morrison, H. and Pinto, J. O.: Intercomparison of bulk microphysics schemes in mesoscale simulations of springtime Arctic mixed-phase stratiform clouds, Mon. Weather Rev., 134, 1880–1900, 2006.
Morrison, H., Curry, J. A., and Khvorostyanov, V. I.: A new double-moment microphysics parameterization for application in cloud and climate models, Part I: Description, J. Atmos. Sci., 62, 1665–1677, 2005.
Morrison, H., Thompson, G., and Tatarskii, V.: Impact of cloud microphysics on the development of trailing stratiform precipitation in a simulated squall line: comparison of one- and two-moment schemes, Mon. Weather Rev., 137, 991–1007, 2009.
Petters, M. D. and Kreidenweis, S. M.: A single parameter representation of hygroscopic growth and cloud condensation nucleus activity, Atmos. Chem. Phys., 7, 1961–1971, doi:10.5194/acp-7-1961-2007, 2007.
Phillips, V. T. J., DeMott, P. J., and Andronache, C.: An empirical parameterization of heterogeneous ice nucleation for multiple chemical species of aerosol, J. Atmos. Sci., 65, 2757–2783, doi:10.1175/2007JAS2546.1, 2008.
Pleim, J. E.: A combined local and non-local closure model for the atmospheric boundary layer. Part 1: Model description and testing, J. Appl. Meteorol. Clim., 46, 1383–1395, 2007a.
Pleim, J. E.: A combined local and nonlocal closure model for the atmospheric boundary layer. Part II: Application and evaluation in a mesoscale meteorological model, J. Appl. Meteorol. Clim., 46, 1396–1409, 2007b.

ACPD
13, 25649–25739, 2013

Pleim, J. E. and Xiu, A.: Development and testing of a surface flux and planetary boundary layer model for application in mesoscale models, J. Appl. Meteor., 34, 16–32, 1995.
Pleim, J. E. and Xiu, A.: Development of a land surface model. Part II: Data assimilation, J. Appl. Meteor., 42, 1811–1822, 2003.
Pleim, J. E., Young, J. O., Wong, D., Gilliam, R. C., Otte, T. L., and Mathur, R.: Two-way coupled meteorology and air quality modeling, in: Air Pollution Modeling and Its Application XIX, edited by: Borrego, C. and Miranda, A. I., ISBN 978-1-4020-8452-2, Springer, the Netherlands, 496–504, 2008.
Prenni, A. J., Petters, M. D., Kreidenweis, S. M., DeMott, P. J., and Ziemann, P. J.: Cloud droplet activation of secondary organic aerosol, J. Geophys. Res., 112, D10223, doi:10.1029/2006JD007963, 2007.
Pruppacher, H. R. and Klett, J. D.: Microphysics of Clouds and Precipitation, 2nd edn., Kluwer Academic Publishers, Dordrecht, the Netherlands, 954 pp., 1997.
Ramanathan, V., Crutzen, P. J., Kiehl, J. T., and Rosenfeld, D.: Aerosols, climate and the hydrological cycle, Science, 294, 2119–2124, 2001.
Randall, D. A.: Parameterizing fractional cloudiness produced by cumulus entrainment, in: Preprints, Workshop on Cloud Microphysics Parameterizations in Global Atmospheric Circulation Models, WMO, Kananaskis, AB, Canada, 1–16, 1995.
Rasch, P. J., Barth, M. C., Kiehl, J. T., Schwartz, S. E., and Benkovitz, C. M.: A description of the global sulfur cycle and its controlling processes in the National Center for Atmospheric Research Community Climate Model Version 3, J. Geophys. Res., 105, 1367–1385, 2000.
Rotstayn, L.: Indirect forcing by anthropogenic aerosols: a global climate model calculation of the effective-radius and cloud-lifetime effects, J. Geophys. Res., 104, 9369–9380, 1999.
Rosenfeld, D.: TRMM observed first direct evidence of smoke from forest fires inhibiting rainfall, Geophys. Res. Lett., 26, 3105–3108, 1999.
Rosenfeld, D.: Suppression of rain and snow by urban and industrial air pollution, Science, 287, 1793–1796, doi:10.1126/science.287.5459.1793, 2000.
Rosenfeld, D. and Lensky, I. M.: Spaceborne sensed insights into precipitation formation processes in continental and maritime clouds, B. Am. Meteorol. Soc., 79, 2457–2476, 1998.
Rosenfeld, D., Dai, J., Yu, X., Yao, Z., Xu, X., Yang, X., and Du, C.: Inverse relations between amounts of air pollution and orographic precipitation, Science, 315, 1396–1398, doi:10.1126/science.1137949, 2007.

ACPD
13, 25649–25739, 2013

Rosenfeld, D., Lohmann, U., Raga, G. B., O'Dowd, C. D., Kulmala, M., Fuzzi, S., Reissell, A., and Andreae, M. O.: Flood or drought: how do aerosols affect precipitation?, Science, 321, 1309–1313, 2008.

Saxena, V. K. and Yu, S. C.: Searching for a regional fingerprint of aerosol forcing in the south-eastern US, Geophys. Res. Lett., 25, 2833–2836, 1998.

Saxena, V. K., Yu, S. C., and Anderson, J.: Impact of stratospheric volcanic aerosols on climate: evidence of aerosol radiative forcing in the southeastern US, Atmos. Environ., 31, 4211–4221, 1997.

Seifert, A., Köhler, C., and Beheng, K. D.: Aerosol-cloud-precipitation effects over Germany as simulated by a convective-scale numerical weather prediction model, Atmos. Chem. Phys., 12, 709–725, doi:10.5194/acp-12-709-2012, 2012.

Seinfeld, J. and Pandis, S.: Atmospheric Chemistry and Physics, John Wiley & Sons, New York, NY, USA, 408–448, 1998.

Simon, H., Bhave, P. V., Swall, J. L., Frank, N. H., and Malm, W. C.: Determining the spatial and seasonal variability in OM/OC ratios across the US using multiple regression, Atmos. Chem. Phys., 11, 2933–2949, doi:10.5194/acp-11-2933-2011, 2011.

Skamarock, W. C., Klemp, J. B., Dudhia, J., Gill, D. O., Barker, D. M., Duda, M. G., Huang, X.-Y., Wang, W., and Powers, J. G.: A description of the advanced research WRF version 3, Technical Note TN-475+STR, NCAR, 2008.

Slingo, A.: Sensitivity of the earth's radiation budget to changes in low clouds, Nature, 343, 49–51, 1990.

Stephen, G. L.: Cloud feedbacks in the climate system: a critical review, J. Climate, 18, 237–273, 2005.

Su, W., Bodas-Salcedo, A., Xu, K.-M., and Charlock, T. P.: Comparison of the tropical radiative flux and cloud radiative effect profiles in a climate model with Clouds and the Earth's Radiant Energy System (CERES) data, J. Geophys. Res., 115, D01105, doi:10.1029/2009JD012490, 2010.

Tao, W.-K., Chen, J.-P., Li, Z., Wang, C., and Zhang, C.: Impact of aerosols on convective clouds and precipitation, Rev. Geophys., 50, 1–62, 2012.

Taylor, K. E. and Penner, J. E.: Response of the climate system to atmospheric aerosols and greenhouse gases, Nature, 369, 734–737, doi:10.1038/369734a0, 1994.

Taylor, P. C.: The role of clouds: an introduction and rapporteur, Surv. Geophys., 33, 609–617, 2012.

Twomey, S.: Pollution and the planetary albedo, Atmos. Environ., 8, 1251–1256, 1974.
Twomey, S.: Aerosols, clouds and radiation, Atmos. Environ., 25, 2435–2442, 1991.
Wong, D. C., Pleim, J., Mathur, R., Binkowski, F., Otte, T., Gilliam, R., Pouliot, G., Xiu, A., Young, J. O., and Kang, D.: WRF-CMAQ two-way coupled system with aerosol feedback: software development and preliminary results, Geosci. Model Dev., 5, 299–312, doi:10.5194/gmd-5-299-2012, 2012.
Wielicki, B. A., Barkstrom, B. R., Harrison, E. F., Lee III, R. B., Smith, G. L., and Cooper, J. E.: Clouds and the Earth's Radiant Energy System (CERES): an earth observing system experiment, B. Am. Meteorol. Soc., 77, 853–868, 1996.
Xiu, A. and Pleim, J. E.: Development of a land surface model. Part I: Application in a mesoscale meteorological model, J. Appl. Meteorol., 40, 192–209, 2001.
Yarwood, G., Rao, S., Yocke, M., and Whitten, G. Z.: Final Report – Updates to the Carbon Bond Chemical Mechanism: CB05, Rep. RT-04-00675, 246 pp., Yocke and Co., Novato, Calif., available at: http://www.camx.com/publ/pdfs/CB05_Final_Report_120805.pdf (last access: 30 September 2013), 2005.
Young, K. C.: Numerical-simulation of wintertime, orographic precipitation – 1. Description of model microphysics and numerical techniques, J. Atmos. Sci., 31, 1735–1748, 1974.
Yu, F., Luo, G., Liu, X., Easter, R. C., Ma, X., and Ghan, S. J.: Indirect radiative forcing by ion-mediated nucleation of aerosol, Atmos. Chem. Phys., 12, 11451–11463, doi:10.5194/acp-12-11451-2012, 2012a.
Yu, F., Luo, G., and Ma, X.: Regional and global modeling of aerosol optical properties with a size, composition, and mixing state resolved particle microphysics model, Atmos. Chem. Phys., 12, 5719–5736, doi:10.5194/acp-12-5719-2012, 2012b.
Yu, H., Kaufman, Y. J., Chin, M., Feingold, G., Remer, L. A., Anderson, T. L., Balkanski, Y., Bellouin, N., Boucher, O., Christopher, S., DeCola, P., Kahn, R., Koch, D., Loeb, N., Reddy, M. S., Schulz, M., Takemura, T., and Zhou, M.: A review of measurement-based assessments of the aerosol direct radiative effect and forcing, Atmos. Chem. Phys., 6, 613–666, doi:10.5194/acp-6-613-2006, 2006.
Yu, S. C.: The role of organic acids (formic, acetic, pyruvic and oxalic) in the formation of cloud condensation nuclei (CCN): a review, Atmos. Res., 53, 185–217, 2000.
Yu, S. C. and Zhang, Y.: An examination of the effects of aerosol chemical composition and size on radiative properties of multi-component aerosols, Atmos. Clim. Sci., 1, 19–32, doi:10.4236/acs.2011.12003, 2011.

Yu, S. C., Saxena, V. K., Wenny, B. N., DeLuisi, J. J., Yue, G. K., and Petropavlovskikh, I. V.: A study of the aerosol radiative properties needed to compute direct aerosol forcing in the southeastern US, J. Geophys. Res., 105, 24739–24749, 2000.
Yu, S. C., Saxena, V. K., and Zhao, Z.: A comparison of signals of regional aerosol-induced forcing in eastern China and the southeastern United States, Geophys. Res. Lett., 28, 713–716, 2001a.
Yu, S. C., Zender, C. S., and Saxena, V. K.: Direct radiative forcing and atmospheric absorption by boundary layer aerosols in the southeastern US: model estimates on the basis of new observations, Atmos. Environ., 35, 3967–3977, 2001b.
Yu, S. C., Kasibhatla, P. S., Wright, D. L., Schwartz, S. E., McGraw, R., and Deng, A.: Moment-based simulation of microphysical properties of sulfate aerosols in the eastern United States: model description, evaluation and regional analysis, J. Geophys. Res., 108, 4353, doi:10.1029/2002JD002890, 2003.
Yu, S. C., Dennis, R., Bhave, P., and Eder, B.: Primary and secondary organic aerosols over the United States: estimates on the basis of observed organic carbon (OC) and elemental carbon (EC), and air quality modeled primary OC/EC ratios, Atmos. Environ., 38, 5257–5268, 2004.
Yu, S. C., Dennis, R., Roselle, S., Nenes, A., Walker, J., Eder, B., Schere, K., Swall, J., and Robarge, W.: An assessment of the ability of 3-D air quality models with current thermodynamic equilibrium models to predict aerosol NO_3^-, J. Geophys. Res., 110, D07S13, doi:10.1029/2004JD004718, 2005.
Yu, S. C., Eder, B., Dennis, R., Chu, S.-H., and Schwartz, S.: New unbiased symmetric metrics for evaluation of air quality models, Atmos. Sci. Lett., 7, 26–34, 2006.
Yu, S. C., Bhave, P. V., Dennis, R. L., and Mathur, R.: Seasonal and regional variations of primary and secondary organic aerosols over the continental United States: semi-empirical estimates and model evaluation, Environ. Sci. Technol., 41, 4690–4697, 2007a.
Yu, S. C., Mathur, R., Schere, K., Kang, D., Pleim, J., and Otte, T. L.: A detailed evaluation of the Eta-CMAQ forecast model performance for O_3, its related precursors, and meteorological parameters during the 2004 ICARTT study, J. Geophys. Res., 112, D12S14, doi:10.1029/2006JD007715, 2007b.
Yu, S. C., Mathur, R., Schere, K., Kang, D., Pleim, J., Young, J., Tong, D., McKeen, S., and Rao, S. T.: Evaluation of real-time $PM_{2.5}$ forecasts and process analysis for $PM_{2.5}$ formation

ACPD
13, 25649–25739, 2013

Aerosol indirect effect in the two-way coupled WRF-CMAQ

S. Yu et al.

over the eastern U.S. using the Eta-CMAQ forecast model during the 2004 ICARTT study, J. Geophys. Res., 113, D06204, doi:10.1029/2007JD009226, 2008.

Yu, S., Mathur, R., Pleim, J., Pouliot, G., Wong, D., Eder, B., Schere, K., Gilliam, R., and Rao, S. T.: Comparative evaluation of the impact of WRF/NMM and WRF/ARW meteorology on CMAQ simulations for $PM_{2.5}$ and its related precursors during the 2006 TexAQS/GoMACCS study, Atmos. Chem. Phys., 12, 4091–4106, doi:10.5194/acp-12-4091-2012, 2012a.

Yu, S. C., Mathur, R., Pleim, J., Pouliot, G., Eder, B., Schere, K., Wong, D., Gilliam, R., and Rao, S. T.: Comparative evaluation of the impact of WRF-NMM and WRF-ARW meteorology on CMAQ simulations for O_3 and related species during the 2006 TexAQS/GoMACCS campaign, Atmos. Pollut. Res., 3, 149–162, doi:10.5094/AP R.2012.015, 2012b.

Zhang, Y.: Online-coupled meteorology and chemistry models: history, current status, and outlook, Atmos. Chem. Phys., 8, 2895–2932, doi:10.5194/acp-8-2895-2008, 2008.

Zhang, Y., Easter, R. C., Ghan, S. J., and Abdul-Razzak, H.: Impact of aerosol size representation on modeling aerosol-cloud interactions, J. Geophys. Res., 107, 4558, doi:10.1029/2001JD001549, 2002.

Zhang, Y., Wen, X.-Y., and Jang, C. J.: Simulating climate-chemistry-aerosol-cloud-radiation feedbacks in continental U.S. using online-coupled WRF/Chem, Atmos. Environ., 44, 3568–3582, 2010a.

Zhang, Y., Liu, P., Liu, X.-H., Jacobson, M. Z., McMurry, P. H., Yu, F., Yu, S. C., and Schere, K. L.: A comparative study of homogeneous nucleation parameterizations, part II. 3-D model simulations and evaluation, J. Geophys. Res., 115, D20213, doi:10.1029/2010JD014151, 2010b.

Zhang, Y., Chen, Y.-C., Sarwar, G., and Schere, K.: Impact of gas-phase mechanisms on WRF/Chem predictions: mechanism implementation and comparative evaluation, J. Geophys. Res., 117, D01301, doi:10.1029/2011JD015775, 2012.

ACPD

13, 25649–25739, 2013

Table 1. Model configurations and components.

Simulation period	1 Aug–15 Oct 2006
Domain	Continental US (CONUS), Eastern Texas
Horizontal grid spacing	12 km (Continental US), 4 km (Eastern Texas)
Number of verticals levels	34 layers
Shortwave radiation scheme	CAM scheme (Collins et al., 2004), rrtmg scheme (Iacono et al., 2008)
Longwave radiation scheme	CAM scheme (Collins et al., 2004), rrtmg scheme (Iacono et al., 2008)
Land–Surface Model	Pleim-Xiu LSM (Pleim and Xiu, 1995; Xiu and Pleim, 2001)
Planetary Boundary Layer	Asymmetrical Convective Model version 2 (ACM2) PBL (Pleim, 2007)
Cloud Microphysics	Morrison et al., 2-monent scheme (Morrison et al., 2009, 2005; Morrison and Pinto, 2006)
Cumulus Parameterization	Kain–Fritsch scheme (Kain and Fritsch, 1990, 1993) for CONUS (12 km), no for 4 km resolution run
Meteorological initial conditions	NAM-218
Meteorological boundary conditions	NAM-218
Gas-phase chemistry	CB05 (Yarwood et al., 2005)
Aerosol module	AERO-6
Chemical BC	GEOS-CHEM simulations (Bey et al., 2001), BCs at 4 km resolution are from the 12 km resolution simulations over the CONUS
Emission inventory	2005 NEI

ACPD
13, 25649–25739, 2013

Table 2. Aerosol species for each mode in AERO6 of CMAQ[a] (see the explanations in the text).

Nucleation (I)	Accumulation (J)	Coarse (K)
ASO4I, ANH4I, ANO3I, APOCI, APNCOMI, AECI, AOTHRI, AH2OI, ANAI, ACLI	ASO4J, ANH4J, ANO3J, AALKJ, AXYL1J, AXYL2J, AXYL3J, ATOL1J, ATOL2J, ATOL3J, ABNZ1J, ABNZ2J, ABNZ3J, ATRP1J, ATRP2J, AISO1J, AISO2J, ASQTJ, AORGCJ, APOCJ, APNCOMJ, AECJ, AOTHRJ, AH2OJ, ANAJ, ACLJ, AISO3J, AOLGAJ, AOLGBJ, AFEJ, AALJ, ASIJ, ATIJ, ACAJ, AMGJ, AKJ, AMNJ	ASO4K, ANH4K, ANO3K, AH2OK, ACLK, ACORS, ASOIL, ASEACAT

[a] Notes: Primary organic aerosol APOAI = APOCI + APNCOMI.
Primary organic aerosol APOAJ = APOCJ + APNCOMJ.
ANAK = 0.8373 · ASEACAT + 0.0626 · ASOIL + 0.0023ACORS.
ASOILJ = 2.2 · AALJ + 2.49 · ASIJ + 1.63 · ACAJ + 2.42 · AFEJ + 1.94 · ATIJ.

Discussion Paper | Discussion Paper | Discussion Paper | Discussion Paper |
ACPD
13, 25649–25739, 2013

Aerosol indirect effect in the two-way coupled WRF-CMAQ

S. Yu et al.

Table 3. Molecular weight ($g\,mol^{-1}$), density ($g\,cm^{-3}$) and hygroscopicity of each aerosol species used in this study (see the explanations in the text).

	Molecular weight	Density	Hygroscopicity
ASO4	96.0	1.8	0.50
ANO3	62.0	1.8	0.50
ANH4	18.0	1.8	0.50
AALK	150.0	2.0	0.14
AXYL	192.0	2.0	0.14
ATOL	168.0	2.0	0.14
ABNZ	144.0	2.0	0.14
ATRP	168.0	2.0	0.14
AISO	96.0	2.0	0.14
ASQT	378.0	2.0	0.14
AISO3	162.0	2.0	0.14
AOLGA	176.4	2.0	0.20
AOLGB	252.0	2.0	0.20
AORGC	177.0	2.0	0.50
APOA	220.0	2.0	0.14
AEC	12.0	2.2	1.0×10^{-6}
AOTHR	200.0	2.2	0.10
ANA	23.0	2.2	1.16
ACL	35.0	2.2	1.16
ACORS	100.0	2.2	0.03
ASOIL	100.0	2.6	0.03

ACPD
13, 25649–25739, 2013

Table 4. Comparison of WRF-CMAQ/CAM and WRF-CMAQ/RRTMG models for operational evaluation of maximum 1 h and 8 h O_3 concentrations on the basis of the AQS data over the continental United States (12 km resolution model grid) and eastern Texas (4 km resolution model grid) for August of 2006. "Domain mean" means the results on the basis of all data at observational sites within the domain. * The results in parentheses are from the simulations of 12 km resolution model grid over eastern Texas domain.

Max O_3	Model	Data points	Domain Mean, ppbv Obs	Domain Mean, ppbv Model	MB, ppbv	RMSE, ppbv	NMB (%)	NME (%)	NMBF (%)	NMEF (%)	r
Over the continental US (12 km resolution model grid)											
All data											
8 h	WRF-CMAQ (CAM)	33 278	50.2	52.9	2.7	12.4	5.3	18.7	5.3	18.7	0.641
8 h	WRF-CMAQ (RRTMG)	33 278	50.2	52.9	2.6	12.3	5.2	18.7	5.2	18.7	0.637
1 h	WRF-CMAQ (CAM)	33 278	56.9	59.4	2.5	14.2	4.5	18.6	4.5	18.6	0.625
1 h	WRF-CMAQ (RRTMG)	33 278	56.9	59.1	2.2	14.1	3.8	18.5	3.8	18.5	0.623
For O_3 > 40 ppbv											
8 h	WRF-CMAQ (CAM)	24 628	56.7	56.7	−0.1	11.5	−0.1	15.0	−0.1	15.0	0.511
8 h	WRF-CMAQ (RRTMG)	24 628	56.7	56.5	−0.3	11.3	−0.4	14.8	−0.4	14.8	0.511
1 h	WRF-CMAQ (CAM)	27 527	62.0	62.4	0.5	13.7	0.7	16.1	0.7	16.1	0.518
1 h	WRF-CMAQ (RRTMG)	27 527	62.0	62.0	0.0	13.5	0.0	15.9	0.0	15.9	0.516
Over the eastern Texas (4 km resolution model grid)*											
All data											
8 h	WRF-CMAQ (CAM)	1854.0	43.1	59.3 (50.2)	16.2 (7.1)	22.0 (14.7)	37.5 (16.4)	42.8 (28.3)	37.5 (16.4)	42.8 (28.3)	0.562 (0.664)
8 h	WRF-CMAQ (RRTMG)	1854.0	43.1	59.5 (50.2)	16.3 (7.1)	21.3 (14.5)	37.8 (16.4)	42.0 (27.8)	37.8 (16.4)	42.0 (27.8)	0.607 (0.656)
1 h	WRF-CMAQ (CAM)	1854.0	51.2	68.1 (57.6)	16.9 (6.5)	25.1 (17.1)	33.1 (12.6)	40.2 (26.6)	33.1 (12.6)	40.2 (26.6)	0.538 (0.644)
1 h	WRF-CMAQ (RRTMG)	1854.0	51.2	67.3 (56.8)	16.2 (5.7)	23.3 (16.8)	31.6 (11.1)	37.7 (26.1)	31.6 (11.1)	37.7 (26.1)	0.606 (0.645)
For O_3 > 40 ppbv											
8 h	WRF-CMAQ (CAM)	996.0	55.7	66.1 (56.4)	10.4 (0.7)	17.7 (12.5)	18.7 (1.2)	25.7 (17.1)	18.7 (1.2)	25.7 (17.1)	0.296 (0.389)
8 h	WRF-CMAQ (RRTMG)	996.0	55.7	66.2 (56.6)	10.5 (0.9)	16.6 (12.7)	18.8 (1.5)	24.6 (17.0)	18.8 (1.5)	24.6 (17.0)	0.357 (0.360)
1 h	WRF-CMAQ (CAM)	1206.0	62.5	74.0 (63.1)	11.5 (0.7)	21.3 (15.6)	18.4 (1.1)	27.1 (18.3)	18.4 (1.1)	27.1 (18.3)	0.362 (0.422)
1 h	WRF-CMAQ (RRTMG)	1206.0	62.5	73.2 (62.3)	10.7 (−0.2)	19.3 (15.9)	17.1 (−0.3)	24.7 (18.4)	17.1 (−0.3)	24.7 (18.4)	0.446 (0.392)

ACPD
13, 25649–25739, 2013

Table 5a. Comparison of observation and models (WRF-CMAQ/CAM and WRF-CMAQ/RRTMG) for $PM_{2.5}$ and its components for each network over the eastern US (longitude $> -100°$) for August of 2006*.

	AIRNow	CASTNet					IMPROVE						STN				
	$PM_{2.5}$	SO_4^{2+}	NH_4^+	NO_3^-	SO_2	TotS	$PM_{2.5}$	SO_4^{2-}	NO_3^-	OC	EC	TC	$PM_{2.5}$	SO_4^{2-}	NH_4^+	NO_3^-	TC
WRF-CMAQ/CAM																	
Mean (Obs)	15.26	5.59	1.62	0.35	0.91	3.16	10.81	4.73	0.28	1.50	0.39	1.89	17.47	4.94	1.58	0.54	4.72
Mean (Model)	16.08	4.05	1.25	0.41	1.83	3.97	9.38	4.14	0.43	1.89	0.61	2.50	17.35	4.55	1.63	0.89	4.83
Number	7318	231	231	231	231	231	489	307	307	484	478	484	817	886	886	850	895
Correlation	0.40	0.81	0.73	0.21	0.78	0.83	0.51	0.57	0.28	0.48	0.58	0.51	0.22	0.49	0.48	0.36	0.32
MB	0.81	−1.54	−0.37	0.07	0.92	0.80	−1.43	−0.59	0.14	0.39	0.22	0.60	−0.12	−0.39	0.04	0.35	0.10
RMSE	10.70	2.43	0.76	0.67	1.30	1.68	8.32	3.68	0.90	1.79	1.05	2.73	12.94	3.64	1.37	1.26	3.26
NMB (%)	5.3	−27.6	−23.0	19.4	101.1	25.3	−13.2	−12.5	50.4	25.9	54.9	31.9	−0.7	−7.9	2.8	64.2	2.2
NME (%)	49.9	33.3	35.0	112.1	105.5	35.6	51.4	53.5	141.9	62.7	97.5	68.0	53.9	53.1	61.5	130.7	48.9
NMBF (%)	5.3	−38.1	−29.9	19.4	101.1	25.3	−15.2	−14.3	50.4	25.9	54.9	31.9	−0.7	−8.5	2.8	64.2	2.2
NMEF (%)	49.9	46.0	45.4	112.1	105.5	35.6	59.2	61.2	141.9	62.7	97.5	68.0	54.3	57.6	61.5	130.7	48.9
WRF-CMAQ/RRTMG																	
Mean (Obs)	15.26	5.59	1.62	0.35	0.91	3.16	10.81	4.73	0.28	1.50	0.39	1.89	17.47	4.94	1.58	0.54	4.72
Mean (Model)	15.25	3.79	1.17	0.38	1.81	3.85	8.99	3.84	0.35	1.86	0.60	2.45	16.39	4.21	1.48	0.74	4.68
Number	7318	231	231	231	231	231	489	307	307	484	478	484	817	886	886	850	895
Correlation	0.40	0.81	0.74	0.21	0.78	0.83	0.51	0.59	0.26	0.50	0.60	0.54	0.23	0.54	0.52	0.34	0.33
MB	−0.02	−1.80	−0.45	0.03	0.90	0.69	−1.82	−0.90	0.06	0.36	0.20	0.56	−1.08	−0.73	−0.11	0.20	−0.04
RMSE	10.20	2.62	0.79	0.64	1.26	1.55	8.02	3.59	0.69	1.68	0.99	2.57	12.56	3.45	1.25	1.06	3.12
NMB (%)	−0.1	−32.1	−27.7	9.7	98.9	21.8	−16.8	−18.9	22.4	23.8	52.2	29.7	−6.2	−14.8	−6.7	37.1	−0.9
NME (%)	48.6	36.3	36.7	107.6	103.0	33.0	51.0	53.2	121.0	59.9	94.0	65.0	52.5	50.0	56.4	115.1	47.8
NMBF (%)	−0.1	−47.4	−38.4	9.7	98.9	21.8	−20.2	−23.3	22.4	23.8	52.2	29.7	−6.6	−17.4	−7.2	37.1	−0.9
NMEF (%)	48.7	53.5	50.8	107.6	103.0	33.0	61.3	65.7	121.0	59.9	94.0	65.0	56.0	58.7	60.5	115.1	48.2

* The unit of Mean, MB, RMSE is $\mu g\,m^{-3}$, SO_2 is ppb, and TotS is total sulfur ($SO_4^{2-} + SO_2$) concentrations ($\mu g\,S\,m^{-3}$).

ACPD
13, 25649–25739, 2013

Table 5b. Comparison of observation and models (WRF-CMAQ/CAM and WRF-CMAQ/RRTMG) for $PM_{2.5}$ and its components for each network over the western US (longitude $< -100°$) for August of 2006*.

	AIRNow	CASTNet					IMPROVE						STN				
	$PM_{2.5}$	SO_4^{2+}	NH_4^+	NO_3^-	SO_2	TotS	$PM_{2.5}$	SO_4^{2-}	NO_3^-	OC	EC	TC	$PM_{2.5}$	SO_4^{2-}	NH_4^+	NO_3^-	TC
WRF-CMAQ/CAM																	
Mean (Obs)	9.15	1.06	0.34	0.37	0.18	0.61	5.61	0.77	0.22	1.83	0.28	2.11	11.37	1.68	0.79	1.26	5.32
Mean (Model)	9.19	0.81	0.23	0.07	0.27	0.65	6.45	0.88	0.11	2.77	0.59	3.36	11.53	1.61	0.42	0.24	4.94
Number	1988	94	94	94	94	94	705	501	501	701	701	701	253	269	269	261	252
Correlation	0.18	0.70	0.32	0.13	0.34	0.48	0.38	0.37	0.24	0.61	0.52	0.60	0.14	0.50	0.35	0.02	0.33
MB	0.04	−0.25	−0.12	−0.30	0.08	0.04	0.84	0.11	−0.12	0.94	0.31	1.25	0.17	−0.07	−0.37	−1.02	−0.37
RMSE	11.63	0.40	0.18	0.47	0.23	0.36	14.51	0.57	0.46	7.11	1.60	8.63	9.69	1.04	0.97	2.25	4.10
NMB (%)	0.4	−23.9	−34.1	−80.6	47.0	6.0	15.0	13.9	−51.9	51.4	110.6	59.2	1.5	−4.2	−47.3	−81.1	−7.0
NME (%)	50.9	29.3	42.9	91.1	77.6	39.4	79.9	51.5	102.9	101.8	153.2	107.3	51.5	42.9	61.7	89.1	48.5
NMBF (%)	0.4	−31.4	−51.7	−415.3	47.0	6.0	15.0	13.9	−107.7	51.4	110.6	59.2	1.5	−4.4	−89.6	−427.9	−7.6
NMEF (%)	50.9	38.5	65.1	469.2	77.6	39.4	79.9	51.5	213.8	101.8	153.2	107.3	51.5	44.8	117.0	470.3	52.2
WRF-CMAQ/RRTMG																	
Mean (Obs)	9.15	1.06	0.34	0.37	0.18	0.61	5.61	0.77	0.22	1.83	0.28	2.11	11.37	1.68	0.79	1.26	5.32
Mean (Model)	8.67	0.80	0.22	0.07	0.27	0.65	6.01	0.86	0.09	2.54	0.54	3.08	10.77	1.52	0.37	0.20	4.65
Number	1988	94	94	94	94	94	705	501	501	701	701	701	253	269	269	261	252
Correlation	0.18	0.70	0.33	0.16	0.36	0.50	0.38	0.38	0.25	0.61	0.52	0.60	0.13	0.48	0.30	−0.01	0.36
MB	−0.48	−0.26	−0.12	−0.30	0.09	0.04	0.40	0.09	−0.14	0.71	0.26	0.97	−0.60	−0.16	−0.42	−1.06	−0.66
RMSE	10.06	0.41	0.19	0.47	0.22	0.35	13.20	0.55	0.39	6.38	1.45	7.76	8.26	1.04	1.00	2.27	3.41
NMB (%)	−5.2	−24.5	−35.9	−82.3	47.5	5.9	7.1	11.6	−61.1	38.6	94.5	46.0	−5.3	−9.5	−53.6	−84.1	−12.5
NME (%)	48.7	29.6	43.6	90.2	77.2	39.0	74.7	49.8	97.4	92.8	140.0	97.4	48.8	41.2	63.9	90.4	45.5
NMBF (%)	−5.5	−32.5	−56.1	−464.6	47.5	5.9	7.1	11.6	−157.0	38.6	94.5	46.0	−5.6	−10.5	−115.5	−528.5	−14.3
NMEF (%)	51.4	39.2	68.0	509.4	77.2	39.0	74.7	49.8	250.3	92.8	140.0	97.4	51.5	45.6	137.8	567.9	52.0

* The unit of Mean, MB, RMSE is $\mu g\,m^{-3}$, SO_2 is ppb, and TotS is total sulfur ($SO_4^{2-} + SO_2$) concentrations ($\mu g\,S\,m^{-3}$).

ACPD
13, 25649–25739, 2013

Table 6. Comparison of observation and models (WRF-CMAQ/CAM and WRF-CMAQ/RRTMG) for $PM_{2.5}$ and its components for each network over the eastern Texas from the simulations of 4 km and 12 km resolution model grids for August of 2006*.

	AIRNow	STN					AIRNow	STN				
	$PM_{2.5}$	$PM_{2.5}$	SO_4^{2-}	NH_4^+	NO_3^-	TC	$PM_{2.5}$	$PM_{2.5}$	SO_4^{2-}	NH_4^+	NO_3^-	TC
	WRF-CMAQ/CAM-4 km						WRF-CMAQ/CAM-12 km					
Mean (Obs)	12.45	12.55	3.32	0.41	1.01	2.71	12.45	12.55	3.32	0.41	1.01	2.71
Mean (Model)	20.59	24.14	3.54	0.32	0.85	6.57	17.06	17.95	1.91	0.17	0.44	5.50
Number	245	17	46	19	46	50	245	17	46	19	46	50
Correlation	0.37	−0.49	0.33	0.41	0.44	0.19	0.38	0.15	0.46	0.70	0.59	0.24
MB	8.14	11.59	0.22	−0.09	−0.17	3.86	4.61	5.41	−1.42	−0.23	−0.58	2.79
RMSE	18.45	17.00	1.92	0.26	0.60	5.36	14.15	9.59	1.94	0.27	0.72	5.00
NMB (%)	65.4	92.4	6.7	−22.2	−16.4	142.7	37.1	43.1	−42.6	−57.3	−56.9	103.1
NME (%)	85.1	112.2	47.7	53.7	46.0	149.4	65.2	60.3	48.6	60.7	60.4	121.2
NMBF (%)	65.4	92.4	6.7	−28.6	−19.7	142.7	37.1	43.1	−74.3	−134.0	−131.8	103.1
NMEF (%)	85.1	112.2	47.7	69.1	55.1	149.4	65.2	60.3	84.7	142.0	139.9	121.2
	WRF-CMAQ/RRTMG-4 km						WRF-CMAQ/RRTMG-12 km					
Mean (Obs)	12.45	12.55	3.32	0.41	1.01	2.71	12.45	12.55	3.32	0.41	1.01	2.71
Mean (Model)	17.06	19.25	3.07	0.16	0.67	5.12	12.70	14.15	1.73	0.06	0.38	4.58
Number	245	17	46	19	46	50	245	17	46	19	46	50
correlation	0.38	−0.44	0.40	0.60	0.57	0.12	0.33	0.10	0.53	0.70	0.64	0.26
MB	4.61	6.71	−0.25	−0.25	−0.34	2.41	0.25	1.60	−1.60	−0.35	−0.64	1.88
RMSE	14.15	12.42	1.70	0.28	0.58	3.89	11.40	5.94	1.99	0.37	0.76	4.01
NMB (%)	37.06	53.4	−7.6	−61.1	−33.8	89.1	2.0	12.7	−48.0	−84.3	−62.9	69.3
NME (%)	65.24	81.7	42.5	62.0	44.8	101.8	61.7	40.9	49.8	84.3	62.9	94.1
NMBF (%)	37.06	53.4	−8.3	−157.0	−51.0	89.1	2.0	12.7	−92.4	−538.6	−169.7	69.3
NMEF (%)	65.24	81.7	46.0	159.2	67.7	101.8	61.7	40.9	95.9	538.6	169.7	94.1

* The unit of Mean, MB, and RMSE is $\mu g\,m^{-3}$.

Table 7a. The same as Table 5a but for September of 2006 for EUS.

	AIRNow	CASTNet					IMPROVE						STN				
	$PM_{2.5}$	SO_4^{2+}	NH_4^+	NO_3^-	SO_2	TotS	$PM_{2.5}$	SO_4^{2-}	NO_3^-	OC	EC	TC	$PM_{2.5}$	SO_4^{2-}	NH_4^+	NO_3^-	TC
WRF-CMAQ/CAM																	
Mean (Obs)	11.84	4.39	0.36	1.35	0.72	2.49	8.01	3.07	0.29	1.27	0.37	1.64	12.04	3.83	1.35	0.59	4.04
Mean (Model)	15.44	3.96	0.54	1.20	1.66	3.69	8.89	3.66	0.52	1.68	0.55	2.23	16.57	4.60	1.69	1.11	4.56
Number	7182	170	170	170	170	170	515	351	351	508	507	508	806	842	842	807	858
correlation	0.48	0.94	0.35	0.86	0.79	0.87	0.49	0.64	0.50	0.48	0.65	0.52	0.50	0.69	0.64	0.53	0.48
MB	3.60	−0.43	0.18	−0.15	0.94	1.20	0.88	0.60	0.23	0.41	0.18	0.59	4.53	0.77	0.34	0.53	0.52
RMSE	10.42	1.03	0.61	0.45	1.18	1.61	8.36	2.78	0.92	1.86	1.05	2.81	11.33	2.73	1.13	1.30	3.37
NMB (%)	30.42	−9.82	50.33	−11.37	130.87	48.26	11.00	19.41	80.65	32.22	49.46	36.07	37.63	19.99	25.10	89.51	12.96
NME (%)	56.18	16.29	109.08	24.14	132.06	51.09	53.56	54.66	151.43	71.91	90.54	74.33	60.07	48.15	57.36	129.95	55.23
NMBF (%)	30.42	−10.89	50.33	−12.83	130.87	48.26	11.00	19.41	80.65	32.22	49.46	36.07	37.63	19.99	25.10	89.51	12.96
NMEF (%)	56.18	18.07	109.08	27.23	132.06	51.09	53.56	54.66	151.43	71.91	90.54	74.33	60.07	48.15	57.36	129.95	55.23
WRF-CMAQ/RRTMG																	
Mean (Obs)	11.84	4.39	0.36	1.35	0.72	2.49	8.01	3.07	0.29	1.27	0.37	1.64	12.04	3.83	1.35	0.59	4.04
Mean (Model)	15.07	3.91	0.53	1.18	1.68	3.70	8.84	3.54	0.54	1.72	0.56	2.28	16.31	4.40	1.62	1.08	4.57
Number	7182	170	170	170	170	170	515	351	351	508	507	508	806	842	842	807	858
Correlation	0.49	0.93	0.32	0.87	0.79	0.87	0.53	0.69	0.42	0.50	0.65	0.53	0.53	0.72	0.68	0.56	0.49
MB	3.23	−0.48	0.17	−0.17	0.96	1.21	0.83	0.47	0.25	0.45	0.19	0.64	4.27	0.57	0.27	0.49	0.53
RMSE	9.83	1.13	0.59	0.44	1.18	1.60	7.44	2.37	0.97	1.79	1.00	2.70	10.56	2.45	1.02	1.28	3.22
NMB (%)	27.29	−10.91	48.26	−12.27	132.81	48.43	10.35	15.35	86.29	35.25	51.55	38.90	35.46	14.81	20.01	83.97	13.04
NME (%)	54.20	18.14	108.30	23.97	134.56	50.77	52.74	51.71	159.45	70.65	89.26	72.93	57.54	45.95	54.00	126.77	53.23
NMBF (%)	27.29	−12.25	48.26	−13.99	132.81	48.43	10.35	15.35	86.29	35.25	51.55	38.90	35.46	14.81	20.01	83.97	13.04
NMEF (%)	54.20	20.36	108.30	27.32	134.56	50.77	52.74	51.71	159.45	70.65	89.26	72.93	57.54	45.95	54.00	126.77	53.23

ACPD
13, 25649–25739, 2013

ACPD
13, 25649–25739, 2013

Table 7b. The same as Table 5b but for September of 2006 for WUS.

	AIRNow	CASTNet					IMPROVE						STN				
	$PM_{2.5}$	SO_4^{2+}	NH_4^+	NO_3^-	SO_2	TotS	$PM_{2.5}$	SO_4^{2-}	NO_3^-	OC	EC	TC	$PM_{2.5}$	SO_4^{2-}	NH_4^+	NO_3^-	TC
WRF-CMAQ/CAM																	
Mean (Obs)	9.80	0.81	0.34	0.29	0.14	0.47	5.17	0.64	0.22	1.68	0.28	1.95	12.03	1.43	0.75	1.33	5.92
Mean(Model)	16.17	0.72	0.09	0.19	0.28	0.63	6.43	0.75	0.16	2.64	0.54	3.17	22.12	1.59	0.70	1.42	11.02
Number	1992	75	75	75	75	75	712	562	562	703	710	706	251	252	252	245	250
Correlation	0.48	0.80	0.07	0.50	0.43	0.58	0.66	0.59	0.28	0.60	0.34	0.57	0.24	0.53	0.29	0.19	0.39
MB	6.37	−0.09	−0.25	−0.10	0.13	0.16	1.26	0.11	−0.06	0.96	0.26	1.22	10.10	0.16	−0.05	0.09	5.11
RMSE	15.19	0.28	0.47	0.16	0.22	0.32	9.53	0.48	0.51	4.81	1.22	5.86	27.76	1.06	1.25	3.53	14.80
NMB (%)	65.01	−11.30	−72.91	−33.06	95.02	34.45	24.29	17.46	−27.57	57.48	93.52	62.71	83.97	11.25	−6.78	6.77	86.34
NME (%)	89.46	22.74	85.92	44.67	107.42	46.94	71.31	48.55	103.08	100.50	141.18	105.74	108.48	48.17	79.37	108.25	112.65
NMBF (%)	65.01	−12.74	−269.13	−49.39	95.02	34.45	24.29	17.46	−38.06	57.48	93.52	62.71	83.97	11.25	−7.27	6.77	86.34
NMEF (%)	89.46	25.64	317.16	66.73	107.42	46.94	71.31	48.55	142.31	100.50	141.18	105.74	108.48	48.17	85.14	108.25	112.65
WRF-CMAQ/RRTMG																	
Mean (Obs)	9.80	0.81	0.34	0.29	0.14	0.47	5.17	0.64	0.22	1.68	0.28	1.95	12.03	1.43	0.75	1.33	5.92
Mean(Model)	15.16	0.71	0.08	0.19	0.28	0.63	5.94	0.74	0.13	2.39	0.50	2.88	20.37	1.47	0.60	1.18	10.21
Number	1992	75	75	75	75	75	712	562	562	703	710	706	251	252	252	245	250
Correlation	0.47	0.80	0.13	0.52	0.43	0.58	0.64	0.56	0.32	0.60	0.33	0.57	0.25	0.51	0.25	0.18	0.40
MB	5.36	−0.10	−0.26	−0.10	0.14	0.16	0.77	0.10	−0.09	0.72	0.22	0.94	8.35	0.04	−0.16	−0.15	4.30
RMSE	13.46	0.28	0.47	0.16	0.22	0.32	8.19	0.49	0.45	4.18	1.13	5.14	22.00	1.03	1.17	3.12	11.75
NMB (%)	54.74	−12.03	−75.47	−34.10	95.21	34.11	14.89	15.82	−39.94	42.83	78.81	48.05	69.40	2.69	−20.73	−11.13	72.66
NME (%)	81.22	22.66	84.16	44.33	107.42	46.88	64.32	47.73	94.15	87.99	127.87	93.06	96.46	45.98	76.83	102.99	100.57
NMBF (%)	54.74	−13.68	−307.65	−51.76	95.21	34.11	14.89	15.82	−66.51	42.83	78.81	48.05	69.40	2.69	−26.15	−12.53	72.66
NMEF (%)	81.22	25.76	343.09	67.27	107.42	46.88	64.32	47.73	156.77	87.99	127.87	93.06	96.46	45.98	96.92	115.89	100.57

The unit of Mean, MB, RMSE is $\mu g\,m^{-3}$, SO_2 is ppb, and TotS is total sulfur ($SO_4^{2-} + SO_2$) concentrations ($\mu g\,S\,m^{-3}$).

Table 8. The same as Table 6 but for September of 2006.

	AIRNow	STN					AIRNow	STN				
	$PM_{2.5}$	$PM_{2.5}$	SO_4^{2}	NH_4^+	NO_3^-	TC	$PM_{2.5}$	$PM_{2.5}$	SO_4^{2}	NH_4^+	NO_3^-	TC
	WRF-CMAQ/CAM-4 km						WRF-CMAQ/CAM-12 km					
Mean (Obs)	12.65	15.05	4.31	1.68	0.50	4.41	12.65	15.05	4.31	1.68	0.50	4.41
Mean (Model)	22.73	27.03	4.47	1.28	0.37	8.66	21.45	27.64	4.38	1.38	0.87	8.38
Number	264	19	48	48	19	52	264	19	48	48	19	52
Correlation	0.40	0.71	0.73	0.65	0.12	0.53	0.33	0.74	0.75	0.63	0.08	0.74
MB	10.08	11.98	0.16	−0.40	−0.13	4.25	8.80	12.59	0.07	−0.29	0.38	3.97
RMSE	19.38	15.18	1.94	1.13	0.47	5.79	20.39	14.40	1.81	1.13	1.20	4.70
NMB (%)	79.66	79.60	3.79	−23.84	−26.29	96.31	69.56	83.63	1.66	−17.46	75.44	89.88
NME (%)	95.57	81.23	32.97	41.37	64.19	100.46	86.95	83.63	33.79	47.61	135.37	91.53
NMBF (%)	79.66	79.60	3.79	−31.30	−35.66	96.31	69.56	83.63	1.66	−21.16	75.44	89.88
NMEF (%)	95.57	81.23	32.97	54.32	87.08	100.46	86.95	83.63	33.79	57.69	135.37	91.53
	WRF-CMAQ/RRTMG-4 km						WRF-CMAQ/RRTMG-12 km					
Mean (Obs)	12.65	15.05	4.31	1.68	0.50	4.41	12.65	15.05	4.31	1.68	0.50	4.41
Mean (Model)	20.68	23.45	4.07	1.16	0.37	7.21	20.53	25.95	4.15	1.27	0.77	7.85
Number	264	19	48	48	19	52	264	19	48	48	19	52
Correlation	0.42	0.78	0.76	0.67	0.18	0.52	0.32	0.60	0.75	0.57	−0.03	0.70
MB	8.03	8.39	−0.24	−0.52	−0.13	2.80	7.88	10.90	−0.16	−0.40	0.28	3.43
RMSE	16.84	10.42	1.73	1.17	0.42	4.17	19.25	13.83	1.79	1.22	1.60	4.20
NMB (%)	63.48	55.76	−5.63	−30.91	−25.44	63.46	62.31	72.39	−3.76	−24.05	55.25	77.81
NME (%)	81.45	56.35	29.46	40.54	62.80	70.61	81.27	72.39	32.49	46.83	147.27	80.14
NMBF (%)	63.48	55.76	−5.97	−44.73	−34.13	63.46	62.31	72.39	−3.91	−31.67	55.25	77.81
NMEF (%)	81.45	56.35	31.22	58.68	84.23	70.61	81.27	72.39	33.76	61.66	147.27	80.14

The unit of Mean, MB, and RMSE is $\mu g\,m^{-3}$.

ACPD
13, 25649–25739, 2013

Aerosol indirect effect in the two-way coupled WRF-CMAQ

S. Yu et al.

Table 9. Comparison of observation and models (WRF-CMAQ/CAM, WRF-CMAQ/RRTMG, WRF/CAM and WRF/RRTMG) for monthly SWCF ($W\,m^{-2}$) over the land and ocean of the eastern US and western US (in parentheses) of the CONUS from 12 km resolution simulations and over the eastern Texas from the 4 km resolution simulations (the results in parentheses are from the 12 km resolution simulation) in August and September of 2006.

	August			September		
	12 km, Land	12 km, Ocean	4 km	12 km, Land	12 km, Ocean	4 km
WRF-CMAQ/CAM						
Mean (Obs)	−60.90 (−37.18)	−52.60 (−62.29)	−33.29 (−34.34)	−55.60 (−34.63)	−50.79 (−49.24)	−37.02 (−36.63)
Mean (Model)	−53.75 (−27.58)	−48.53 (−68.02)	−31.58 (−24.06)	−54.97 (−33.01)	−58.62 (−54.78)	−32.61 (−33.57)
Number	982 (1385)	1124 (997)	309 (79.00)	866 (1104)	1080 (783)	256 (55.00)
correlation	0.96 (0.96)	0.90 (0.91)	0.70 (0.82)	0.91 (0.94)	0.95 (0.90)	0.79 (0.91)
MB	7.15 (9.60)	4.08 (−5.73)	1.71 (10.29)	0.63 (1.62)	−7.83 (−5.53)	4.41 (3.06)
RMSE	10.29 (11.10)	14.53 (19.08)	6.89 (11.68)	6.56 (5.53)	11.76 (11.45)	6.34 (5.71)
NMB (%)	−11.74 (−25.82)	−7.75 (9.20)	−5.13 (−29.95)	−1.13 (−4.67)	15.41 (11.24)	−11.90 (−8.36)
NME (%)	−14.41 (−27.14)	−24.12 (−25.51)	−16.09 (−30.98)	−9.10 (−11.81)	−18.85 (−17.26)	−13.67 (−12.98)
WRF-CMAQ/RRTMG						
Mean (Obs)	−60.90 (−37.18)	−52.60 (−62.29)	−33.29 (−34.34)	−55.60 (−34.63)	−50.79 (−49.24)	−37.02 (−36.63)
Mean (Model)	−47.23 (−24.76)	−40.14 (−53.17)	−30.90 (−21.14)	−63.26 (−37.84)	−67.43 (−60.09)	−38.15 (−38.78)
Number	982 (1385)	1124 (997)	309 (79.00)	866 (1104)	1080 (783)	256 (55.00)
correlation	0.96 (0.95)	0.93 (0.92)	0.45 (0.85)	0.91 (0.95)	0.95 (0.89)	0.85 (0.91)
MB	13.67 (12.42)	12.46 (9.12)	2.38 (13.21)	−7.66 (−3.21)	−16.64 (−10.85)	−1.13 (−2.15)
RMSE	14.74 (14.13)	14.25 (15.44)	9.55 (14.21)	10.76 (7.25)	20.55 (16.22)	4.42 (6.27)
NMB (%)	−22.45 (−33.40)	−23.69 (−14.64)	−7.16 (−38.45)	13.77 (9.27)	32.75 (22.03)	3.05 (5.87)
NME (%)	−22.72 (−34.62)	−24.13 (−20.12)	−22.41 (−38.45)	−16.13 (−15.73)	−33.73 (−26.57)	−9.12 (−13.53)
WRF/CAM						
Mean (Obs)	−60.90 (−37.18)	−52.60 (−62.29)	−33.29 (−34.34)	−55.60 (−34.63)	−50.79 (−49.24)	−37.02 (−36.63)
Mean (Model)	−51.13 (−39.54)	−98.18 (−75.41)	−25.42 (−67.60)	−73.91 (−44.80)	−100.61 (−104.76)	−30.03 (−48.61)
Number	982 (1385)	1124 (997)	309 (79.00)	866 (1104)	1080 (783)	256 (55.00)
correlation	0.37 (0.39)	−0.69 (−0.54)	0.75 (0.28)	0.60 (0.78)	0.18 (0.41)	0.85 (0.65)
MB	9.77 (−2.36)	−45.57 (−13.12)	7.86 (−33.26)	−18.31 (−10.18)	−49.82 (−55.52)	6.98 (−11.98)
RMSE	22.29 (17.10)	65.55 (53.41)	10.71 (46.63)	27.79 (17.96)	59.71 (62.96)	8.33 (26.28)
NMB (%)	−16.04 (6.34)	86.64 (21.07)	−23.63 (96.84)	32.93 (29.39)	98.09 (112.74)	−18.87 (32.70)
NME (%)	−31.26 (−37.33)	−101.43 (−74.98)	−27.89 (−102.13)	−37.42 (−35.08)	−98.19 (−112.76)	−19.12 (−51.08)
WRF/RRTMG						
Mean (Obs)	−60.90 (−37.18)	−52.60 (−62.29)	−33.29 (−34.34)	−55.60 (−34.63)	−50.79 (−49.24)	−37.02 (−36.63)
Mean (Model)	−39.36 (−27.71)	−78.20 (−51.05)	−23.84 (−43.09)	−65.77 (−40.67)	−92.61 (−94.48)	−26.57 (−44.63)
Number	982 (1385)	1124 (997)	309 (79.00)	866 (1104)	1080 (783)	256 (55.00)
correlation	0.72 (0.59)	−0.52 (−0.54)	0.76 (0.34)	0.57 (0.76)	0.10 (0.35)	0.84 (0.62)
MB	21.54 (9.47)	−25.60 (11.24)	9.44 (−8.74)	−10.17 (−6.04)	−41.82 (−45.23)	10.44 (−7.99)
RMSE	25.30 (17.63)	45.41 (49.62)	11.54 (27.39)	22.69 (14.95)	54.15 (54.49)	11.32 (24.53)
NMB (%)	−35.37 (−25.46)	48.67 (−18.04)	−28.37 (25.46)	18.29 (17.44)	82.33 (91.86)	−28.21 (21.82)
NME (%)	−37.99 (−37.94)	−69.04 (−68.10)	−30.56 (−55.10)	−29.66 (−28.01)	−82.69 (−92.08)	−28.25 (−50.55)

ACPD
13, 25649–25739, 2013

Aerosol indirect effect in the two-way coupled WRF-CMAQ

S. Yu et al.

Table 10. Same Table 9 but for monthly LWCF in August and September of 2006.

	August			September		
	12 km, Land	12 km, Ocean	4 km	12 km, Land	12 km, Ocean	4 km
			WRF-CMAQ/CAM			
Mean (Obs)	30.26 (30.33)	29.34 (21.97)	25.36 (27.45)	29.65 (25.84)	34.16 (27.89)	27.06 (28.03)
Mean (Model)	21.83 (19.97)	23.47 (15.84)	26.04 (20.67)	18.56 (16.68)	34.93 (28.24)	21.53 (21.38)
Number	982 (1404)	1124 (1013)	309 (79.00)	866 (1108)	1080 (783)	256 (55.00)
correlation	0.78 (0.85)	0.77 (0.90)	0.59 (0.82)	0.77 (0.87)	0.85 (0.88)	0.90 (0.76)
MB	−8.43 (−10.36)	−5.86 (−6.13)	0.68 (−6.78)	−11.08 (−9.17)	0.77 (0.35)	−5.53 (−6.65)
RMSE	8.76 (11.05)	6.71 (7.03)	7.47 (7.45)	11.44 (9.61)	5.90 (4.84)	7.04 (8.89)
NMB (%)	−27.86 (−34.15)	−19.99 (−27.90)	2.69 (−24.69)	−37.39 (−35.46)	2.25 (1.25)	−20.44 (−23.74)
NME (%)	27.91 (34.18)	20.44 (28.28)	23.41 (24.93)	37.66 (35.92)	13.97 (13.74)	22.22 (28.85)
			WRF-CMAQ/RRTMG			
Mean (Obs)	30.26 (30.33)	29.34 (21.97)	25.36 (27.45)	29.65 (25.84)	34.16 (27.89)	27.06 (28.03)
Mean (Model)	20.95 (19.58)	21.21 (14.33)	23.29 (19.86)	18.69 (16.15)	31.66 (25.49)	23.13 (20.05)
Number	982 (1404)	1124 (1013)	309 (79.00)	866 (1108)	1080 (783)	256 (55.00)
correlation	0.75 (0.85)	0.79 (0.91)	0.63 (0.82)	0.80 (0.89)	0.87 (0.89)	0.86 (0.77)
MB	−9.31 (−10.75)	−8.13 (−7.64)	−2.07 (−7.59)	−10.96 (−9.69)	−2.50 (−2.40)	−3.93 (−7.97)
RMSE	9.63 (11.42)	8.66 (8.37)	7.38 (8.17)	11.27 (10.07)	5.56 (4.82)	6.31 (9.22)
NMB (%)	−30.76 (−35.45)	−27.70 (−34.79)	−8.15 (−27.64)	−36.96 (−37.51)	−7.32 (−8.62)	−14.52 (−28.45)
NME (%)	30.80 (35.47)	27.80 (34.81)	24.07 (27.84)	37.19 (37.82)	13.34 (14.15)	20.57 (29.54)
			WRF/CAM			
Mean (Obs)	30.26 (30.33)	29.34 (21.97)	25.36 (27.45)	29.65 (25.84)	34.16 (27.89)	27.06 (28.03)
Mean (Model)	37.28 (46.10)	81.49 (55.94)	26.39 (76.03)	23.22 (19.77)	50.28 (50.90)	26.21 (25.28)
Number	982 (1404)	1124 (1013)	309 (79.00)	866 (1108)	1080 (783)	256 (55.00)
correlation	0.31 (0.27)	−0.23 (0.55)	0.65 (−0.10)	0.10 (0.54)	−0.30 (−0.20)	0.86 (0.67)
MB	7.02 (15.77)	52.15 (33.97)	1.03 (48.58)	−6.42 (−6.07)	16.12 (23.01)	−0.85 (−2.75)
RMSE	18.64 (22.29)	61.99 (47.38)	8.79 (54.47)	15.07 (10.45)	32.85 (33.46)	6.44 (17.69)
NMB (%)	23.20 (52.00)	177.77 (154.64)	4.06 (177.01)	−21.66 (−23.49)	47.20 (82.52)	−3.13 (−9.82)
NME (%)	32.84 (56.35)	178.14 (159.98)	28.18 (177.01)	39.66 (32.59)	62.71 (87.55)	21.31 (54.15)
			WRF/RRTMG			
Mean (Obs)	30.26 (30.33)	29.34 (21.97)	25.36 (27.45)	29.65 (25.84)	34.16 (27.89)	27.06 (28.03)
Mean (Model)	26.98 (29.23)	61.25 (38.51)	22.02 (43.34)	22.61 (18.95)	44.92 (46.00)	21.82 (22.98)
Number	982 (1404)	1124 (1013)	309 (79.00)	866 (1108)	1080 (783)	256 (55.00)
correlation	0.24 (0.43)	−0.16 (0.61)	0.65 (0.06)	0.09 (0.54)	−0.31 (−0.22)	0.87 (0.66)
MB	−3.28 (−1.10)	31.91 (16.55)	−3.34 (15.89)	−7.04 (−6.89)	10.76 (18.11)	−5.24 (−5.05)
RMSE	9.64 (9.14)	40.06 (26.74)	7.77 (25.71)	15.05 (10.85)	28.73 (28.98)	7.05 (16.31)
NMB (%)	−10.84 (−3.63)	108.78 (75.33)	−13.18 (57.91)	−23.74 (−26.67)	31.51 (64.92)	−19.36 (−18.03)
NME (%)	23.05 (23.02)	110.43 (89.61)	25.85 (65.80)	40.75 (34.80)	56.11 (74.25)	22.63 (50.45)

ACPD
13, 25649–25739, 2013

Table 11. Same Table 9 but for monthly COD in August and September of 2006.

	August			September		
	12 km, Land	12 km, Ocean	4 km	12 km, Land	12 km, Ocean	4 km
			WRF-CMAQ/CAM			
Mean (Obs)	6.86 (4.99)	5.17 (6.09)	2.66 (3.72)	8.43 (7.30)	6.21 (6.01)	6.06 (5.71)
Mean (Model)	5.83 (2.39)	5.21 (5.85)	2.35 (1.83)	8.05 (5.21)	6.80 (6.44)	3.63 (4.67)
Number	790 (924)	738 (513)	255 (45.00)	987 (1195)	826 (509)	580 (63.00)
correlation	0.82 (0.91)	0.87 (0.92)	0.11 (0.50)	0.85 (0.93)	0.89 (0.90)	0.64 (0.84)
MB	−1.02 (−2.59)	0.04 (−0.24)	−0.30 (−1.89)	−0.38 (−2.08)	0.58 (0.43)	−2.44 (−1.04)
RMSE	1.85 (2.70)	2.02 (1.53)	1.04 (2.00)	1.64 (2.34)	1.91 (1.46)	3.02 (1.78)
NMB (%)	−14.92 (−52.02)	0.83 (−4.01)	−11.43 (−50.74)	−4.47 (−28.56)	9.39 (7.15)	−40.22 (−18.28)
NME (%)	22.16 (52.03)	34.23 (21.09)	27.92 (50.74)	14.82 (28.81)	25.14 (20.01)	40.72 (25.35)
			WRF-CMAQ/RRTMG			
Mean (Obs)	6.86 (4.99)	5.17 (6.09)	2.66 (3.72)	8.43 (7.30)	6.21 (6.01)	6.06 (5.71)
Mean (Model)	3.67 (1.44)	2.83 (2.95)	1.90 (1.02)	5.35 (3.48)	4.46 (3.93)	3.43 (3.06)
Number	790 (924)	738 (513)	255 (45.00)	987 (1195)	826 (509)	580 (63.00)
correlation	0.81 (0.90)	0.90 (0.88)	0.59 (0.64)	0.85 (0.93)	0.91 (0.89)	0.55 (0.87)
MB	−3.18 (−3.55)	−2.34 (−3.15)	−0.76 (−2.70)	−3.08 (−3.82)	−1.76 (−2.08)	−2.63 (−2.66)
RMSE	3.43 (3.67)	2.52 (3.47)	1.05 (2.75)	3.43 (4.02)	2.12 (2.32)	3.27 (2.94)
NMB (%)	−46.43 (−71.10)	−45.19 (−51.63)	−28.60 (−72.56)	−36.49 (−52.32)	−28.26 (−34.56)	−43.44 (−46.48)
NME (%)	46.62 (71.10)	45.23 (51.63)	32.95 (72.56)	36.70 (52.32)	29.32 (34.61)	43.82 (46.48)
			WRF/CAM			
Mean (Obs)	6.86 (4.99)	5.17 (6.09)	2.66 (3.72)	8.43 (7.30)	6.21 (6.01)	6.06 (5.71)
Mean (Model)	2.42 (1.28)	1.62 (1.56)	0.70 (1.43)	10.00 (6.59)	10.84 (10.05)	1.22 (6.05)
Number	790 (924)	738 (513)	255 (45.00)	987 (1195)	826 (509)	580 (63.00)
correlation	0.54 (0.81)	0.18 (0.81)	0.55 (−0.23)	0.67 (0.85)	0.75 (0.76)	0.10 (0.73)
MB	−4.44 (−3.70)	−3.55 (−4.53)	−1.96 (−2.29)	1.57 (−0.70)	4.63 (4.04)	−4.84 (0.34)
RMSE	4.79 (3.94)	4.14 (5.09)	2.08 (2.45)	3.40 (1.79)	5.55 (4.65)	5.35 (2.22)
NMB (%)	−64.72 (−74.27)	−68.62 (−74.33)	−73.64 (−61.53)	18.65 (−9.62)	74.53 (67.28)	−79.80 (5.99)
NME (%)	65.11 (74.27)	69.70 (74.33)	73.67 (61.64)	28.20 (18.65)	74.87 (67.38)	79.81 (28.66)
			WRF/RRTMG			
Mean (Obs)	6.86 (4.99)	5.17 (6.09)	2.66 (3.72)	8.43 (7.30)	6.21 (6.01)	6.06 (5.71)
Mean (Model)	0.72 (0.31)	0.45 (0.37)	0.34 (0.26)	6.78 (4.46)	7.48 (6.70)	0.56 (4.08)
Number	790 (924)	738 (513)	255 (45.00)	987 (1195)	826 (509)	580 (63.00)
correlation	0.71 (0.89)	0.42 (0.72)	0.61 (0.59)	0.66 (0.84)	0.73 (0.72)	0.06 (0.72)
MB	−6.13 (−4.67)	−4.72 (−5.73)	−2.32 (−3.47)	−1.65 (−2.83)	1.26 (0.69)	−5.50 (−1.63)
RMSE	6.41 (4.93)	5.15 (6.31)	2.43 (3.52)	2.88 (3.24)	2.55 (1.86)	5.96 (2.38)
NMB (%)	−89.43 (−93.71)	−91.33 (−93.96)	−87.33 (−93.12)	−19.56 (−38.85)	20.35 (11.56)	−90.76 (−28.57)
NME (%)	89.43 (93.71)	91.33 (93.96)	87.33 (93.12)	28.04 (39.98)	29.91 (21.73)	90.76 (34.72)

ACPD

13, 25649–25739, 2013

Aerosol indirect effect in the two-way coupled WRF-CMAQ

S. Yu et al.

Table 12. Same Table 9 but for monthly cloud fractions in August and September of 2006.

	August			September		
	12 km, Land	12 km, Ocean	4 km	12 km, Land	12 km, Ocean	4 km
			WRF-CMAQ/CAM			
Mean (Obs)	0.51 (0.38)	0.50 (0.56)	0.34 (0.35)	0.52 (0.37)	0.52 (0.51)	0.37 (0.38)
Mean (Model)	0.47 (0.35)	0.47 (0.58)	0.38 (0.31)	0.51 (0.34)	0.54 (0.49)	0.33 (0.35)
Number	560 (1031)	644 (764)	276 (61.00)	556 (888)	713 (685)	168 (43.00)
correlation	0.92 (0.97)	0.91 (0.86)	0.74 (0.94)	0.95 (0.97)	0.97 (0.87)	0.93 (0.78)
MB	−0.05 (−0.03)	−0.03 (0.02)	0.04 (−0.04)	−0.01 (−0.03)	0.01 (−0.01)	−0.04 (−0.02)
RMSE	0.06 (0.05)	0.05 (0.11)	0.07 (0.05)	0.04 (0.05)	0.04 (0.09)	0.07 (0.05)
NMB (%)	−9.08 (−8.37)	−5.67 (2.85)	11.13 (−11.21)	−2.84 (−7.98)	2.60 (−2.89)	−11.75 (−6.52)
NME (%)	9.42 (10.79)	8.92 (13.36)	17.06 (11.81)	5.34 (10.65)	5.49 (9.05)	14.48 (10.58)
			WRF-CMAQ/RRTMG			
Mean (Obs)	0.51 (0.38)	0.50 (0.56)	0.34 (0.35)	0.52 (0.37)	0.52 (0.51)	0.37 (0.38)
Mean (Model)	0.43 (0.34)	0.44 (0.51)	0.35 (0.30)	0.48 (0.33)	0.51 (0.45)	0.37 (0.35)
Number	560 (1031)	644 (764)	276 (61.00)	556 (888)	713 (685)	168 (43.00)
correlation	0.92 (0.97)	0.91 (0.90)	0.84 (0.93)	0.94 (0.97)	0.95 (0.74)	0.91 (0.70)
MB	−0.08 (−0.05)	−0.06 (−0.05)	0.02 (−0.05)	−0.05 (−0.04)	−0.01 (−0.05)	0.00 (−0.03)
RMSE	0.08 (0.06)	0.07 (0.10)	0.05 (0.06)	0.06 (0.05)	0.04 (0.13)	0.06 (0.06)
NMB (%)	−15.28 (−12.19)	−12.38 (−8.69)	4.50 (−14.74)	−9.22 (−11.05)	−1.77 (−10.76)	−1.22 (−8.16)
NME (%)	15.30 (14.52)	12.64 (13.85)	12.64 (14.91)	9.65 (12.30)	6.09 (14.45)	15.02 (12.41)
			WRF/CAM			
Mean (Obs)	0.51 (0.38)	0.50 (0.56)	0.34 (0.35)	0.52 (0.37)	0.52 (0.51)	0.37 (0.38)
Mean (Model)	0.58 (0.59)	0.75 (0.76)	0.38 (0.80)	0.59 (0.39)	0.72 (0.72)	0.35 (0.50)
Number	560 (1031)	644 (764)	276 (61.00)	556 (888)	713 (685)	168 (43.00)
correlation	−0.20 (0.48)	−0.72 (0.14)	0.79 (−0.69)	0.71 (0.86)	0.01 (0.39)	0.93 (−0.02)
MB	0.07 (0.21)	0.25 (0.20)	0.04 (0.45)	0.06 (0.02)	0.19 (0.21)	−0.03 (0.12)
RMSE	0.16 (0.26)	0.32 (0.30)	0.07 (0.49)	0.15 (0.10)	0.26 (0.28)	0.07 (0.27)
NMB (%)	13.69 (54.86)	49.70 (35.47)	10.54 (127.18)	11.61 (5.43)	37.01 (41.77)	−7.42 (31.05)
NME (%)	23.43 (55.49)	53.58 (41.82)	17.49 (127.18)	21.70 (22.08)	37.83 (43.45)	14.79 (57.15)
			WRF/RRTMG			
Mean (Obs)	0.51 (0.38)	0.50 (0.56)	0.34 (0.35)	0.52 (0.37)	0.52 (0.51)	0.37 (0.38)
Mean (Model)	0.53 (0.53)	0.72 (0.68)	0.38 (0.71)	0.56 (0.38)	0.70 (0.70)	0.34 (0.49)
Number	560 (1031)	644 (764)	276 (61)	556 (888)	713 (685)	168 (43.00)
correlation	0.08 (0.50)	−0.62 (−0.02)	0.78 (−0.62)	0.69 (0.85)	−0.05 (0.35)	0.93 (−0.02)
MB	0.02 (0.15)	0.21 (0.12)	0.04 (0.35)	0.03 (0.01)	0.17 (0.19)	−0.04 (0.11)
RMSE	0.12 (0.20)	0.28 (0.27)	0.08 (0.40)	0.14 (0.10)	0.26 (0.26)	0.07 (0.27)
NMB (%)	3.98 (38.62)	42.66 (20.72)	11.30 (100.80)	6.19 (2.26)	33.09 (37.74)	−9.93 (28.42)
NME (%)	16.56 (40.58)	47.05 (39.27)	18.00 (100.89)	21.01 (21.84)	35.58 (39.89)	16.04 (58.83)

ACPD
13, 25649–25739, 2013

Table 13. Comparison of observation (PRISM) and models (WRF-CMAQ/CAM, WRF-CMAQ/RRTMG, WRF/CAM and WRF/RRTMG for monthly precipitation (inch month^{-1}) over the land of the eastern US and western US from 12 km resolution simulations and over the eastern Texas from the 4 km resolution simulations in August and September of 2006.

	August			September		
	12 km (East)	12 km (West)	4 km	12 km (East)	12 km (West)	4 km
			WRF-CMAQ/CAM			
Mean (Obs)	3.86	1.58	1.77	3.99	1.48	3.35
Mean (Model)	5.40	2.91	1.39	3.12	1.40	2.72
Number	28 391	25 527	25 085	28 391	25 680	25 088
correlation	0.45	0.75	0.10	0.63	0.77	0.20
MB	1.54	1.33	−0.37	−0.87	−0.08	−0.63
RMSE	3.14	2.43	1.79	1.78	0.75	2.44
NMB (%)	39.96	83.77	−21.13	−21.81	−5.58	−18.81
NME (%)	59.46	94.98	71.46	35.01	35.14	54.04
			WRF-CMAQ/RRTMG			
Mean (Obs)	3.86	1.58	1.77	3.99	1.48	3.35
Mean (Model)	5.84	3.03	1.49	3.27	1.45	3.56
Number	28 391	25 527	25 085	28 391	25 680	25 088
correlation	0.43	0.77	0.23	0.62	0.77	0.33
MB	1.98	1.45	−0.27	−0.71	−0.03	0.21
RMSE	3.61	2.56	1.71	1.78	0.75	2.66
NMB (%)	51.34	91.30	−15.40	−17.85	−2.32	6.22
NME (%)	67.58	100.97	69.03	34.33	35.15	54.46
			WRF/CAM			
Mean (Obs)	3.86	1.58	1.77	3.99	1.48	3.35
Mean (Model)	4.38	3.44	1.24	2.40	1.23	2.94
Number	28 391	25 527	25 085	28 391	25 680	25 088
correlation	0.39	0.66	0.26	0.51	0.65	0.36
MB	0.52	1.86	−0.53	−1.59	−0.26	−0.42
RMSE	5.40	3.13	1.57	2.37	0.90	2.12
NMB (%)	13.38	117.52	−30.00	−39.89	−17.30	−12.39
NME (%)	70.66	127.25	63.49	47.06	42.54	45.27
			WRF/RRTMG			
Mean (Obs)	3.86	1.58	1.77	3.99	1.48	3.35
Mean (Model)	3.93	3.56	1.25	2.45	1.25	2.85
Number	28 391	25 527	25 085	28 391	25 680	25 088
correlation	0.44	0.57	0.25	0.50	0.63	0.36
MB	0.07	1.98	−0.52	−1.54	−0.24	−0.50
RMSE	2.71	3.56	1.56	2.36	0.91	2.10
NMB (%)	1.87	124.83	−29.20	−38.58	−16.06	−14.87
NME (%)	50.34	141.06	63.38	46.24	42.66	45.13

ACPD
13, 25649–25739, 2013

Aerosol indirect effect in the two-way coupled WRF-CMAQ

S. Yu et al.

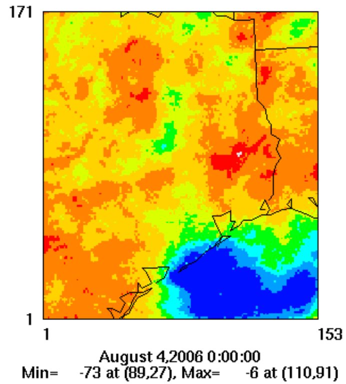

(a)

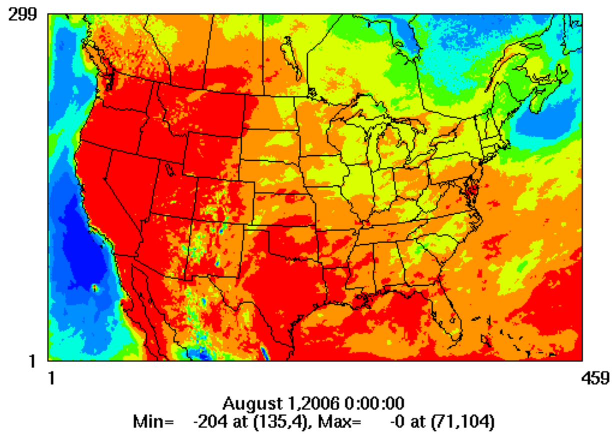

(b)

Fig. 1. The model domains of WRF-CMAQ for **(a)** a 4 km resolution model grid over east Texas and **(b)** a 12 km resolution model grid over the continental US for the results of SWCF in August of 2006.

ACPD
13, 25649–25739, 2013

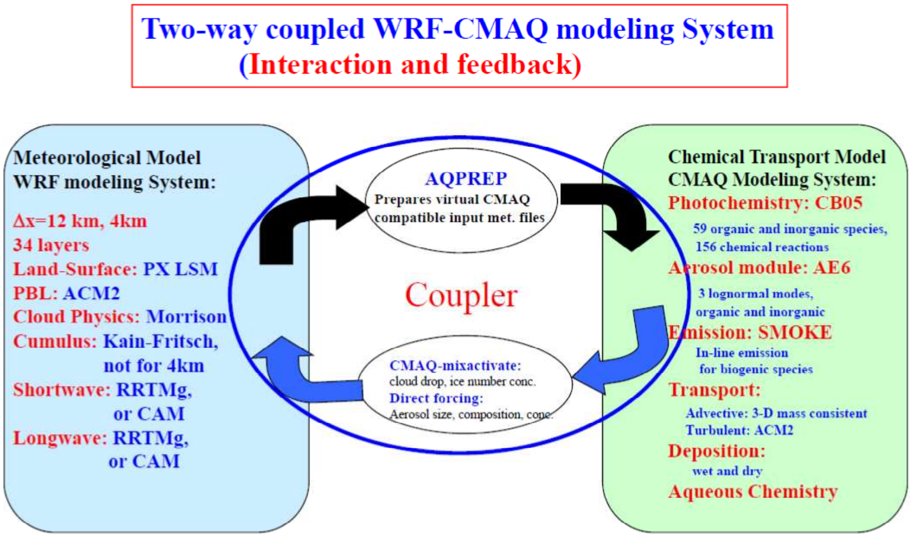

Fig. 2. The two-way coupled WRF-CMAQ modeling system.

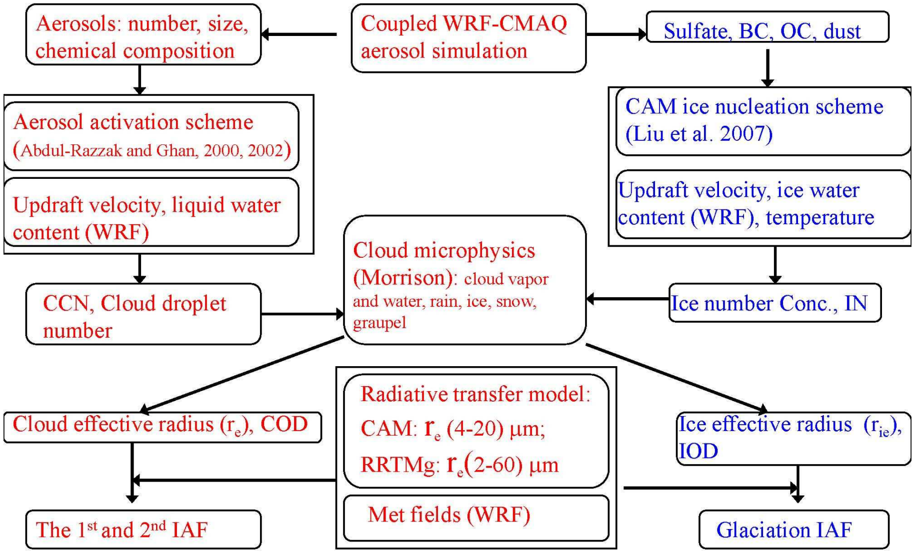

Fig. 3. Flow diagram for calculation of aerosol indirect effect (AIE) in the two-way coupled WRF-CMAQ modeling system.

ACPD
13, 25649–25739, 2013

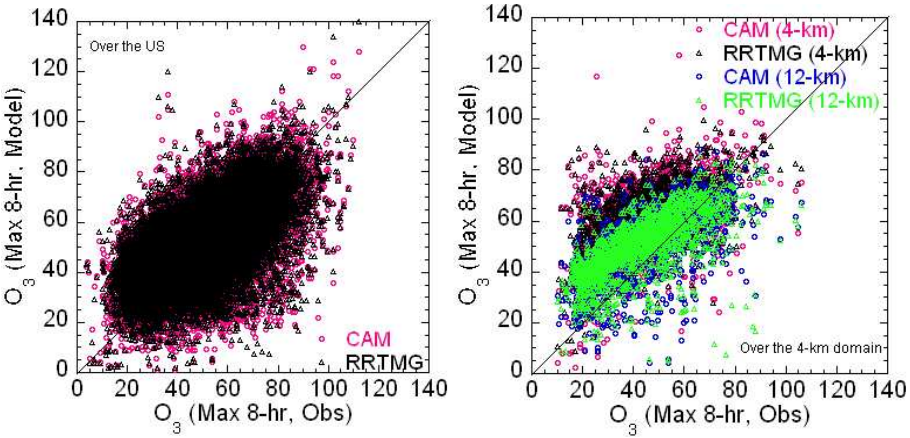

(a) (b)

Fig. 4. Scatter plots of the modeled (CAM (WRF-CMAQ/CAM) and RRTMG (WRF-CMAQ/RRTMG)) and observed 8 h O_3 concentrations (ppbv) at the AIRNow monitoring sites **(a)** over the continental US (12 km resolution model grid); **(b)** the results over eastern Texas from the simulations at 4 km and the 12 km resolution model grids.

ACPD
13, 25649–25739, 2013

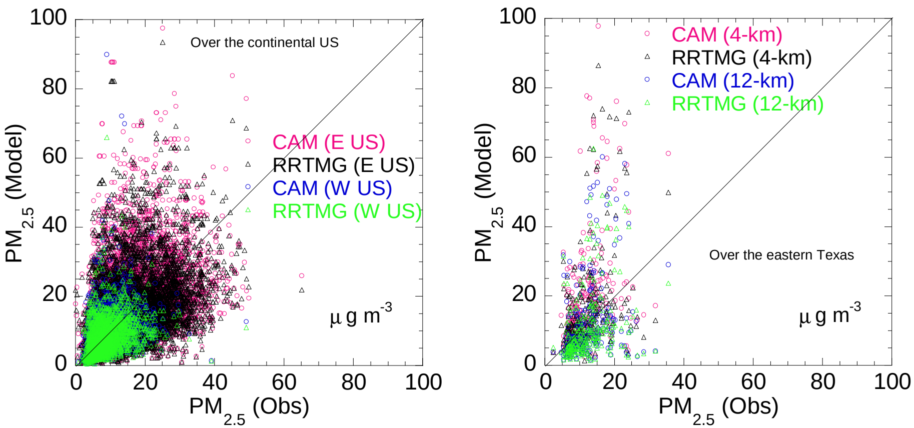

(a) (b)

Fig. 5. Scatter plots of the modeled (CAM (WRF-CMAQ/CAM) and RRTMG (WRF-CMAQ/RRTMG)) and observed daily $PM_{2.5}$ concentrations at the AIRNow monitoring sites **(a)** over the continental US (12 km resolution model grid); **(b)** over eastern Texas from the simulations at 4 km and the 12 km resolution model grids.

ACPD
13, 25649–25739, 2013

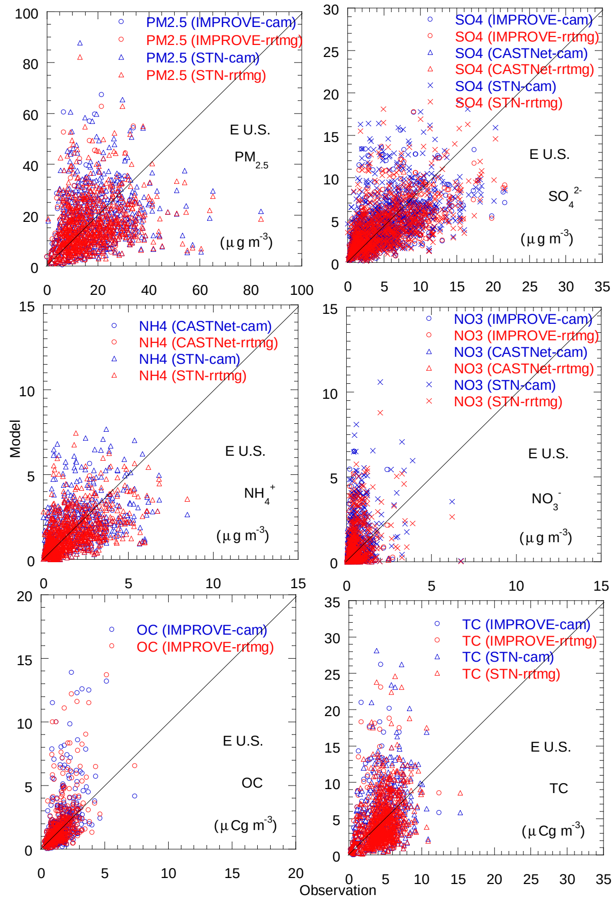

Fig. 6a. Comparison of observed and modeled (CAM (WRF-CMAQ/CAM) and RRTMG (WRFCMAQ/RRTMG)) $PM_{2.5}$ and its chemical composition at the IMPROVE, CASTNet and STN sites over the eastern US (longitude > 100°).

ACPD
13, 25649–25739, 2013

Aerosol indirect effect in the two-way coupled WRF-CMAQ

S. Yu et al.

Title Page
Abstract | Introduction
Conclusions | References
Tables | Figures
◀| |▶
◀ ▶
Back | Close
Full Screen / Esc
Printer-friendly Version
Interactive Discussion

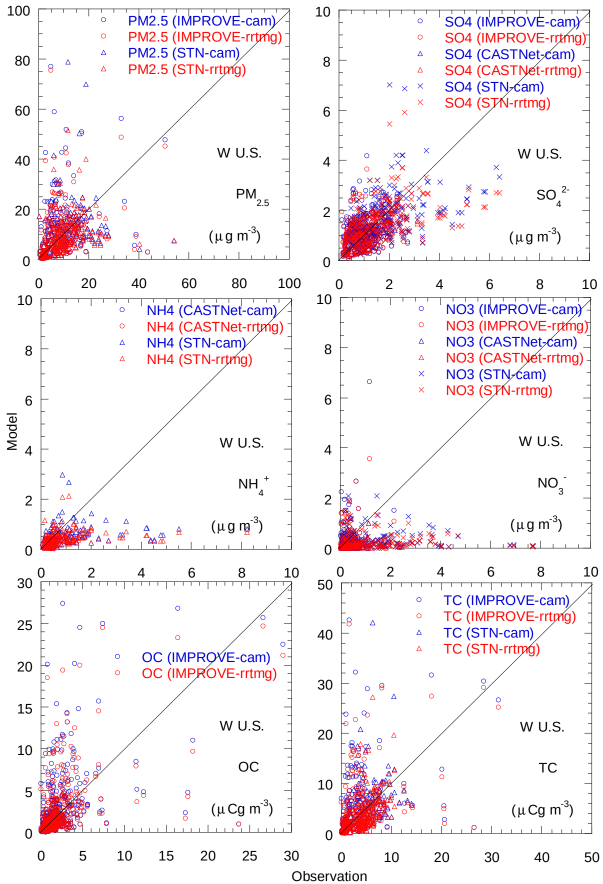

Fig. 6b. Comparison of observed and modeled (CAM (WRF-CMAQ/CAM) and RRTMG (WRFCMAQ/RRTMG)) $PM_{2.5}$ and its chemical composition at the IMPROVE, CASTNet and STN sites over the western US (longitude < 100°).

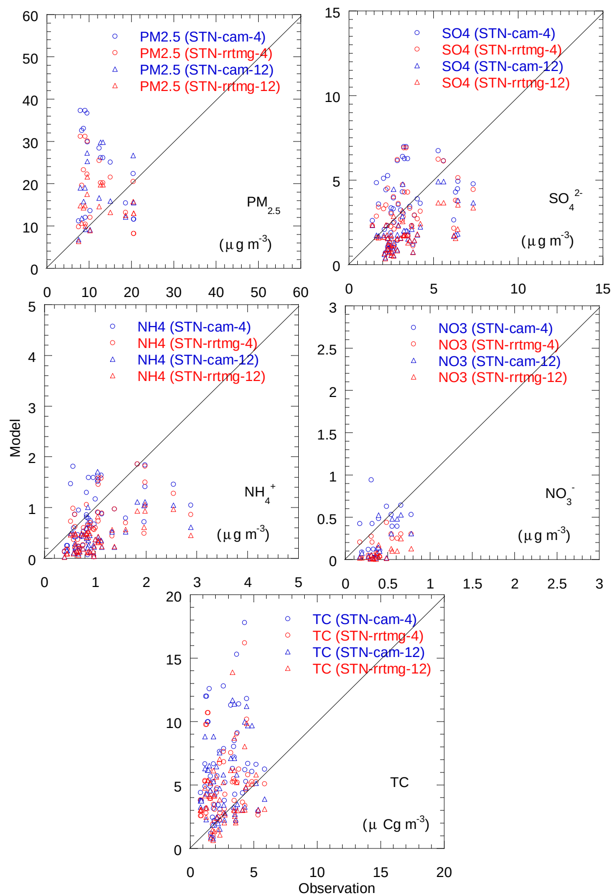

Fig. 7. Comparison of observed and modeled (CAM (WRF-CMAQ/CAM) and RRTMG (WRFC-MAQ/RRTMG)) $PM_{2.5}$ and its chemical composition at the STN sites over the eastern Texas from the simulations at 4 km and the 12 km resolution model grids.

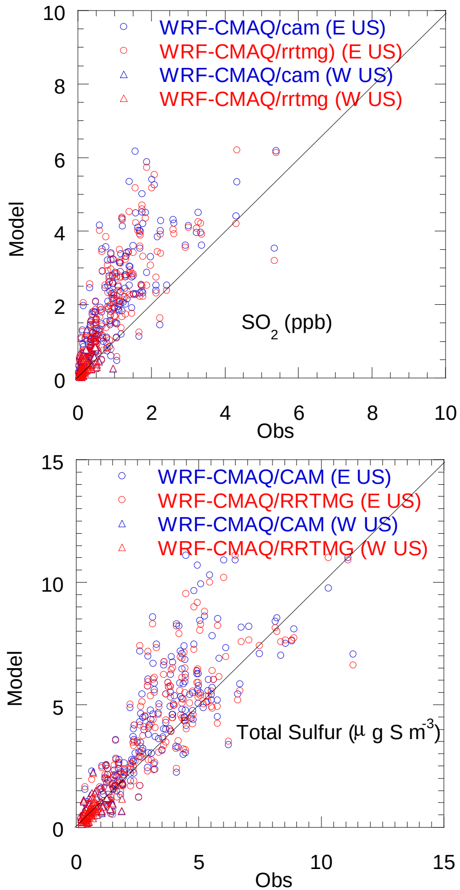

Fig. 8. Comparison of observed and modeled (WRF-CMAQ/CAM and WRFCMAQ/RRTMG) SO_2 and total sulfur ($SO_4^{2-} + SO_2$) concentrations at the CASTNet over the continental US.

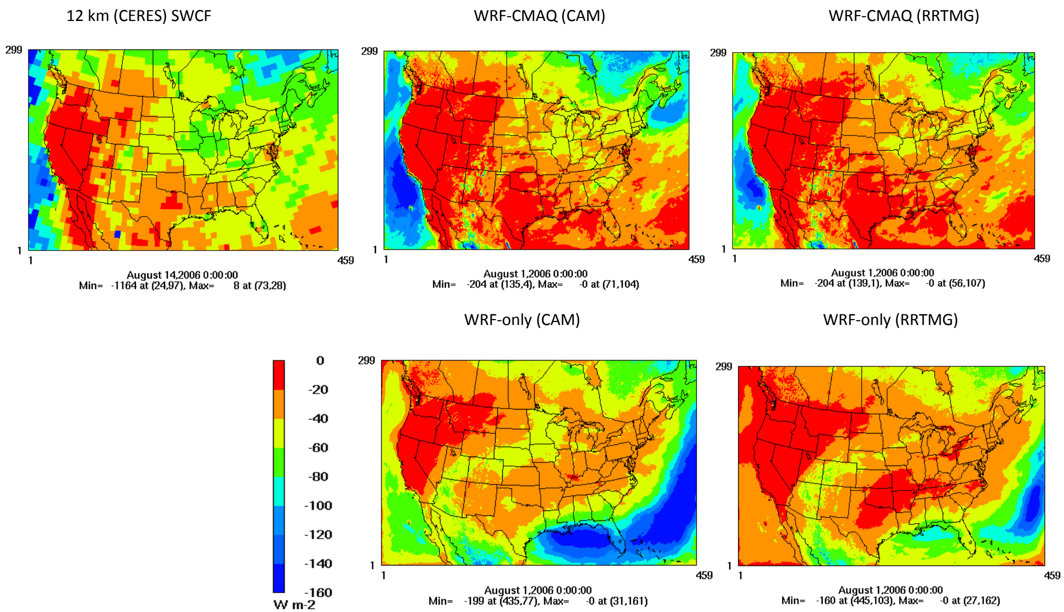

Fig. 9. Monthly domain means of SWCF for the CERES observations and model results of WRF-CMAQ/CAM, WRF-CMAQ/RRTMG, WRF-only/CAM and WRFonly/RRTMG on the basis of 12 km resolution simulation over the CONUS for August of 2006.

ACPD
13, 25649–25739, 2013

Title Page
Abstract | Introduction
Conclusions | References
Tables | Figures
◀| |▶
◀ ▶
Back | Close
Full Screen / Esc
Printer-friendly Version
Interactive Discussion

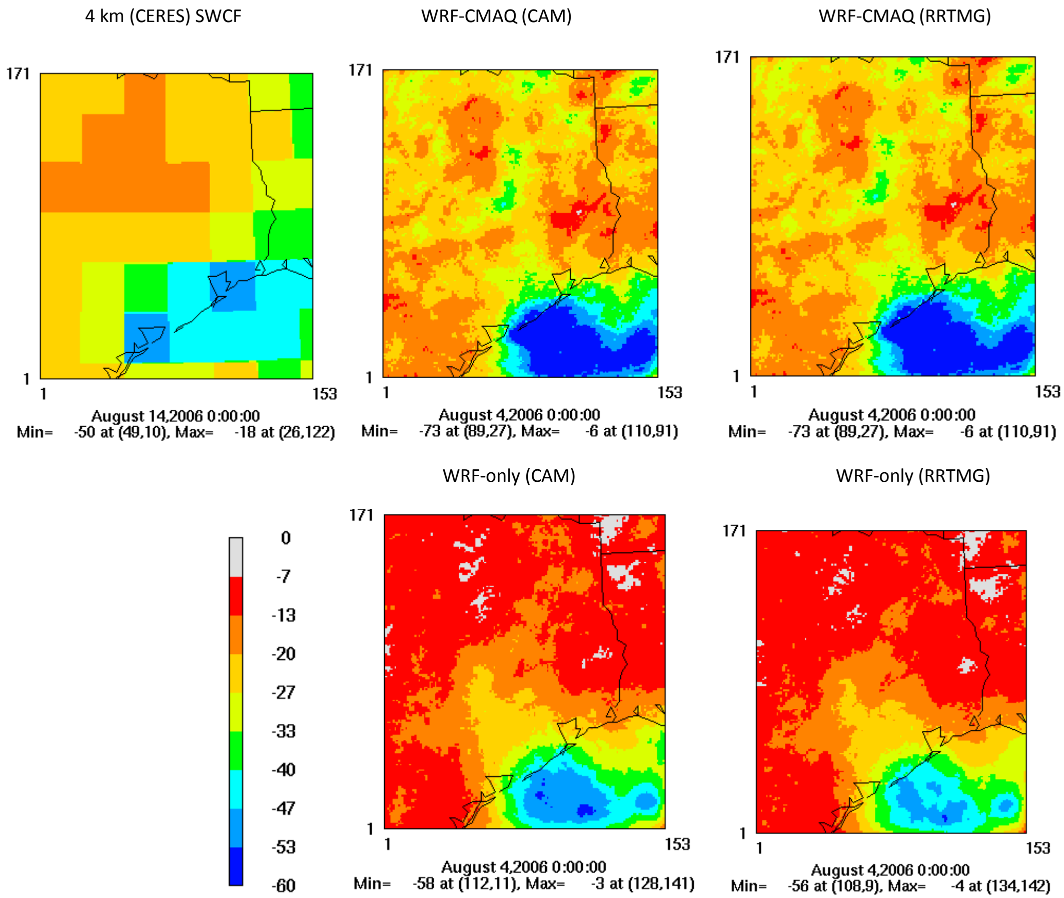

Fig. 10. Same as Fig. 9 but for the eastern Texas domain on the basis of the 4 km resolution simulation for August of 2006.

ACPD
13, 25649–25739, 2013

Aerosol indirect effect in the two-way coupled WRF-CMAQ

S. Yu et al.

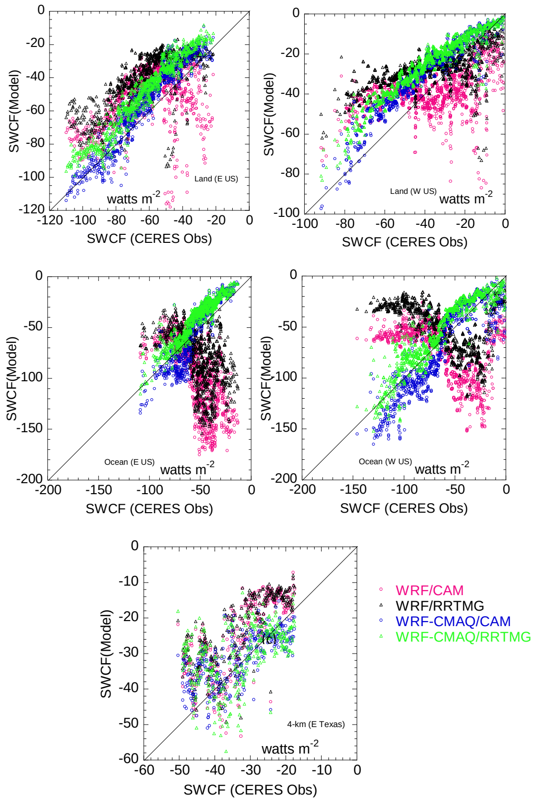

Fig. 11. Scatter plots of modeled (WRF-CMAQ/CAM, WRF-CMAQ/RRTMG, WRF/CAM and WRF/RRTMG) and observed monthly mean SWCF over the land, and ocean of the eastern and western US for the 12 km resolution simulations (see Fig. 9) and over the eastern Texas domain for the 4 km resolution simulations (see Fig. 10) for August of 2006.

ACPD
13, 25649–25739, 2013

Title Page
Abstract | Introduction
Conclusions | References
Tables | Figures
◀I | ▶I
◀ | ▶
Back | Close
Full Screen / Esc
Printer-friendly Version
Interactive Discussion

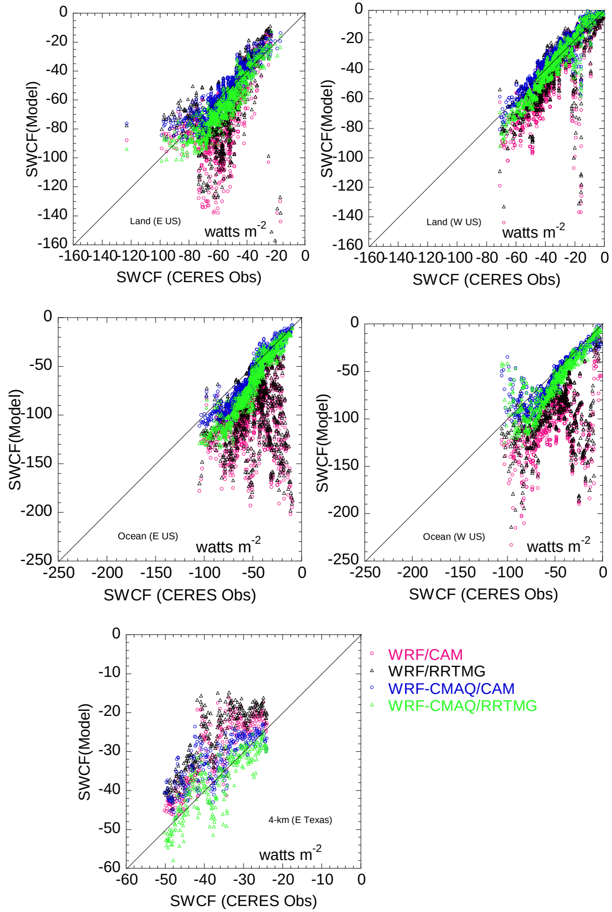

Fig. 12. Same as Fig. 11 but for September of 2006.

ACPD
13, 25649–25739, 2013

Aerosol indirect effect in the two-way coupled WRF-CMAQ

S. Yu et al.

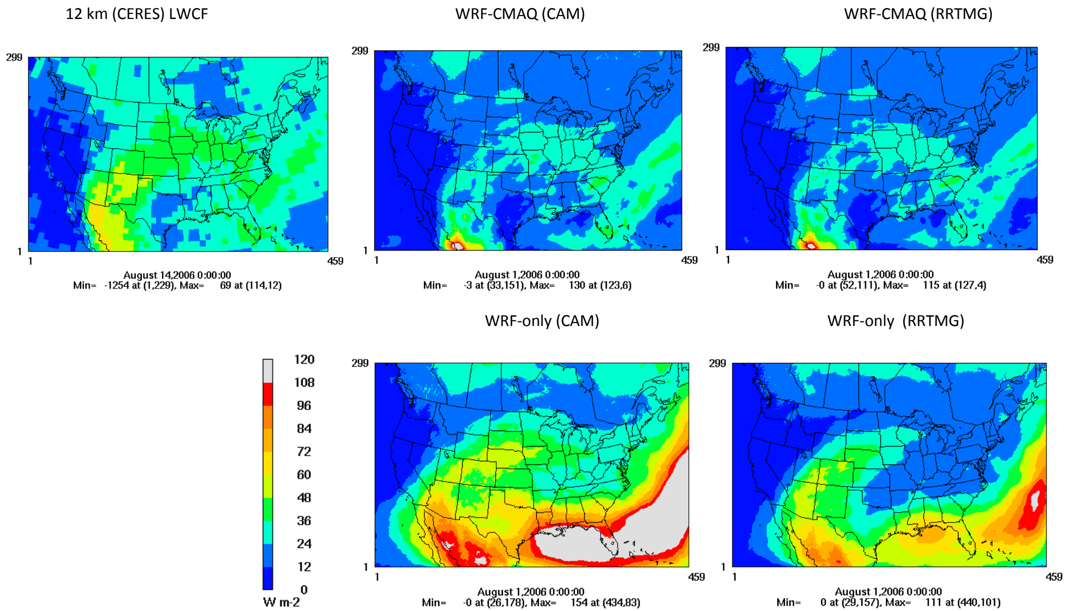

Fig. 13. Same as Fig. 9 but for LWCF.

ACPD
13, 25649–25739, 2013

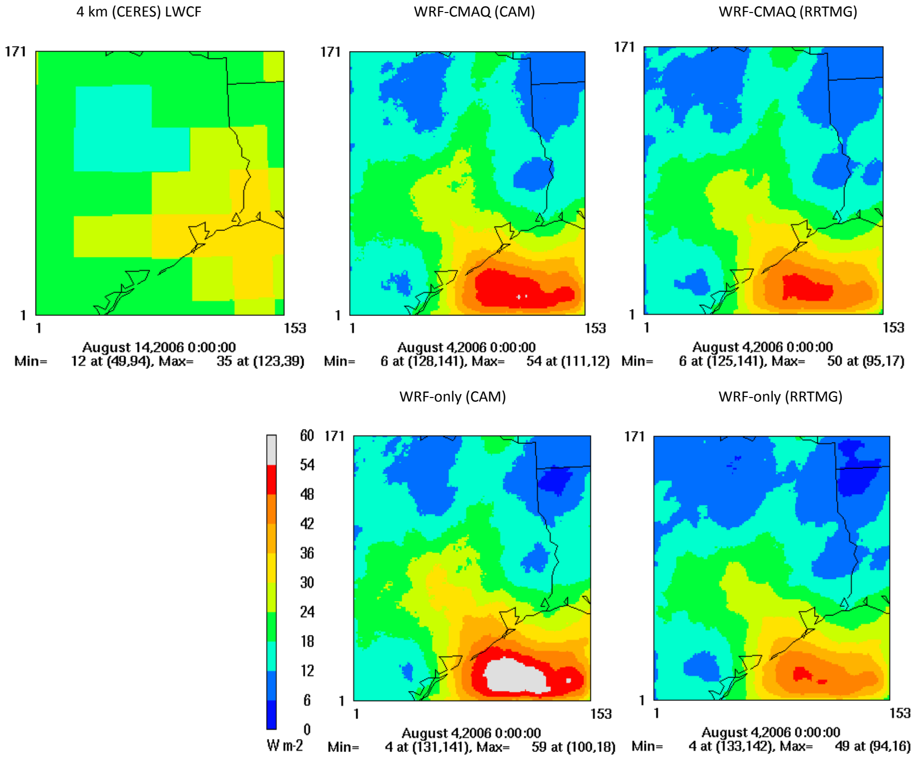

Fig. 14. Same as Fig. 10 but for LWCF.

ACPD
13, 25649–25739, 2013

Aerosol indirect effect in the two-way coupled WRF-CMAQ

S. Yu et al.

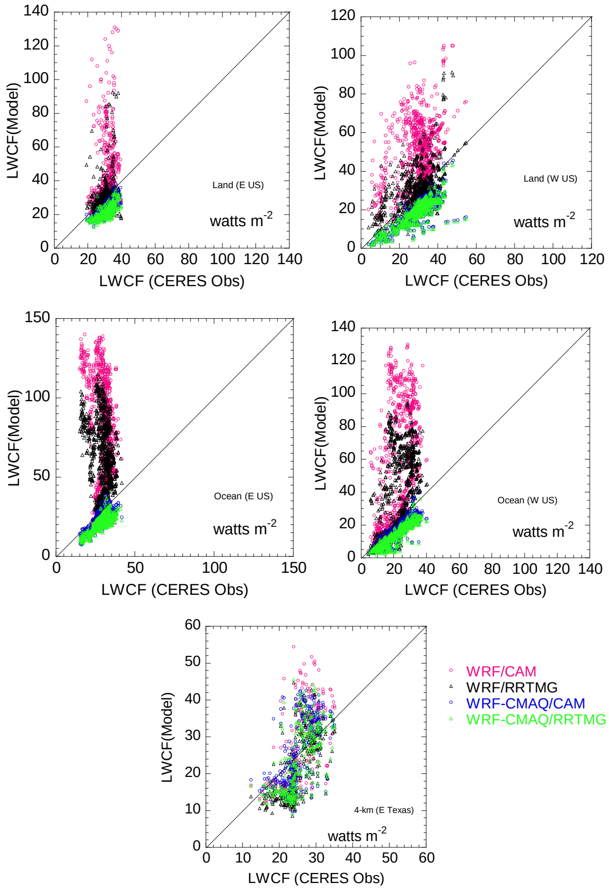

Fig. 15. Same as Fig. 11 but for LWCF.

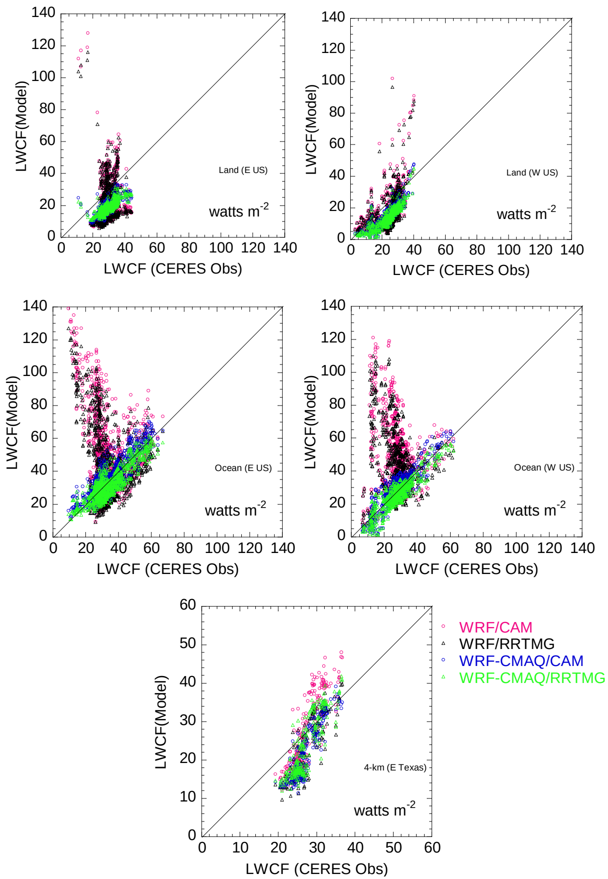

Fig. 16. Same as Fig. 15 but for September of 2006.

ACPD
13, 25649–25739, 2013

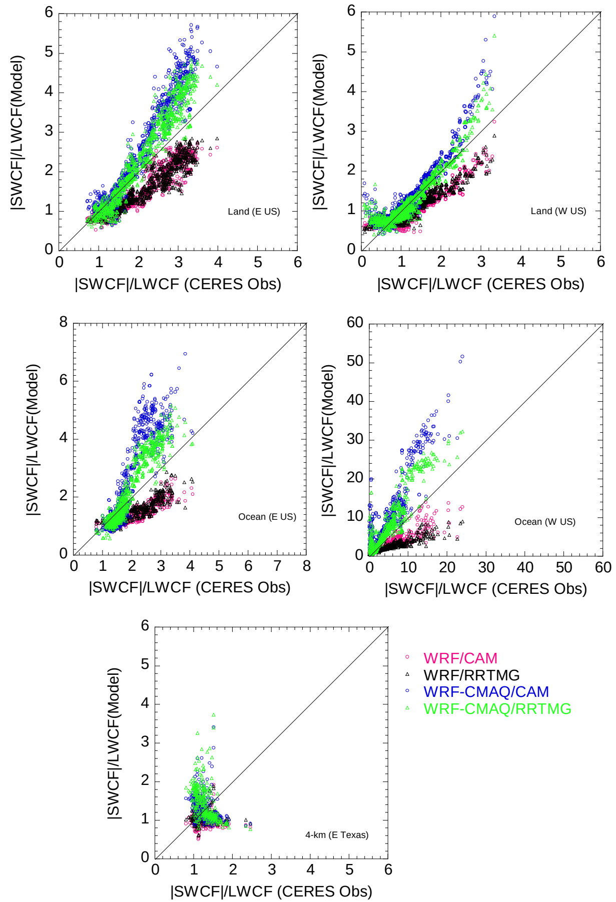

Fig. 17. Same as Fig. 11 but for the ratios of monthly mean absolute (SWCF) to LWCF for August of 2006.

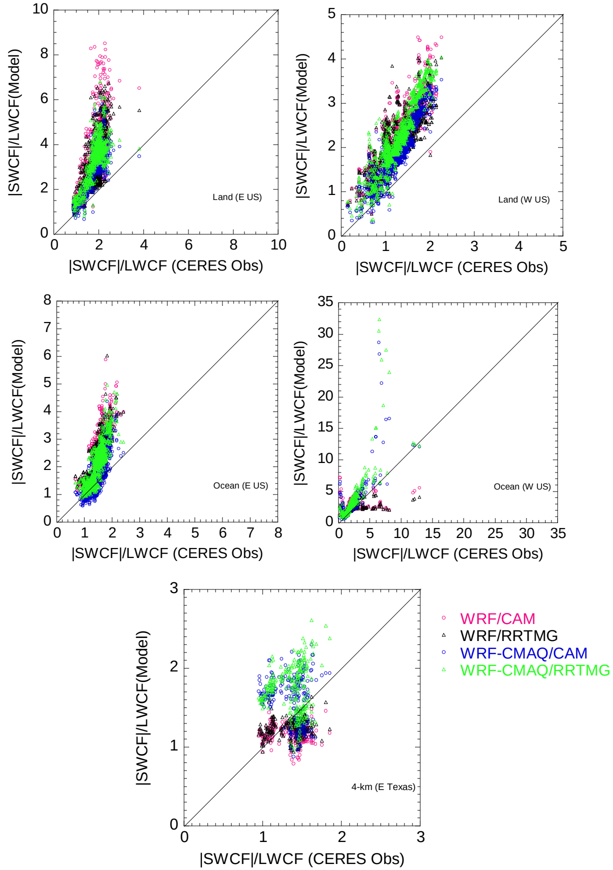

Fig. 18. Same as Fig. 17 but for September of 2006.

ACPD
13, 25649–25739, 2013

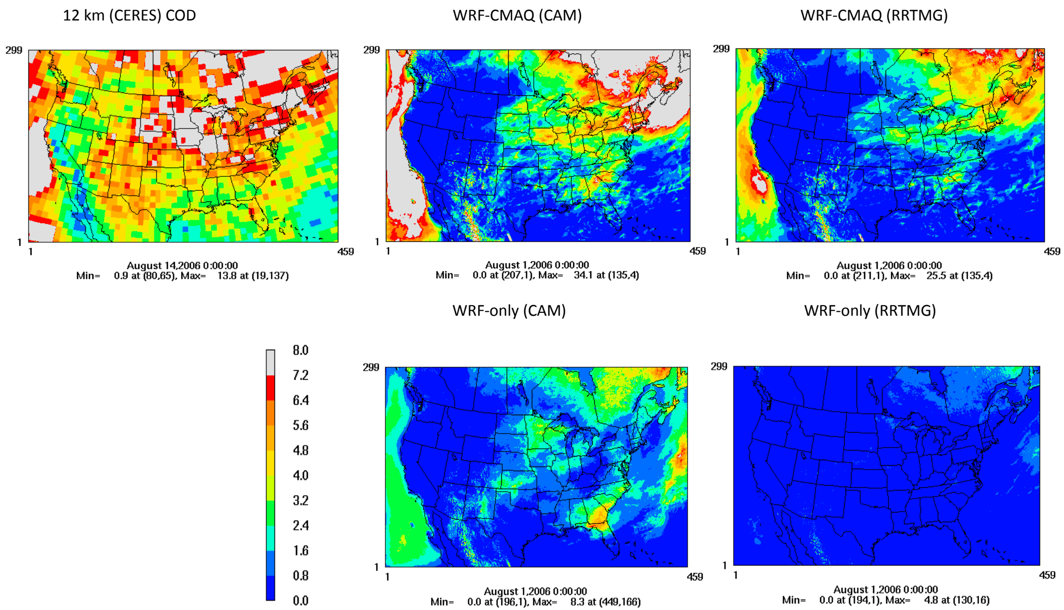

Fig. 19. Same as Fig. 9 but for COD for August of 2006.

ACPD
13, 25649–25739, 2013

Aerosol indirect effect in the two-way coupled WRF-CMAQ

S. Yu et al.

Title Page
Abstract
Introduction
Conclusions
References
Tables
Figures
◀
▶
Back
Close
Full Screen / Esc
Printer-friendly Version
Interactive Discussion

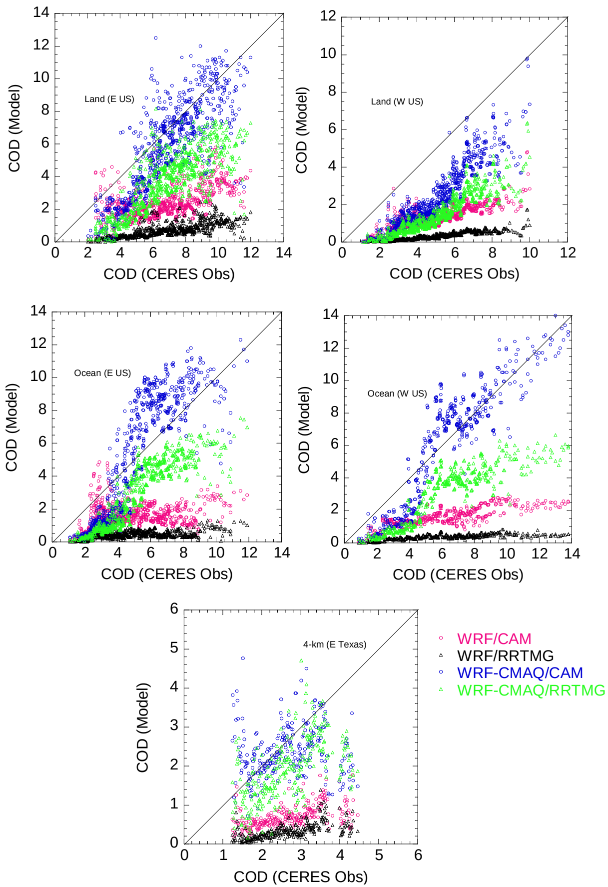

Fig. 20. Same as Fig. 11 but for COD for August of 2006.

ACPD
13, 25649–25739, 2013

Aerosol indirect effect in the two-way coupled WRF-CMAQ

S. Yu et al.

Title Page
Abstract Introduction
Conclusions References
Tables Figures
◀ ▶
Back Close
Full Screen / Esc
Printer-friendly Version
Interactive Discussion

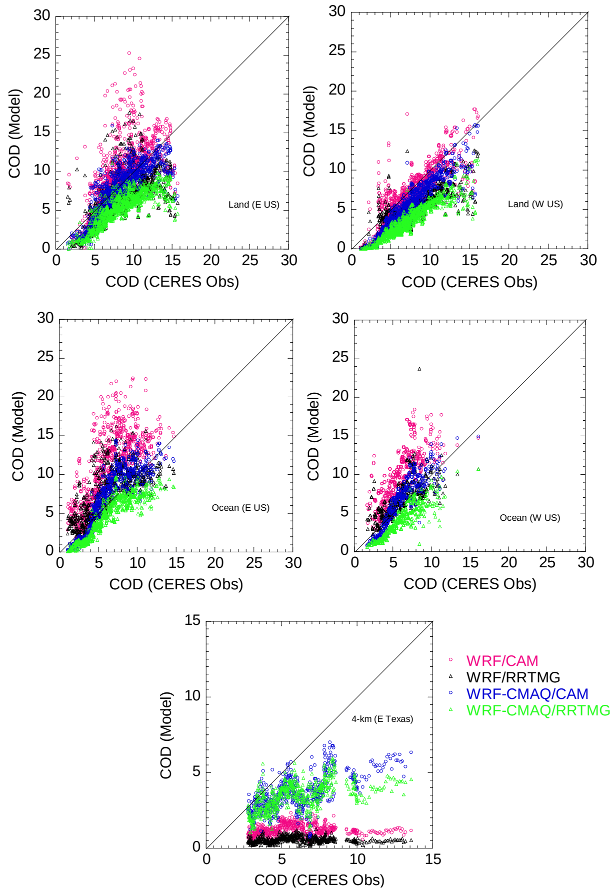

Fig. 21. Same as Fig. 11 but for COD for September of 2006.

ACPD
13, 25649–25739, 2013

Aerosol indirect effect in the two-way coupled WRF-CMAQ

S. Yu et al.

Title Page
Abstract | Introduction
Conclusions | References
Tables | Figures
◂ | ▸
◂ | ▸
Back | Close
Full Screen / Esc
Printer-friendly Version
Interactive Discussion

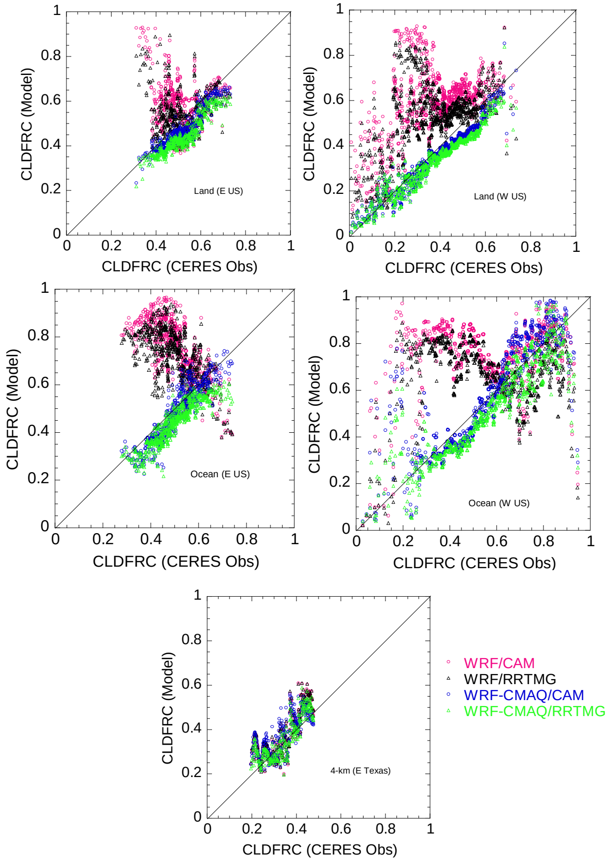

Fig. 22. Same as Fig. 11 but for cloud fractions (CLDFRC) for August of 2006.

ACPD
13, 25649–25739, 2013

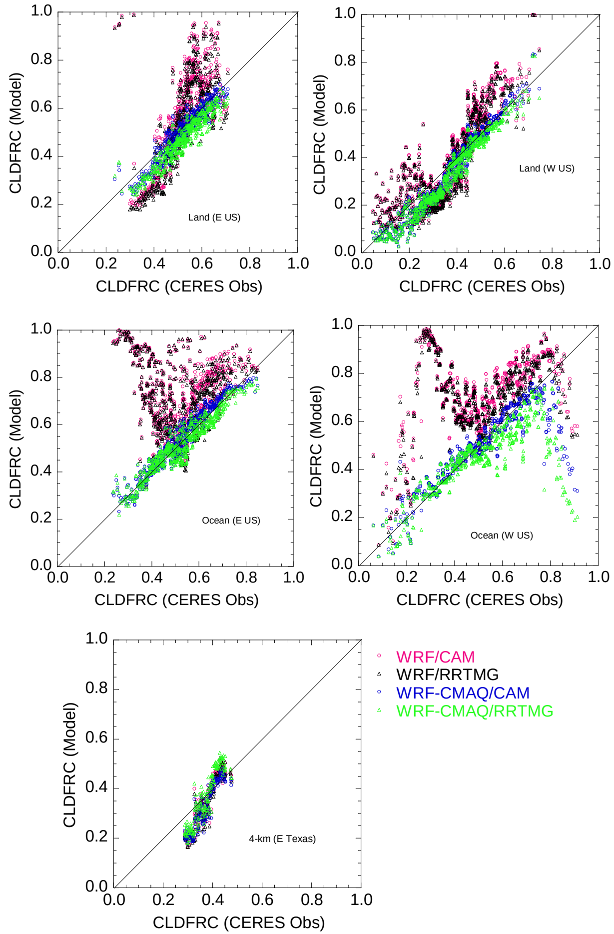

Fig. 23. Same as Fig. 11 but for cloud fractions (CLDFRC) for September of 2006.

ACPD
13, 25649–25739, 2013

Aerosol indirect effect in the two-way coupled WRF-CMAQ

S. Yu et al.

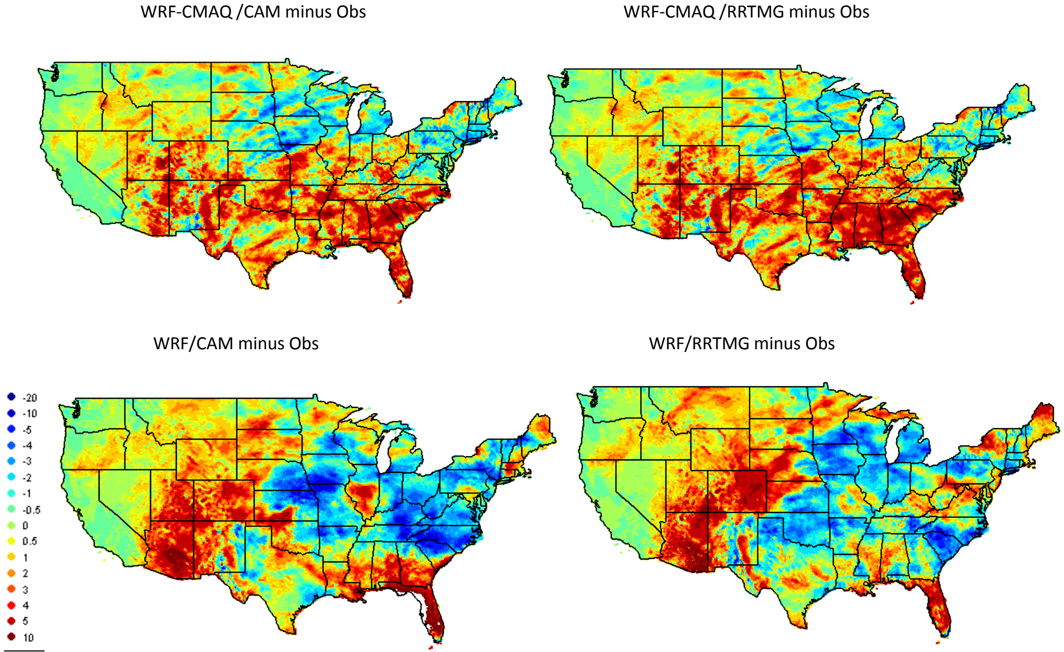

Fig. 24. The difference (inch month^{-1}) of monthly domain means of precipitation between the observations and model results of WRF-CMAQ/CAM, WRFCMAQ/RRTMG, WRF-only/CAM and WRF-only/RRTMG on the basis of 12 km resolution simulation over the CONUS for August of 2006.

ACPD
13, 25649–25739, 2013

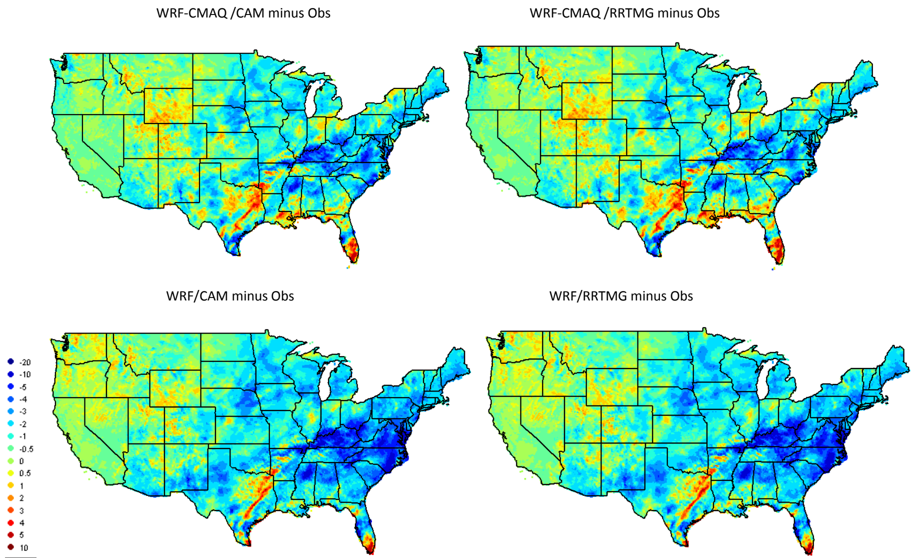

Fig. 25. Same as Fig. 24 but for September of 2006.

ACPD
13, 25649–25739, 2013

Aerosol indirect effect in the two-way coupled WRF-CMAQ

S. Yu et al.

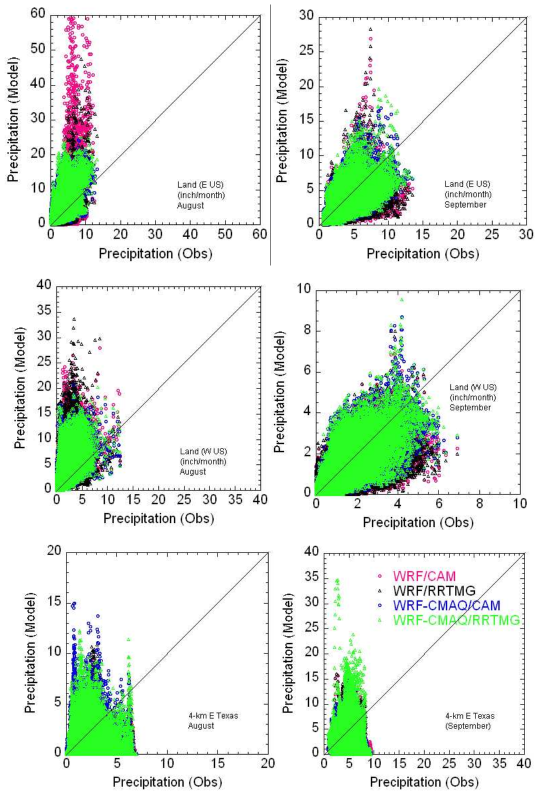

Fig. 26. Scatter plots of modeled (WRF-CMAQ/CAM, WRF-CMAQ/RRTMG, WRF/CAM and WRF/RRTMG) and observed monthly mean precipitation (inch/month) over the land of the eastern and western US for the 12 km resolution simulations and over the eastern Texas domain for the 4 km resolution simulations for August and September of 2006.

ACPD
13, 25649–25739, 2013